Spatiotemporal characterization of post-stroke myelin density changes and their contribution to functional recovery using a novel label-free in vivo imaging technique

by

Eszter Wendlandt

A thesis submitted in partial fulfillment of the requirements for the degree of

Master of Science

Department of Psychiatry
University of Alberta

Abstract

Myelin is an essential component of nervous system functioning: it supports axonal metabolism, enables saltatory conduction to allow for precise timing across cortical networks to regulate information processing and is increasingly recognized as an integral type of adult experience-dependent structural plasticity. As such, myelin's role is aiding the neuroplastic reorganization of the brain after stroke has recently received considerable attention, but significant gaps in knowledge remain, chief amongst them the widely differing timecourse and spatial distribution of myelination changes reported across various studies. To help characterize these post-stroke changes in myelin, particularly in the immediate vicinity of the primary site of injury, we investigated the utility of a novel label-free in vivo imaging technique called Spectral Confocal Reflectance Microscopy (SCORE) capable of stably tracking individual superficial cortical myelinated fibers over a period of weeks. We concurrently tracked changes in the integrity and density of axons projecting to or passing through the same peri-lesional areas originating in the contralesional homotopic regions and simultaneously monitored meso-scale functional activation of the cortex in response to somatosensory stimuli of the fore- and hindlimb to gauge the extent of functional recovery occurring in somatosensory processing, given that the stroke model used specifically targeted the forelimb somatosensory representation. The pole test and the cylinder test were also utilized as an indices of behavioral recovery. Furthermore, we administered the atypical antipsychotic quetiapine - a known pro-myelinating agent - to see whether its myelin boosting effect was observable following an ischemic injury as well and to further help evaluate the functional significance of post-stroke myelin densities in aiding functional recovery. We showed longitudinal imaging of both GFP-expressing contralateral crossing fibers and SCORE-imaged myelinated fibers are stable and powerful

techniques for evaluating the changing architecture of the post-stroke brain: though a severe deficit in both types of fiber densities are evident immediately in the days following stroke, robust recovery to baseline levels particularly in the density of contralaterally projecting crossing fibers was apparent within 2 weeks after the initial injury. Myelin density, however, particularly in regions close to the stroke core, remained persistently decreased even at 4 weeks post-stroke. Quetiapine treatment increased the density of intact contralateral crossing fibers, but more dramatically helped partially alleviate the chronic myelin deficit observed surrounding the infarct core. Despite these effects, however, quetiapine did not significantly boost the timecourse or extent of the functional recovery of somatosensory processing or behavioral recovery. Nevertheless, myelin density was still shown to be a significant predictor of the size of both forelimb and hindlimb stimulation activated cortical responses, indicating that though myelination appears to play some role in contributing to functional recovery, it does so in concert with other, potentially more influential mechanisms of recovery. Alternatively, functional patterns of cortical activity dictated by rehabilitative training may be necessary to induce more functional patterns of myelination across the recovering cortical networks than was observed in our model of quetiapine administration with no directed sensorimotor rehabilitation.

Preface

This thesis is an original work by Eszter Wendlandt. The research project, of which this thesis is a part, received research ethics approval from the University of Alberta Research Ethics Board, Project Number AUP361. No part of this thesis has been previously published.

I dedicate this thesis to my wonderful husband - because he told me I had to, and because I couldn't have done it without him.

Acknowledgements

I would like to thank my supervisor for his constant patience, support and insight throughout this process, as well as all my labmates for their unfailing willingness to show me how the microscope works, particularly Mischa Bandet. I'd also like to thank my amazing parents and all my crazy siblings for being a continuous source of inspiration and support in my life, and my fantastic in-laws for their steadfast understanding.

Table of Contents

List of Tables

List of Figures

Chapter 1

Introduction

1.1 Background Information

1.1.1 Ischemia

Impact and Potential Therapies

Over the past few decades, the focus of neuroscience has shifted towards a more holistic view of the central nervous system (CNS), with growing appreciation of the multiplicity and complex interplay between the various glial and neuronal populations that collaborate to produce the intricate patterns of activity of the brain. Stroke research itself is a great example of this shifting interest, with a recent explosion of studies focusing on the glial contribution to the disease pathophysiology and their impact on behavioral recovery [1, 2]. Many consider this change key to improving post-stroke care [3] - a much needed improvement, given that stroke is leading cause of adult disability and the third leading cause of death in Canada [4] and its prevalence is projected to continue rising given the aging population [5].

By far the most frequent type of stroke is the acute ischemic variety, accounting for as much as 87% of all strokes [6]. This type of stroke is caused by a blockage of blood vessels in the brain leading to greatly restricted delivery of oxygen and glucose to the affected regions resulting in eventual tissue death. To date, the only FDA-approved treatment for ischemic stroke remains tissue plasminogen activator (TPA) [7], which itself is severely limited both by its constrained applicability and poor efficacy [8, 9]. TPA is a classic example of a neuroprotective treatment - an intervention whose primary aim is to

limit the extent of the damage caused by the bout of ischemia. Though numerous such therapies have been developed in animal models, translation remains a major roadblock to effective stroke management in human populations [10]. And whereas neuroprotection is certainly an important branch of stroke treatment, its feasability is necessarily limited to the hours and days following the initial insult during which time the region surrounding the stroke core - the area with the most severely compromised blood flow - undergoes ongoing cell death [11]. This so-termed penumbral region then is the primary target of neuroprotective therapies that aim to limit the extent of this spatial expansion of the stroke core. The other, complementary arm of stroke treatment is instead centered on enhancing whatever recovery naturally occurs in the brain. To this end, tremendous effort has been expanded to understand precisely the endogeneous mechanisms through which the brain reorganizes itself after an injury - a phenomenon called neuroplasticity. Here too, the role glial cells play is being increasingly recognized as crucial to a complete understanding of post-injury neuroplasticity that will ultimately enable us to fully exploit and even extend the self-regenerating capabilities of our nervous system. Though this approach has definitely yielded a number of positive results in animal models of stroke and has shown some promise across human populations (for an in-depth review see [12]), significant gaps in knowledge remain.

Photothrombotic Animal Model of Ischemia

Such mechanistic questions are perhaps best explored using animals models, and a number of rodent stroke model have been developed - each with its unique set of strengths and weaknesses [13, 14]. Photothrombosis is one such model originally described in Watson et al., 1985 [15], that involves the systemic injection of the photoactive dye Rose Bengal, which, upon illumination, produces singlet oxygen which in turn causes peroxidative damage to the endothelium, subsequent platelet aggregation and thrombus formation and consequently blood flow cessation. It generates a highly reproducible, precisely localized form of permanent focal ischemia, characterized by a specific spatiotemporal evolution of neuronal damage and glial reactivity. The infarct core, for example, expands over the first 24-48 hours after the initial insult - with ongoing apoptotic and necrotic cell death

occurring rapidly [16] - but shrinks considerably over the course of the weeks following [17]. Surrounding the lesion core is a so-called demarcation zone that evolves over the course of around 7 days, and is identified primarily by the location of the CSPG-rich glial scar deposited principally by reactive astrocytes that form a tight ring around the infarct core [18]. Activated microglia and macrophages expressing Iba-1 show a similar timeline of activation to astrocytes - peaking around 4 days after the initial injury but, unlike astrocytes, invade the infarct core itself, as well as the demarcation zone and show overall reduced normalization to baseline densities over the following weeks as compared to GFAP-reactive astrocytes [17]. The rim of cortex surrounding this glial scar is known as the peri-infarct region, and is considered to be the area of greatest injury-induced structural and functional plasticity in the weeks following the initial insult [19, 20]. Though both the generally small infarct volume and regional specificity of this stroke model make it an attractive candidate from the translational perspective, certain aspects of its pathophysiology diverge significantly from the ischemia seen in humans. One major difference is the complete absence of reperfusion, which is a common occurrence in humans and may significantly alter the specific pathophysiology of post-stroke recovery [21, 22]. In addition, photothrombotic stroke generally induces simultaneous vasogenic and cytotoxic edema, as imaged via an increase in T2-weighted MRI signals concurrent to a decrease in the apparent diffusion of water [23, 24], whereas stroke in humans in comparison in specifically characterized by a delayed onset of vasogenic edema [25]. Lastly, photothrombotic ischemia is thought to produce a much smaller penumbra than ones typically seen with human patients; however, this orthodoxy is increasingly challenged as the size of the penumbra in humans may be smaller than originally believed [26]. Indeed, in the photothrombotic stroke model, the primary site of hypoperfusion is surrounded by a rim of $\sim$ 400 uM experiencing progressive hypoperfusion and cell death [27].

Mechanisms of Cell Death

Crucially important, however, is to note that apoptotic cell death following the initial injury occurs even in areas of the cortex not directly experiencing hypoperfusion - in other words, in regions outside of the penumbra [27] and within the border zone of the

ischemic infarct. Even in photothrombotic stroke, is an ongoing process lasting days after the intial insult [16]. Ischemia immediately leads to a severe energy deficit in operating neurons, who are consequently unable to maintain ionic gradients across their cell membranes and depolarize, rapidly releasing large amount of vesicular glutamate into the extracellular space [28–30]. Meanwhile this glutamate elevation is further exacerbated by the reverse-transport of glutamate by the glutamate transporter, caused by a reversal in the sodium ion gradient [31]. This rapid elevation of extracellular glutamate leads to even more Na+ influx that further compromises the already energy-deficient neuron and leads to direct excitotoxic injury through the activation of NMDAR channels and the subsequent entry of Ca2+ ions, which in turn may directly activate pathways of apoptotic cell death [32]. Even mildly elevated intracellular Ca2+, however, may lead to enhanced activity of NOS-1 and heightened generation of NO, as well as other reactive oxygen species generated by the mitochondria, which may combine with oxygen to produce the particularly toxic peroxynitrite, which may in turn directly severely damage DNA and thus activate pathways of apoptosis [33, 34]. This extensive injury of course results in rapid and substantial immune activation across much of the ipsilesional hemisphere, and infiltrating immune cells may release their own cocktail of lethal cytokines, further compromising both the core regions but surrounding cortex as well. Reactive oxygen species and pro-inflammatory molecules will also work to open the blood-brain-barrier (BBB), leading to vasogenic edema, swelling and further import of various immune cells [35, 36]. Given this complex cascade of evolving damage, it is not surprising that the effects of a temporally limited ischemic injury extend well beyond the scope of the initial insult, both temporally and spatially with secondary degeneration of distant cortical regions occurring sometimes over days after the initial insult [37]. Overlapping with this evolving damage, however, is the emergence of pro-regenerative mechanisms involving structural and functional plasticity that work to reorganize the cortical networks responsible for information processing that were lethally injured during the ischemic episode.

1.1.2 Functional plasticity

Functional remapping of cortical sensorimotor representations is fairly well-characterized meso-scale phenomenon that's thought to underlie much of true behavioral recovery that occurs following stroke. It's most comprehensively studied within the context of small targeted infarcts that damage a particular sensory or motor representation, and describes the apparent re-emergence of these cortical map weeks following the initial insult at distinct, functionally "remapped" spatial locations that previously performed processing other than their newly remapped function [38–40]. Current common methodologies to image stimulus-evoked cortical activity include PET scans and fMRI, which provide the distinct advantage of repeated imaging over a period of weeks following the initial injury, as compared to the use of voltage sensitive dyes, which can only be utilized acutely, but provide significantly better spatial and temporal resolution. A compromise between these extremes is represented by intrinsic optical signal imaging (IOS), which measures a minute cortical reflectance dip attributed to a local rise in deoxyhemoglobin that results from the increased metabolic demands of active neuronal tissue [41] and provides fairly good spatial resolution ($\sim$ 100 uM) with minimal invasiveness.

Using these techniques, the changing cortical activation patterns following a disturbance can be stably tracked and visualized. The precise peri-infarct location of the remapped representation, for example, has been shown to vary significantly with the exact location of the ischemic infarct - presumably due to the specific pattern of intact intracortical and cortico-thalamic (or thalamo-cortical) structural connections that survive the initial impact and hence provide the neural substrate for potentially taking over the processing of the specific function that was lost. Following a targeted forelimb somatosensory stroke for example, the emergent forelimb somatosensory representation has been shown to remap both into the primary motor cortex (M1) [42], as well as into the hindlimb somatosensory representation (H1) and the regions lateral to it [43]. Interestingly, there is some evidence to indicate that the spatial extent of the remapping may be modality-specific, as the infarcted primary motor cortex, in contrast to the somatosensory data, does not significantly encroach into the forelimb somatosensory representation,

but appears to remain largely constrained to the immediate border zone of the infarct [44].

The timecourse of these changes also appears to vary relative to the size and location of the injury, with likely some continual recovery in responsitivity occurring over the first months after the initial injury [45] - however, the exact timeline of these changes remains relatively unexplored and shows considerable heterogeneity across studies. Following very small strokes of the primary visual cortex, for example, the bulk of remapping seems to occur within 14 days of the injury [46], whereas the reorganization of the barrel cortex shows some limited recovery 7 days post-stroke but significant changes only at the next timepoint assessed, at 28 days post-stroke [47]. In contrast, forelimb somatosensory remapping appears largely absent at 7 and 14 days post-stroke, but is eminently visible by 28 days post-stroke, yet its specific configuration may continue changing even beyond this timepoint [42, 43]. This is particularly interesting, given the altered characteristics of information processing in these newly established networks. For example, the amplitude of activity elicited by immediately neighbouring M1 cortical regions became significantly more uncorrelated following a targeted injury, especially when targeted to the FL somatosensory representation, indicating a significantly more diffuse primary motor map than that observed prior to stroke [44]. The dynamics of somatosensory responsive cortical activity is likewise altered following remapping, with persistently lower amplitudes of cortical response, that exhibit a slower onset and a significantly prolonged pattern of depolarization [42]. Neurons within the remapped somatosensory representations of digits in monkeys and raccoons also show larger sensory receptive fields following ischemic damage [48, 49], similar to the decrease in limb-specificity seen in neurons following forelimb remapping in mice [43], though this result again may be sensitive to precise stroke volume and location [50].

The functional significance of the cortical remapping response was most clearly demonstrated using classic serial ablation. Castro-Alamancos & Borrell, 1995 [51] demonstrated first the strong temporal correlation between the functional remapping of the forelimb primary motor cortex into peri-infarct tissue and the occurrence of motor behavioral

recovery, then demonstrated that subsequent ablation of the newly remapped cortical region re-instated the original motor deficits observed, despite the spatially identical ablation of cortical tissue in control animals resulting in no such deficits. This convincingly illustrates that the newly established motor representation of the forelimb was functionally performing the same information processing previously performed by the uninjured forelimb motor representation. Similar results have now been demonstrated using muscimol inactivation of the newly remapped region [52] and functional imaging studies demonstrate a similarly strong positive correlation between peri-lesional somatosensory remapping and behavioral recovery [53].

In humans studies as well there is a preponderance of evidence indicating functional remapping of sensorimotor representations after stroke, though the exact locations of newly established activation patterns vary significantly across subjects given the precise location and size of the initial insult, as in the animal data [54–57]. Interestingly, there is some disagreement across studies regarding the general trend in the size of motor response driven cortical activation over time. Some studies report an initially heightened, but diffuse activation in multiple cortical regions shortly after the initial insult whose eventual shrinking and increasing localization over time is associated with significant behavioral recovery [58], while others contend that its the increasing size of the injured sensorimotor representation in the peri-lesional cortex that drives functional recovery [59]. These discrepancies may be compatible however when one considers the differing timeline and cortical areas investigated in these studies - indeed, multiple investigators report an initial contralateral remapping response whose attenuation over time appears concurrent to the reappearance of peri-lesional patterns of activation that together predict behavioral recovery [60, 61]. Longitudinal imaging within the same subjects demonstrates that this functional plasticity extends well-beyond the initial period of substantive behavioral recovery - generally estimated at around 3 months - with ongoing behaviorally relevant remapping reported at 4 months and even at 2 years after ischemia [59, 62]. This is especially true with the concurrent administration of intensive rehab therapies, that result in simultaneous improvement of behavioral deficits and greater peri-lesional

representations of the injured functions - gains that remain stable for years [63, 64]. This rehab-dependent functional remapping response has also been noted in animal work, particularly with monkeys, with some studies reporting only minimal functional recovery without the concurrent administration of some rehabilitative treatment [65]. This raises the question of what specific plasticity mechanisms on the scale of individual neurons may underlie the meso-scale remapping of sensorimotor functions.

With relatively small strokes, part of the original sensorimotor representation may be completely spared, with recovery evident upon the strengthening of its existing connections. Another proposed mechanisms is the existence of a latent subthreshold connectome that is spared by injury and provides an existing structural substrate for the post-injury propagation of the type of sensorimotor information whose primary cortical processing network was damaged [66, 67]. There is some evidence indicating that such a network exists: neurons dedicated to processing incoming sensory information from a specific limb, for example, have been shown to receive synaptic inputs from the non-preferred limb as well [68] and whereas their receptive fields eliciting suprathreshold activity are generally finely tuned to specific types of somatosensory inputs, a wide variety of somatosensory inputs can elicit their subthreshold activation [69, 70]. Voltage sensitive dye imaging also reveals a wide network of functionally connected brain regions that reliably exhibit subtreshold propagation of activity [71, 72]. Such latent connections may be unmasked and synaptically strengthened over the period of weeks and months following an injury and contribute to the functional re-emergence of cortical sensorimotor maps. The other major proposed mechanism is true structural rewiring via axonal sprouting amongst intracortical, interhemispheric and subcortical-cortical connections. Indeed, multiple tracer studies demonstrate significantly altered patterns of local, peri-infarct intracortical connections following stroke [73–76], as well as substantial rewiring of long-distance intrahemispheric subcortical connection [42]. Axon sprouting has also been demonstrated from the contralateral hemisphere, in both the cortifugal and corticospinal tracts, that is, under certain conditions, associated with the successful remapping of motor representations [77–79]. Just recently, axonal sprouting of thalamo-cortical fibers was also imaged [80]. These

newly formed connections, just as the latent subthreshold connectome, requires continued synaptic remodelling to work effectively.

Indeed, a large body of in vivo imaging and immunohistochemical work demonstrates the incredible plasticity of dendritic spines and the synapses they form in the peri-infarct regions following stroke [81]. Though initially a rapid loss of dendritic spines is evident in the immediate ischemic border (<200 uM) [21], within 1 to 2 weeks this initial loss transforms into a greatly upregulated rate of spine turnover, with overall more gain than loss, with eventual recovery to baseline levels by 6 weeks within a millimeter of the stroke core [42]. Further from the core, others have noted an overall increase in the number of dendritic spines compared to baseline conditions [82]. All these plastic changes natively seem to occur over the first months following the initial injury, and there is some evidence of an initially-growth promoting microenvironment in the peri-lesional areas that lessens gradually with time [83, 84]. A number of pro-plasticity interventions have been investigated with some success that aim to extend and enhance the opening of this window of plasticity to maximize gains through the antagonism of growth-inhibitory molecules such as CSPGs and myelin associated proteins [85–89]. Though this type of naive recovery could certainly contribute to the functional improvements observed, some studies suggest that experience through rehab could greatly improve behavioral recovery - or is even a necessary requisite for the true remapping of the functions lost. For example, Nudo et al., 1996 [65] showed little to no native functional remapping of the monkey somatosensory representation of finger digits following a targeted injury, but a significant increase in post-injury remapped representation size when rehabilitative therapy was administered. This is somewhat different than the substantial spontaneous sensorimotor remapping observed in rodents, but again, some studies suggest such functional remapping may actually be reflective of compensatory behaviors rather than true behavioral recovery. Nishibe et al., 2010 [90] demonstrated this possibility quite elegantly using a targeted forelimb motor cortex focal injury, and followed spontaneous functional remapping and behavioral recovery over a period of weeks after the initial insult. Though the animals demonstrated significant behavioral improvements concurrent to the reappearance of the forelimb motor

representation, the authors subsequently demonstrated that the remapped forelimb representation was actually redistributed with an enlarged representation of the proximal limb while digit representation was reduced, suggesting the remapping reflected the development of compensatory motor mechanisms rather than true recovery of the original motor function. However, the true extent to which such compensatory plasticity contributes to behavioral recovery across a variety of species, sensorimotor modalities, and injury sizes remains unclear. Also important to note is that non-directed use of the paretic limb may also occur spontaneously to varying degrees during the weeks following the initial injury and may consequently drive some of the naive recovery observed - confounding the notion of truly spontaneous, non-experience-dependent post-injury plasticity.

1.1.3 Contralateral Crossing Fibers

One source of possible plasticity that was briefly discussed above involves the activation of the contralesional, intact hemisphere; though precisely how it influences functional recovery remains elusive. Its potential for involvement in the plastic remapping of the damaged sensorimotor function is clearly demonstrated by its dramatically increased responsitivity to ipsilateral somatosensory input within 30-50 minutes of stroke onset, that appears to be mediated through a network of uncrossed subcortical inputs [91]. A similar increase in the activity of the uninjured hemisphere in response to tasks involving the ipsilateral limb is observed in humans as well, especially in the subacute phase of the injury [58]. Multiple lines of evidence, however, suggest that its appearance likely signals poorer prognosis, either passively or as an active participant in aberrant, maladaptive plasticity. Evidence suggests that significant increases in contralesional activity in response to ipsilateral inputs correlate significantly with the size of the injury, and hence indicate substantially decreased sparing in the ipsilesional cortical networks where most gainful functional remapping is expected to occur [53]. As such, contralateral hemispheric involvement shortly after injury may simply be an indicator of lesion size and hence predict poorer recovery. Indeed, chronic hyperexcitability of the contralesional hemisphere is associated with worse behavioral outcomes [58, 92, 93] - further evidence compatible with the idea that enhanced contralateral cortical activity after injury signals not a

functional remapping response but rather the severe malfunctioning of the ipsilesional hemisphere. Interestingly, this response appears to be a uniquely induced by injury-mediated mechanisms, as pharmacological inhibition of the ispilateral cortex or thalamus fails to reproduce the same pattern of contralateral disinhibition [91]. It's important to note, however, that not all investigators report enhanced contralesional activity - [94], for example, demonstrates instead severely depressed spontaneous and sensation-induced neuronal responses in the contralesional homotopic areas that share direct axonal connections to the injured region. The precise mechanisms underlying such contrasting results are not yet understood. Yet the functional significance of contralesional homotopic activity to behavioral recovery appears negligible, as the contralateral hemisphere appears to demonstrate no meaningful functional remapping of the original (ipsilateral) sensorimotor representation [95]. Indeed, when chronic stroke patients receive intensive training on a motor task involving the use of their paretic hand, one of the most salient plastic changes that occur is a decrease in contralesional patterns of activation and a concomitant increase in perilesional activity [61], which suggests persistent contralesional responsitivity may actually represent a maladaptive pattern of activation, or at least a nonfunctional one.

Some people contend, however, that beyond its potential as an indicator of the extent of the damage to the perilesional cortex, enhanced activity in the contralesional hemisphere following stroke is in itself detrimental to recovery. This observation relates to the putative reciprocal transcallosal interhemispheric inhibition proposed to help mediate normal unilateral motor function via the suppression of mirror movements. Following stroke, the decreased inhibitory output from the damaged hemisphere is predicted to cause consequent disinhibition in the contralesional side, ultimately resulting in increased inhibition of the ipsilesional cortex. This idea has received considerable interest in human studies, where the phenomenon of interhemispheric inhibition was first demonstrated [96]. Imaging data in stroke patients shows, for example, increased contralesional inhibitory output immediately prior to movements of the paretic hand. In healthy controls, in contrast, there is significant attenuation of this interhemispheric inhibition prior to movement - a

salient difference, and one that significantly predicts behavioral recovery [97, 98]. Further evidence favoring the interhemispheric inhibition model is the functional improvements in movements of the affected hand gained following the rTMS-mediated inhibition of the contralesional cortex [99, 100]. These effects, however, have yet to be replicated in animal models of stroke.

Though this phenomenon of interhemispheric inhibition is thought to be mediated primarily by transcallosal fibers connecting contralateral homotopic brain areas [101], as mentioned above, injury also induces heightened innervation of the contralesional limbs from the contralesional cortex [77–79], though the functional relevance of this type of plasticity remains unclear. A number of studies, for example, report that increasing ipsilateral innervation of the paretic hand is negatively correlated to functional outcomes [102–104], while others show significant improvements in recovery following enhanced ipsilateral connectivity [79, 105]. The key mediator, it seems, may be stroke volume: it appears it is only is larger strokes that destroy a significant portion of the descending corticospinal tract originating in the ipsilesional cortex that enhanced innervation of the cortalesional spinal cord by contralesional motor neurons results in functional benefit. Indeed, within this context, the subsequent ablation of the contralateral cortex will serve to re-instate the original behavioral deficits that were partially recovered following the initial injury, demonstrating clearly the functional contributions of the contralesional cortex [106].

1.1.4 Myelin

Myelin is the lipid-rich, cocentric, compact wrapping formed by elongated oligodendrocyte processes in the CNS that ensheath axon segments and whose earliest identified function was to enable saltatory conduction of action potentials - a high-fidelity, energetically efficient method of electric signal propagation [107, 108]. With continued research, however, myelin's role has been greatly expanded and now subsumes other functions like providing trophic and metabolic support to axons, and is increasingly recognized as a form of learning-related plasticity via its ability to fine tune conduction speeds within higher order networks to alter information processing pathways [109, 110]. Myelin, as mentioned

above, is formed by oligodendrocytes (OLs) that differentiate from NG2+/PDGFR-a+ oligodendrocyte precusor cells (OPC); developmentally, this process occurs in tightly regulated spatial and temporal waves [111] and is regulated by a whole host of diverse signalling molecules [112, 113]. The regional specificity of various CNS OPC populations and their unique signalling mechanisms is being increasingly recognized [114, 115], and may signal an opportunity to be able to differentially target local OPC populations.

Once developmental myelination patterns are established, however, there is surprisingly little turnover amongst OLs - after age 5 in the human brain, about 0.3% [116]. Despite such stability, OLs continue to be generated from OPCs throughout life - indeed, as many as 30% of adult OLs are newly formed in the murine brain [117] - and actively participate in adult-stage myelin remodelling. A number of striking examples of such experience-dependent changes in myelination in adulthood were recently demonstrated in both animal and human studies. For example, prolonged social isolation in adult mice have been shown to result in fewer and thinner myelin sheaths, with no concomitant decrease in OL cells, and impaired cognition - deficits that are both reversed by social reintroduction [118]. Conversely, driving cortical activity using optogenetic stimulation of the premotor cortex of awake and behaving mice has been shown to increase OPC proliferation, subsequent oligodendrogenesis and drive both cortical and subcortical myelination [119]. The specific functional importance of such newly formed myelin was perhaps most convincingly demonstrated by McKenzie et al., 2014 [120], where a conditional ablation of myelin regulatory factor - a transciption factor necessary for OPC maturation - impaired the ability of mice to learn a new complex motor skill, despite the manipulation having no impact on existing myelination patterns. In humans as well, the acquisition of a new complex motor task, such as learning to play to piano or to juggle, has been associated with region-specific changes in white matter content [121, 122]. Such activity-driven changes in myelination may include thickening of the myelin sheath, or alterations in the number of myelin nodes or the shortening of internode length that can work to modulate signal conduction speeds [123]. This may be particularly important in controlling information processing in cortical networks, where large portions of axon seg-

ments are only intermittently myelinated, especially in more superficial layers - indeed, a myelin gradient can be reliably observed across the different cortical layers, despite similarities across their axonal and somas' diameters [124]. Though previous orthodoxy held that most of the cortical myelination observed enwraps excitatory axons targeting subcortical or distal cortical areas, recent work demonstrates that as much as 40% of myelin in layers 2/3 is targeted to inhibitory PV+ basket cells [125], and recent evidence suggests that myelination may indeed be differentially regulated by different neuronal subtypes [126].

This phenomenon of activity-dependent myelination is also borne out by in vitro studies which demonstrate the electrically silenced axons myelinate poorly [127], though the exact mechanism by which electrical activity induces the differentiation of OPC into myelinating OLs remains unclear. Vesicular release of glutamate from active axons, however, appears to play an important role and its blockade by tetanus toxin administration reduces the number of myelin sheaths formed [128]. Through which exact OPC and OL-expressed neurotransmitter channels the action of the released glutamate is mediated by is debated - with some authors demonstrating the importance of OPC-AMPAR channel activation in promoting the survival of differentiating OPCs [129], and others highlighting an OL-NMDAR dependent pathways for maintenance and adjustments to the myelin sheaths [130]; yet others suggest it's non-synaptic axono-glial junctions that underlie these effects [131]. Regardless of the exact mechanism, however, activity-dependent myelin plasticity is certainly an important form of adaptive cortical plasticity necessary for the acquisition and maintenance of complex behaviors.

In vitro studies also make abundantly clear the extent of the metabolic support provided to axon segments by the oligodendrocyte processes enwrapping them, primarily through a lactate shuttle system, such that when lactate transporters are blocked, ATP balance within axon segments is poorly maintained under normal working conditions [132]. Further evidence suggests that this metabolic support may be fine-tuned to the particular needs of the various axon segments a single OL enwraps, with highly active axons signalling through increased glutamatergic output to OL-NMDAR channels that

in turn result in increased OL-surface expression of glucose transporters to enhance their capacity for energy generation [133]. Without the metabolic support provided by its enwrapping myelin sheaths, axonal integrity is seriously compromised over the long term [134, 135], as is abundantly evident in various de- and dysmyelinating diseases such as multiple sclerosis, where progressive axonal degeneration is a classic feature of the disease pathophysiology [136].

Generally, however, remyelination following a demyelinating injury is robustly observed, though evidence indicates that early remyelination may be thinner with shorter internode length than normal [137, 138], however such morphological alterations may be only temporary [139]. Resident OPCs evenly distributed across the CNS continually monitor their local microenvironments and respond to various CNS insults - even ones not specifically targeting OLs - and participate in the remyelinating response, in concert with newly proliferating OPCs in the subventricular zone, than then migrate to the site of injury [140]. Though initial studies reported that OPCs may also differentiate into astrocytes as well as neurons [117, 141], recently a number of additional fate mapping studies has demonstrated that in vivo under homeostatic conditions, OPCs seem to give rise to exclusively to OLs [142, 143]. Despite their limited fate upon differentiation, OPCs themselves perform a number of integral functions in the adult CNS. For example, they respond to ongoing network activity by forming both pre and post-synaptic contacts across neuronal synapses and express receptors for both the major excitatotry and inhibitory neurotransmitters glutamate and GABA [144, 145]. In addition, the cleavage of their highly expressed surface proteoglycan NG2 appears to be activity dependent and functionally relevant to synaptic modulation as its blockade impairs long term potentiation [146]. They may also participate in the formation of the growth inhibitory glial scar [147, 148], and may help modulate the inflammatory response via the direct secretion of pro-inflammatory cytokines or signalling molecules to aid the recruitment of other immune cells [149]. They are also one of the initial generators of MMP-9, an enzyme that participates in the cleavage of extracellular matrix proteins, and therefore may also contribute to the opening of the blood brain barrier [150]. Driving OPC proliferation

after an injury with the goal of boosting myelination may therefore inadvertently impact a multitude of other post-injury mechanisms, and perhaps not all beneficial.

Indeed, boosting post-injury myelination in and of itself may serve to overall increase the growth retarding effects of myelin-associated proteins such as NoGo-A and OMgp. These proteins, along with MAG, have been long recognized to cause the collapse and retraction of regenerating adult CNS neuronal growth cones, as demonstrated both in vitro and in vivo [151–153] and would normally serve to stabilize established neuronal networks in the adult CNS. Though MAG is normally expressed only along the inner folds of the compact myelin sheath, and thus does not exert an inhibitory effect under conditions of normal myelination, following a CNS injury it's released from damaged myelin in its diffusable form, which exhibits very potent growth inhibitory activity even at sites distant to the original myelin damaging injury [154, 155]. The major signalling pathway mediating myelin's growth inhibitory effects has been studied extensively and involves the receptor complex NgR1-p75NTR-LINGO-1 which results in the downstream activation Rho-kinase [156, 157]; The specific characterization of this cascade has provided multiple potential points of intervention to alleviate myelin's growth retarding effect, many of which have been shown to boost axonal plasticity following a CNS injury (for a review see [158]). Others, however, have proposed a slightly more nuanced interpretation of the functional relevance of this myelin-mediated inhibition, contending instead that parallel myelinated tracts create a inhibitory-molecule lined tunnel insulated by growth-permissive astrocytic processes that serve to constrain the direction of travel of growth cones, making them bullet-shaped cones, thereby actually guiding and speeding up the process of neurite extension [159]. Indeed, myelin seems to support parallel but not perpendicular axonal growth [160, 161], and there is evidence for axonal regeneration in the adult CNS along myelinated tracts even in adult neurons [162]. However, these theories extend only to white matter tracts - in grey matter, myelin-induced collapse of neurite extension remains, making cortical pro-myelinating therapies following an injury potentially harmful to axonal plasticity and consequently, counterintuitively detrimental to functional recovery.

1.1.5 Myelin in Stroke

Abundant in vitro evidence demonstrates the exceptional vulnerability of OLs and particularly pre-OLs to hypoxic-ischemic injury. This vulnerability is conferred by their exceptionally high membrane-bound iron stores, which become mobilized following hypoxia [163] and fuel the generation of reactive oxygen species [164], which are particularly damaging to OLs due to their relative scarcity of reduced glutathione [33]. The high metabolic rate necessary for the proper maintenance of the large myelin sheaths further contributes to the increased generation of reactive oxygen species as a byproduct of mitochondrial ATP synthesis and renders OLs particularly sensitive to conditions of glucose deprivation [165]. OL cell bodies also primarily express the specific AMPAR subunits most permeable to Ca2+ influx upon activation by glutamate, predisposing OLs to excitotoxic injury [166], which is further amplified by additional Ca2+ influx mediated by OL-expressed P2X(7) ATP-channels [167]. The specific contribution of OL-expressed NMDAR channels, however, remains controversial, with some studies reporting significant neuroprotection and improved functional outcomes with an NMDAR allosteric modulator that preferentially partitions into OL membranes [168], and others demonstrating no effect or even poorer protection and recovery of axon function with NMDAR blockade, especially in aging white matter [169]. Lastly, microglial infiltration and activation in response to ischemic injury can also damage and even kill OLs and pre-OLs directly through the release of TNF-a [170], and may further exacerbate the apoptotic pathways outlined above via the increased release of glutamate and reactive oxygen species [171]. For a thorough review of this topic, refer to [172].

The dynamics of OL and myelin pathophysiology after ischemic stroke in vivo, in comparison, are far from resolved and may be highly dependent on the precise targeting, severity, developmental timing and mechanism of induction of the hypoxic-ischemic injury, as well as the precise cortical/subcortical location at which it is assessed. Multiple studies, for example, report a gradual and sustained increase in myelin-associated proteins PLP and MBP mRNA and immunostaining in peri-infarct areas following tMCAO, peaking around a week after the initial insult, suggesting minimal OL death and dam-

age in the peri-infarct regions that is well-compensated in the short term [173–175]. In contrast, other investigations show immediate deficits in myelin density in peri-infarct regions within days of MCAO ischemia [176–178], while others demonstrate a delayed decrease in MBP immunostaining that becomes increasing evident only after weeks have elapsed [179]. These technique, however, may fail to detect more subtle forms of OL dysfunction that seem to occur within hours of ischemia onset such as the OL accumulation of the microtubule-associated protein tau [180] or the unraveling, swelling, vacuolation and disorganization of the myelin sheath that is observed hours before the appearance of necrotic neurons and mirrors the pattern of enhanced OL sensitivity to ischemic damage observed in vitro [181].

The timeline of the recovery of myelin density is likewise quite variable across different studies: while some report a chronic myelin deficit 56 days after the initial MCA disruption [176] or even as far out as 12 weeks in the case of global ischemic injury [182], other observe robust peri-infarct recovery within 1-2 weeks after an initial MCAO-induced reduction [178]. Location-specific changes in myelin content have also been assessed, with one group showing a persistent decrease in Luxol Fast Blue staining in the striatum and internal capsule at 4 weeks, but intact myelin density at the corpus callosum and anterior commissure [183], and others reporting decreased Luxol Fast Blue staining precisely in the corpus callosum and anterior commissure, and actually enhanced myelin density in the caudoputamen and internal capsule at 3 and 10 days following MCAO [184]. McIver et al., 2010 [185] conducted an elegant investigation to map more precisely the timeline of tMCAO-induced changes in white matter OLs, where they utilized an MBP-promoter specific GFP-expressing lentivirus injected into the ipsilesional corpus callosum a week before ischemia to be able to longitudinally track changes to labelled OLs in vivo over the course of a week. Using this technique, they demonstrated severe fragmentation of both proximal and distal myelinating OL processes at 1 and 2 days after ischemia, as well as an overall reduced number of GFP+-OLs at 2 days. By 7 days post-stroke, however, both the number and process density of OLs were statistically equivalent to sham animals', demonstrating rapid and robust recovery of OL process extension in the peri-infarct area

following an initially severe dieback.

The timecourse of myelin changes has also been studied in deep white matter targeted small strokes induced by the vasoconstrictor ET-1, and, similar to what was observed using EM in MCAO, showed severe axonal and myelin damage within 24 hours of ischemia in the peri-infarct regions, and though much of the myelin debris here was phagocytosed over the course of the following week, significant myelin damage was still observed 7 days after the initial injury, even in areas of where axonal integrity was relatively preserved [186, 187]. Interestingly, MBP immunostaining showed instead a progressive decrease over the course of a week [188], though this discrepancy may be due to the specific locations imaged, as myelin damage in this stroke model actually shows gradual outward expansion over time [187]. Recently, a photothrombotic equivalent of the ET-1 small white matter stroke was developed and its consequent myelin damage characterized through the use of EM [189]. Here too, within hours of initial ischemia onset, nodular swelling and loosening of the myelin sheath was evident with a continued unpacked, whorled appearance of myelin for the first week following injury. From weeks one through three, myelin appearance began to normalize, but unmyelinated and thinly myelinated axons persisted even at the 3 week timepoint. Throughout this time axonal diameter was actually also increased, resulting in the particularly decreased g-ratios observed. These investigations clearly demonstrate substantial ongoing myelin pathology following even very small white matter ischemia, but whether such results translate to cortical myelination following similarly sized strokes remains to be seen. Indeed, with the remarkably variable timecourse and extent of myelin deficits observed in cortical region following MCAO, a precise characterization of cortical myelin changes following ischemia remain elusive.

In contrast, the functional benefits of improved post-ischemic myelination are well replicated across both human and animal studies. White matter hyperintensities on T2 weighted MRI images - a surrogate marker for myelin and axonal loss - are an important prognostic for functional recovery, including disability scores [190, 191], cognitive impairement [191, 192], verbal learning ability, memory impairements and deficits in

executive functioning [192, 193]. Similarly, gains in diffusion tensor imaging based fractional anisotrophy values - a proxy measure of microstructural white matter integrity - are strongly predictive of motor task learning in chronic stroke patients [194], and chronic hemispheric asymmetry in myelin water content is shown to be significantly associated with persistent deficits in upper limb function [195].

In animals models of ischemia, a number of pro-myelinating and myelin-protective therapeutics have likewise been demonstrated to improve post-stroke functional recovery. In tMCAO, for example, administration of cornel iridoid glycoside (CIG) from 6 hours on after ischemia onset was demonstrated to significantly alleviate myelin pathology as assessed in the corpus callosum 7 days post-stroke, as well as decrease GFAP and microglial activation, and concurrently improve motor, somatosensory and memory performance on a variety of behavioral tasks [196]. Similarly in global ischemia, the hypoglycemic agent metformin - which has been shown to readily cross the blood brain barrier and potentially improve brain energy metabolism and protect against inflammation [197] - was shown to significantly attenuate ischemia-hypoxia induced myelin deficits in the corpus callosum which translated to clear improvements in the open field task and Morris water maze [198]. In subcortical ET-1 strokes as well, transplantation of adipose derived mesenchymal stem cells into the stroke core 1 day after the initial injury resulted in a smaller lesioned area, less apoptotic cell death, enhanced axonal sprouting, improved markers of immunohistochemical markers of myelination and better DTI-visualized tract connectivity at 28 days after injury. At 7 days after the initial injury, the only significant alteration was enhanced MBP staining intensity, yet behavioral deficits were mitigated in some tests even 1 day after treatment [199]. A similar pattern emerged with subcortical ET-1 stroke followed by BDNF treatment, with improvements in histological myelin density and DTI-visualized tractography becoming apparent only at 28 days after the initial insult [200]. Here, however, the functional benefits of the treatment were likewise delayed until the 28 days timepoints. Interestingly, there was also a significant decrease in NoGo-A levels with BDNF treatment, despite an overall increase in myelination - the same direction of results as seen in [199], though there differences in NoGo-A levels

were not statistically significant. These studies strongly support the idea that boosting myelin recovery in the post-ischemic brain, particularly in white matter tissue, could be an important therapeutic target that may readily translate to tangible improvements in behavioral recovery.

1.1.6 Quetiapine

Though the mechanism of action of the atypical antipsychotic quetiapine was classically thought to be mediated via its antagonism at the D2 receptor [201] - similar to the mechanism of action of first generation antipsychotics - continued research has greatly expanded our understanding of the myriad of ways in which quetiapine plays a role in the regulation of the central nervous system. Though quetiapine is primarily used to treat schizophrenia, it is also FDA approved for use in bipolar disorder and as an adjunct therapy for major depressive disorder - though is considered effacious as a stand-alone therapy for MDD and generalized anxiety disorder as well [202]. Its receptor binding profile, as well as it's metabolite's (norquetiapine's), exhibits a complex pattern of partial binding affinity to a wide variety of ion channels, G-protein couples receptors and neurotransmitter transporters, most prominent of which are its H1 receptor antagonism, antagonism of the norepinephrine transporter [203], and its partial agonism of the 5-HT1A receptor [202]; yet it also shows some binding affinity to various adrenergic, muscarinic, dopaminergic and other serotonergic receptors [204].

In addition to its host of heteregenous effects at the classic neurotransmitter receptors and transporters, quetiapine is now recognized to be a fairly potent pro-myelinating agent. This effect is most well-replicated in the cuprizone-induced demyelination model, where it was first demonstrated that co-administration of quetiapine with cuprizone partially alleviates the curprizone-induced decrease of MBP+ labelling in the corpus callosum and cerebral cortex, and in addition increases the number of GST-pi positive cells in the corpus callosum [205]. This myelin protection was also shown to fully reverse the behavioral deficits commonly observed in curprizone-treated mice, such as spatial memory impairments on the Y-maze, increased anxiety in the open field test, deficits in prepulse inhibition, and decreased social interactions [206, 207]. In addition to preventing myelin

breakdown, quetiapine has also been shown to accelerate the remyelination that ensues over the month following the withdrawal of cuprizone - potentially through facilitating the differentiation of OPC to myelinating OLs, as shown by a faster recovery of MBP+ immunostaining and GST-pi cell density concomitant to an accelerated decrease of the initially 8-fold uptick of NG2+ cell densities. As before, these changes are accompanied by a parallel acceleration of behavioral recovery on the Y-maze task in quetiapine-treated animals [208]. Interestingly, quetiapine's effects seem to be confined to conditions of myelin-injury as sham animals treated with quetiapine consistently fail to show enhanced myelin densities. In line with what was observed in vivo, in vitro quetiapine has been shown to promote OPC differentiation into myelinating OLs [209], and to drive preferential NPC differentiation toward CNPase+ and MBP+ expressing cells and decrease differentiation toward GFAP+ expressing cells, in a dose-dependent manner, as well as dramatically enhance MBP+ expression in embryonic rat neocortical aggregate cultures [207]. It was also demonstrated to induce NPC mitogenesis though only in the presence of the growth factors FGF2 and EGFP. The specific mechanisms through which quetiapine exerts it's pro-myelinating effect, however, has remained elusive. For example, it's been shown to enhance phosphorylation of the ERK signalling pathway [207], and counteract the curprizone-induced downregulation of the Notch signalling pathway - antagonizing which seemed to ameriolate quetiapine's pro-myelinating effect [206]. It may also help boost the biosynthesis of cholesterol, resulting in enhanced OPC to OL differentiation [210].

In addition to its potential direct effects in OPCs, quetiapine also acts as an immunomodulator - in vitro it's been shown to decreased TNF-a and NO release from activated microglia [211], potentially through downregulation of STIM1 channels leading to decreased intracellular Ca2+ signalling and the prevention of the nuclear translocation of NK-kb p65 [212]. In vivo, chronic administration of quetiapine in APP/PS-1 double transgenic mice decreases microglial infiltration into the hippocampus [213], and in EAE (a mouse model of multiple sclerosis), quetiapine has been shown to significantly improve symptom severity potentially through the suppression of CD4(+)/CD8(+) T cell infiltra-

tion into the spinal cord, as well as through limiting local glial activation [214]. However, other authors have reported no significant alteration of microglial or astrocytic activity with quetiapine treatment following a demyelinating injury [208].

Besides its immunomodulating role, quetiapine may also help reduce oxidative stress via reducing the production of intracellular reactive oxygen species [215], and increasing the expression of SOD-1, as was shown in PC12 cells experiencing serum withdrawal [216]. This increase in SOD-1 specific activity was also observed in patients with schizophrenia being treated with quetiapine [217]. Growth factors are yet another potential pathway through which quetiapine may exert its effects - indeed, chronic quetiapine treatment in vivo reverses chronic-stress or NMDAR antagonism induced decreases in hippocampal and cortical BDNF and FGF-2 [218, 219], and in vitro counters the reduction of synaptic proteins synaptophysin, PSD-85 and BDNF that occurs with B27 media supplementation deprivation in hippocampal slices [220].

In PC12 cell cultures, quetiapine was also shown to downregulate p75NTR receptor expression [216] - a receptor markedly increased in a number of disease models, including ischemia, with the purported function of driving apoptosis upon neurotrophin binding [221, 222]. In addition, p75NTR has also been shown to bind directly to the Nogo receptor as well as to the ganglioside GT1b and thus form the signal transduction component of the receptor complex to the myelin-associated protein MAG, which results in the activation of Rho-kinase that works to ridify the cytoskeleton and prevent axonal elongation [223]. Quetiapine in turn then may help limit myelin's inhibitory effect on axonal plasticity.

The limited research that exists on quetiapine's effects in stroke are almost all centered on its potential neuroprotective effects in global cerebral ischemia. These studies reliably demonstrate that pre-treatment with quetiapine protects against ischemia-induced neuronal death in the hippocampus and the striatum, in addition to enhancing remyelination and reducing hippocampal GFAP reactivity [224–226]. Functionally, this translates to the attenuation of ischemia-induced memory impairments [225], and of heightened depressive and anxious behaviors [226]. Only one study thus far has investigated quetiapine's effects

in focal ischemia, where similar to its reported role in global ischemia, quetiapine was found to be neuroprotective, significantly reducing the number of TUNEL+ cells in the penumbra 3 days after the initial insult [227]. Interestingly, Bi et al., 2009 [228] reported that following global cerebral ischemia, pre-treatment with quetiapine was found to actually decrease hippocampal neurogenesis, potentially through the suppression of NF-kB p65/50 signalling - the same mechanism whereby quetiapine purportedly decreased microglial release of TNF-a and NO [212].

1.2 Aims of the Current Study

In this investigation, we aimed to assess the utility of a novel in vivo imaging technique called Spectral Confocal Reflectance Microscopy (SCORE), as first described by Schain, Hill & Grutzendler, 2014 [229], to track patterns of myelination following an ischemic injury. This label-free technique allows for the longitudinal tracking of single cortical myelinated fibers, mostly restricted to superficial cortical layers, but could prove very useful to precisely characterize the timecourse and spatial distribution of myelin density changes following a precise spatially delimited ischemic injury given that it could be used to follow myelination patterns over weeks within the same cortical regions of the same animals. Given the highly contradictory literature on the topic of post-stroke myelination outlined above, it could be a powerful tool to help resolve some of these discrepancies, help assess the efficacy of proposed pro-myelinating agents and study the functional role of myelination patterns in post-stroke recovery.

To this end, concurrent to longitudinally tracking post-stroke myelination changes using SCORE imaging, we also administered quetiapine to a subset of animals receiving ischemic injuries to evaluate whether the same type of pro-myelinating effect of quetiapine as was observed in various models of demyelinating injuries described above would translate to post-stroke cortical myelination recovery and to see whether SCORE imaging could resolve this potential pro-myelinating effect. In addition, we aimed to assess whether such an effect would result in a significant alteration in functional recovery following an ischemic injury, by targeting the ischemic injury specifically to the forelimb

somatosensory representation and utilizing intrinsic optical signal imaging, simultaneously to appraising SCORE-visualized cortical myelin densities, to track the changing patterns of cortical activation in response to both forelimb and hindlimb somatosensory stimuli over a period of weeks following the initial injury to assess the timecourse, spatial reorganization and extent of ongoing functional plasticity in both the quetiapine-treated and untreated post-stroke brain. Further, two additional behavioral tests were also consistently administered to assess changes in sensorimotor behavior after stroke, namely the cylinder test and the pole test.

In addition to tracking post-stroke changes in patterns of myelination using SCORE imaging, we also investigated the feasability of longitudinally tracking axons projecting or passing through the peri-infarct cortical areas that project transcallossaly from the homotopic contralesional cortex, visualized using eGFP expression, with the aim of assessing ongoing axonal injury in the peri-infarct cortex and evaluating the potential functional contributions of contralesional innervation of the peri-infarct cortex, given the complicated literature presented above about the functional role the contralesional cortex may play in supporting or hindering functional plasticity.

Chapter 2

Methods

2.1 Surgical Procedures

2.1.1 Animals

Data was acquired from 52 male and female C57BL/6 mice, aged 5-8 months, sequentially from 5 cohorts overall. Animals were housed in standard conditions, in group of two-five, maintained on a 12 hour light/dark cycle and fed ad libitum. All procedures followed guidelines set forth by the Canadian Council for Animal Care and were approved by the Health Sciences Animal Care & Use Committee at the University of Alberta.

2.1.2 Cranial Window Implantation and Cortical eGFP Injection

Cranial windows were constructed on all animals using previously described procedures with minor modifications [42, 230]. During the same procedure contralateral cortical eGFP injections were administered. Animals were placed in a clean, paper-towel lined anaesthesia induction chamber, with oxygen supplied at a 1000 ml/min flow rate and an isoflurane vaporizer on at 3%. Mice were monitored until recumbent and subsequently administered an intraperitoneal dexamethasone injection (0.2 mg/kg). They were then transferred to and secured in a stereotaxic frame, where a nosecone ensured continual isoflurane supply at 2% with oxygen:nitrous oxide flow rates at 700:300 mL/min. Body temperature was maintained at a constant 37 degrees Celsius using a rectal probe coupled to a thermal feedback regulator. Toe-pinch tests were performed immediately prior to surgery to ensure adequate anesthetic depth. Following a subcutaneous injection of

0.005 mL bupivacaine (2.5 mg/mL), the scalp was removed and a high-speed dental drill was used to roughen the skull surface and create 5-7 small dimples on either side of the sagittal suture for maximal glue adherence. A small hole through the cranial bone was drilled 1.9 mm to the left of the sagittal suture and 0.9 mm anterior to bregma, and 0.6 uL of the undiluted viral vector pAAV9.hSyn.eGFP.WPRE.bGH from UPenn Vector Core was injected using a Hamilton syringe. 0.3 uL was injected at a depth of 0.8 mm from the cortical surface at 0.1 uL/min, the syringe was left at that depth for 2 minutes then pulled out to a cortical depth of 0.3 mm where a further 0.3 uL was injected at 0.1 uL/min, with an additional 2 minute waiting period afterwards before the syringe was removed from the cortical surface. Vetbond was then applied to the small craniotomy as a sealant. The FL and HL sensory cortices to the right of the sagittal suture were located using stereotaxic coordinates: an oval centered 2.0 mm lateral to midline and 0.25 mm posterior to bregma with a rostral-caudal diamater of 3.5 mm and lateral diamater of 3.0 mm was first drawn onto the cranial surface, and the dental drill again used to thin the thus-delineated circular section of skull until transparent, whereby the bone fragment was removed using fine-tipped forceps. Leaving the dura intact, a circular 5 mm glass coverslip was secured over the craniotomy using dental cement and Vetbond glue, along with a custom-made lightweight aluminium headplate to make repeated imaging of the same cortical areas easier. Intracranial bleeds were controlled using gelfoam sponges, as needed. Following surgery, all mice received a subcutaneous injection of buprenorphine (3.25 mg/ kg) to control post-op pain. After anesthesia termination, mice were recovered at 1000 mL/min oxygen flow rate through the nosecone until a blink response was apparent, transferred to a paper-towel lined recovery cage with heating pad until fully conscious and finally returned to their home cages for a three week recovery period during which maximal viral expression occurred. Post-surgery, mice were monitored daily for changes in weight, movement and appearance for up to 1 week, and every 3 days thereafter. Note that cohort 1 - a total of 3 animals included in the final analysis (2 stroke and 1 sham) - also received an experimental ipsilesional intrathalamic injection of AAV1.CB7.CI.mCherry.WPRE.RBG viral vector from UPenn Vector Core, but given the technical difficulty and imprecise targeting observed, this procedure was no longer

applied in other cohorts going forward.

2.1.3 Photothrombotic Stroke

All photothrombosis procedures were carried out in accordance with procedures described by Watson et al., 1985 [15], immediately following the conclusion of the baseline image acquisition sessions. Animals were randomized to the sham condition or photothrombotic stroke condition at this time. The procedure itself was carried out as follows: Briefly, under 1.5% isoflurane aneasthesia (oxygen:nitrous oxide 800:200 mL/min) and still secured in a stereotaxic frame, mice were administered an intraperitoneal injection of Rose Bengal(RB) solution prepared immediately prior to injection at a concentration of 15 mg/mL in 0.9% saline and administerd to a final titration of 150 mg/kg. During the 5-minute waiting period for systemic RB distribution, the region of sensory cortex responsive to cFL stimulation (as delineated by IOS imaging collected during baseline data acquisition) was identified using surface vasculature and all other exposed brain regions covered with a small piece of black electrical tape. The cFL was then illuminated using collimated green laser light for 15 minutes. All animals received a subcutaneous injection of 0.05 mL buprenorphine immediately prior to aneasthesia termination, to aid recovery and control post-op pain. Sham stroke controls underwent the same procedure, with an injection of saline solution instead of Rose Bengal. Mice appearance, movement and weight were monitored daily for 1 week post-stroke.

2.1.4 Euthanasia and Brain Extraction

Animals were placed in a clean, paper-towel lined anaesthesia induction chamber, with oxygen supplied at a 1000 ml/min flow rate and an isoflurane vaporizer on at 5%. Mice were monitored until recumbent and subsequently administered an intraperitoneal injection of Euthanyl diluted 1:1 in 0.9% saline at a final concentration of 6.6 mL/kg. Once animals were deeply aneasthetized as assessed by the toe-pinch reflex, a V incision was made along their chest cavity, and a small gauge blunted needle tip connected via plastic tubing to a syringe filled with 0.9% saline was inserted into their left ventricle. An incision was made to the liver and 15 mL of saline flushed through their system at a rate of 3

mL/min, followed by a similarly administered 4% PFA circulatory system flush to a total volume of 30 mL of PFA. The head was subsequently removed and the brain carefully extracted from the skull cavity and placed in a light-sealed container in 4% PFA at 4 degrees Celsius for storage.

2.2 Image Acquisition and Analysis

2.2.1 IOS Image Acquisition

IOS images were collected in all animals using previously described procedures [43] with minor alterations. A Leica SP5 confocal microscope with x2.5 magnification lens (NA=0.07) coupled to a Dalsa 1M60 Pantera 12-bit camera with a depth of focus set to 250 microns below the cortical surface were used for IOS image capture. Pre-written scripts prescribing stimulus and data collection patterns were implemented using Spike2 and XCAP-standard version 2.2 imaging software and frame grabber (EPIX), respectively. Cortical illumination was achieved using red (wavelength = 635 nm) light-emitting diodes centered on the cranial window. Light source intensity, regulated by a DC power supply, was set to maximize the contrast between surface blood vessels and the cortex using visual inspection. At longer wavelengths, the dip in cortical reflectance is increasingly dominated by light scattering in the tissue, as caused by metabolic and electrical activity, which provides the tightest spatial correlation to regions of underlying neural activity and the least amount of blood vessel artifacts [231].

Anaesthesia induction and maintenance procedures followed those described in the section for chronic window implementation, except all imaging was conducted at 1.25% isoflurane saturation (with oxygen:nitrous oxide at 800:200 mL/min). Prior to each IOS session, an overview image of the surface vasculature was taken to visually evaluate blood vessel stability and remapping and to serve as a position-reference for subsequent SCORE imaging. These images were collected at an exposure time of 500 ms, using green light for cortical illumination.

Subsequently, IOS signals from the exposed somatosensory cortices at a depth focus of around 250 uM were collected concomitant to a regimen of alternating contralateral

hindlimb (cHL) and forelimb (cFL) stimulation, ensured using transistor-transistor logic. Vibrotactile stimuli at 100 Hz, lasting 1 second each, were played into piezo electrodes secured to either limb, with an interstimulus interval of 20 seconds to allow for complete metabolic relaxation [232]. Over the course of 40 trials per limb, IOS collection at a frame rate of 10 Hz lasted a total of 3 seconds per trial - 1 second before stimulus onset to create a baseline map, and 2 seconds during and post-stimulus to capture the peak of the reflectance change.

2.2.2 IOS Imaging Data Quantification

All IOS data analysis was carried out using custom-software coded in Python. Each frame within the full image stack containing the 31 frames obtained prior to and after the delivery of the vibrotactile stimulus were normalized to the average of the first 8 frames, and frames 10-26 (inclusive) were selected for further analysis - from hereon referred to as the response frames. This was done for each of the 40 trials per limb, with a small number of trials overall excluded based on the automated criterion that the average intensity across their response frames was $>$ or $<$ than the average plus or minus three times the standard deviation of the average intensity across all response frames of all trials for that animal at that imaging session. The non-excluded response frames from every trial were then averaged together. To obtain the maps of the cortical areas activated by the incoming somatosensory stimulus, the trial-averaged response frames were averaged together. The resulting image was enhanced using global histogram equalization and a tv-chamboille denoising algorithm. This image was then thresholded at top 20% of all pixel intensities, and a median filter with a disk size of 25 pixels was applied to obtain the final map. A mask to exclude everything outside a centered circular area with a 50-pixel wide border to the edge of the image was applied to restrict the analysis to the cranial window itself, and suprathreshold pixel groups less than 1000 pixels large were also excluded. The final suprathreshold areas obtained this way were then overlaid onto the overview images of the cranial windows collected at each imaging session and assessed along 3 major axis: visually, using the total number of suprathreshold pixels (somatosensory map size), and using the absolute coordinates for the center of mass of

each map image.

2.2.3 2-photon eGFP and SCORE Image Acquisition

2 photon imaging visualization of contralesionally injected eGFP expression in the ipsilesional peri-infarct cortex and SCORE imaging was carried out immediate after IOS image acquisition. Due to time-constraints, only two representative image stacks were collected per session - one proximal to infarct core on the cFL-cHL boundary, a region known to exhibit remapping of cFL activity after cFL targeted stroke, and one distal to injury at the opposite edge of the cHL functional map. Stack depths were set to capture the entire imageable region of the cortex expressing eGFP and the entire imageable depth at which SCORE-visible fibers could be resolved (i.e.: stacks ran from the meninges to complete darkness), spanning from 40 - 200 microns below the pial surface depending on image quality, capturing cortical layers I-II. Surface vasculature and distinct stable structural markers from the cranial window were used in combination for inter-session position-matching to allow for repeated data collection from the same cortical areas. eGFP stacks were collected first, with starting depth set to the first visible GFP-expressing fibers; SCORE stacks were subsequently collected at the same imaging locations with the same starting depths but usually more superior stack end depths. The same procedure was then repeated at the second imaging location.

All imaging stacks were collected using a Leica SP5 confocal microscope with water immersion lens (Leica 25x, NA=0.9), set to 1024x1024 xy pixel resolution at a zoom of 1x and 8-bit depth resolution. Line averaging was set to 2 and frame averaging to 4. Smart gain and negative noise were adjusted separately for each image using visual inspection to maximize image quality at stack midpoint, whereas z step-size was invariable set to 0.98 microns. For eGFP imaging, a tunable Coherent laser was set to 950 nm wavelenth, and photodetection was achieved using Leica's NDD HyD photodetector set to capture the wavelength range 525-560 nm. SCoRe imaging procedures followed closely that outlined in the original paper by [229]. Laser light at wavelengths of 458 nm, 576, 633 nm were used as the incident rays, whose reflectance pattern were collected using a pinhole diameter set at airy unit 1. Three separate PMT photodetectors set to capture light within a ± 5

nm wavelength band, centered around each of the four incident wavelength (i.e. for an incident ray of 576 nm, the corresponding photodetector will be set to range 571-581 nm).

2.2.4 eGFP+ Fiber Density and SCORE-imaged Fiber Density Quantification

All quantification of eGFP and SCORE image stacks was carried out using custom software written in Python. First both stacks were rotated in the z-direction using the same parameters to correct for the ultra bright meninges artefact seen in SCORE stacks, which results in significant aberrations in any analysis that involves intensity thresholding. Angles of rotation were calculated as follows: all images within a SCORE image stack were scaled by an absolute value such that the last 5 images of each stack had an average intensity of exactly 15. A mean filter with disk size 31 was then applied to each image, which were then thresholded with an absolute value of 70. Because above the bright meningeal artefact images were dark, any pixels across the entire stack that had suprathreshold pixels anywhere directly below it were re-coded as being suprathreshold themselves. The thus-obtained binary stacks were summed across the depth dimension and subsequently collapsed using maximum values across both the row and column dimension, thus obtaining 2 lists of 1024 values each reflecting the depth that the bright meninges were calculated to reach along each dimension of the image. Straight lines were fit across these values, and the rotation angles calculated as the arctangent of their slopes. These rotation angles were then applied to both the GFP and SCORE imaging stacks to obtain stacks with consistent depths relative to the meninges across the entire width and length of the images. The last image within the rotated SCORE stack that had meningeal artefact was then found and everything above it including itself were removed from further analysis in both the SCORE and GFP stacks. Further trimming was applied to remove any additional black spaces created around the imaging stack as a result these rotations.

Following this pre-processing, the SCORE stack was analyzed using the Meijering fiber filter algorithm found in the Skimage Python package with sigmas set at (1,3) and the

alpha parameter set at 10. This filter can be used to detect continuous edges such as those formed by a neurite. The filtered stack was then re-scaled to have a mean intensity value of 25 and 5 uM thick mean projections were created for the entire depth of the stack. A gaussian local threshold was applied to the mean projections with a block size of 55, and an offset of -3 and any objects containing less than 25 2-connected suprathreshold pixels were removed. A probabilistic hough-line transform was then applied to these images with a line length of 20 pixels and a permissible gap of 1 pixel - this was particularly important near the top of the stack because despite efforts described above, some minor meningeal bright artefact was commonly observed near the top of the stacks that was consistently identified as "fiberous" by the meijering filter, but did not have the characteristic long straight lines that are seen in true myelinated fibers. A custom filtering algorithm based on a number of exclusion criterion was then applied to each connected component of the binarized mean projections. Connected components that at any point were thicker than or equal to 10 pixels were excluded. Connected components that had overall fewer or an equal number of lines than their total number of pixels divided by 300 were excluded, unless the mean projection being considered was deeper than 20 uMs below the meningeal artefact and the particular connected component's overall length was at least 5 times greater than its overall width and its overall width was smaller than or equal to 10 pixels. This latter concession was necessary since lower throughout the stack of mean projections, fiber lengths became much shorter and thus consistently failed to meet the hough line based criterion and at such depths accidental mischaracterization of meningeal artefact as fibers was no longer an issue. The total number of suprathreshold pixels in the thus-filtered binarized mean projection stack was then calculated and was understood to reflect the total number of pixels within the original imaging stack that were deemed to be myelinated fibers.

After applying the same rotational preprocessing to the GFP stack as applied to the SCORE stack, 5 uM thick max projections were obtained from across the entire depth of the GFP stacks and used for all subsequent analyses. Two separate thresholds were calculated for each max projection and then multiplied together for the final binary image

of the GFP fibers. The first threshold used the intensity value of the 1% brightest pixels from the 10 darkest 25x25 pixel wide image regions as an absolute threshold for the entire image, the idea being that the darkest imaging regions will necessarily be the blood vessels running through the cortex that should contain absolutely no fibers but that this value itself would be more sensitive to small variations in background brightness across GFP stacks than a threshold set at an absolute value would be completely insensitive to. The second threshold applied to the stack of max projections was a local gaussian threshold within a block size of 55 and an offset of -3. In both binary images connected components with less than 10 pixels altogether were removed. The two binary images obtained this way were, as mentioned above, multiplied and again connected components with less than 25 pixels altogether were removed to filter out salt and pepper noise. Finally, a custom filter was applied similar to what was used in the SCORE analysis to exclude bright, blebby, non-fibrous objects that were suprathreshold across both intensity-based analyses. Each connected component was removed if it had more suprathreshold pixels than 50% of the total area of its convex full image and if additionally the its total length was smaller than 3 times its width. As before, the total number of suprathreshold pixels in the thus-filtered binarized max projection stack was then calculated and was understood to reflect the total number of pixels within the original imaging stack that were deemed to be GFP-expressing fibers.

In one last additional processing step, the 5 uM max projections from the rotated and trimmed GFP stacks were max projected across all depths, median filtered with a disk of size 30 and its intensity values rescaled for improved contrast across the image. These images were then binarized at a minimum intensity of 230 and all subthreshold pixels were taken to reflect either regions of the image subsumed by the infarct core or by blood vessels - a true tissue mask was thus created that excluded regions of the image that could not contain any GFP+ or SCORE fibers such as the infarct core and blood vessels. This tissue mask was consequently used as a mask across all images within the binarized SCORE and GFP stacks to calculate final values of myelinated fiber and GFP-expressing fiber densities by counting the total number of suptrathreshold pixels from the binarized

SCORE and GFP stacks against the total number of pixels from the tissue mask. The thus-obtained density measures then reflect the total number of fibers imageable at any timepoints within regions of the image where fibers are expected to appear.

2.2.5 Exclusion Criterion

Individual imaging timepoint were excluded from the final analysis based on the criterion that at that particular timepoint the animal had to have a complete dataset including behavioral data and imaging data from all three imaging modalities. In addition, animals whose windows had deteriorated and were consequently euthanized and their brains extracted prior to T28 were also excluded to avoid confounding the effects of stroke volume. Animals whose windows had deteriorated but whose brains were extracted at T28 were included in the analysis, but only at the timepoints where their windows had remained intact. Window deterioration was assessed at each imaging session based on the extent of the blurring observed particularly in the SCORE image stacks as compared to the images obtained at the previous imaging session and the baseline imaging session, and all timepoints going forward plus the timepoint where the noticeable degradation of the window was observed plus one timepoint sooner were excluded from further analysis.

2.3 Behavioral Testing

Two behavioral tests were administered prior to each imaging session. Animals were taken to behavioral rooms and allowed to acclimate for half an hour prior to testing. The pole test was consistently administered before the cylinder test.

2.3.1 Pole Test

The pole test was conducted similarly to how it was first described by Ogawa et al., 1985 [233] for use in assessing MPTP-injection related bradykinesia, but later adopted for use in evaluating post-stroke motor deficits [234]. Training on the pole task was done over a period of three days prior to the baseline data acquisition session. During each training and testing day, animals were placed in a clear large rectangular cage bottom with bedding, a playtube, and a 50 cm vertical wooden pole placed at the center of the

cage. Animals were allowed to acclimate within this setup for 3 minutes prior to the commencement of testing and rest for 1 minute between each trial. A total of 10 trials were administered per session, and each trial was video recorded and later scored by a blind observer. Within each session, the animal was grasped by their tail and placed nose-up at the top of the pole and allowed to climb down. During the first 5 training trial on the first day of training, animals were placed nose-down near the top of the pole to practice the climbing motion itself and familiarize themselves with the setup. Each trial was later scored as the distance it took for the mouse to complete their turn on their pole relative to the full height of the pole. If the animal failed to turn and instead slid down or backed down the full height of the pole, a score of 1 was assigned. If the animal climbed over the top of the pole instead of turning, that particular trial was immediately discarded and re-administered. Animals who failed to turn on average at or above 50% of the full height of the pole at baseline were excluded from all pole tests analyzes.

2.3.2 Cylinder Test

The cylinder test was administered similar to procedures described by Schaar, Brenneman and Savitz, 2010 [235] and Li et al., 2004 [236]. Animals were given a rest period of at least 15 minutes between their pole test session and cylinder test administration, then were placed inside a glass cylinder of diameter ∼10 cm placed on top of clear plexiglass plate with a videocamera placed below. Animals were kept inside the cylinder until they had performed 25 distinct rears against the side of the cylinder or for a period of 30 minutes, whichever came first. Each session was later video scored by a blind observer and the first paw to touch the glass at each instance of rearing behavior was recorded as Left, Right or Bilateral. Each rear was considered complete once both forelimbs touched the bottom of the cylinder again. Two baseline cylinder sessions were administered to better gauge pre-stroke spontaneous limb preference and averaged together to obtain a baseline score to which all subsequent timepoints were normalized.

2.4 Immunohistochemical Analysis

2.4.1 Slide Preparation

Following brain extraction and at least 3 days of PFA immersion, brains were transferred to a 30% sucrose solution for another 3 day period, after which they were cryoprotected using a thick coating of OCT solution that was gradual frozen in a dry-ice cooled isopentane solution and stored in -20 degrees Celsius for at least a day prior to sectioning. Brains were cryosectioned into 25 uM thin slices from +2.0 mm to -2.5 mm relative to bregma with 5 series created and every 2nd slice thrown within a series. Slides were stored at -20 Celsius until immunohistochemical processing, a summary of which is outlined briefly below.

Slides were allowed to warm to room temperature over a period of 20 minutes, and then washed three times with PBS-1x for 10 minutes each. 1 mL of 10% Universal Blocker solution in 90% PBS-Tx was placed on top of each slide for 1 hour and was then replaced by 1 mL of primary antibody solution that was left incubating overnight. The following morning two PBS-Tween washes for 10 minutes each were done, followed by another 10 minute wash with PBS-1x. Slides were then incubated with 1 mL of secondary antibody solution for exactly 1 hour, which was followed by two more 10 minute PBS-Tween washed and a final 10 minute PBS-1x wash. Following the final wash, slides were coverslipped using a DAPI fluorescent mount with clear nail polish applied around the sides of the slides as a sealant. All slides were stored in the cold room until imaging.

2.4.2 Antibody Solutions

Antibody solutions were prepared immediate prior to application with 2% Universal Blocker, 2% Bovine Serum Albumin, and 96% PBS-Tx. Goat anti-GFAP antibody was obtained from ABCAM (cat. no. AB53554) and diluted at 1:250; the paired secondary antibody for visualization was donkey anti-goat antibody conjugated to AlexaFluor-546 from ThermoFished Scientific (cat. no. A-11056) and diluted at 1:200. Rabbit anti-NeuN antibody was obtained from EMD Millipore (cat. no. ABN78) and diluted at 1:500; the paired secondary antibody for visualized was donkey anti-rabbit antibody conjugated to

AlexaFluor-647 from ThermoFished Scientific (cat. no. A-11056) and diluted at 1:200. Rat anti-MBP antibody was obtained from EMD Millipore (cat. no. MAB386) and diluted at 1:100; the paired secondary antibody for visualization was donkey anti-rat antibody conjugated to Dylight649 from ThermoFisher Scientific (cat. no. SA5-10029) diluted at 1:200. Goat anti-PDGFRalpha antibody was obtained from R&D Systems (cat. no. AF1062) and diluted at 1:100; the paired secondary antibody for visualized was donkey anti-goat antibody conjugated to AlexaFluor-546 from ThermoFished Scientific (cat. no. A-11056) and diluted at 1:200.

2.4.3 Slide Imaging

Stained slides were imaged using an inverted epifluorescent Leica microscope with 5x or 25x magnifications at resolutions of 1.83 uM/pixels or 0.4581 uM/pixels, respectively, using Leica's CFP, GFP, Y3 or Y5 filter cubes as appropriate. Ideal image acquisition parameters were determined on a few trial slides and thereafter utilized across imaging to maintain consistency for any subsequent intensity-based analysis. For the analysis of the stroke size, tile scans of the affected hemisphere were collected using a 5x magnification objective lens across every section where a stroke cavity was evident. For the analysis of the myelin-related immunomarkers assessed - namely MBP and PDGFR-alpha - three images were obtained from areas underneath the infarct core, three from regions medial to the infarct core and three from regions lateral to the infarct core using the 25x magnification objective lens. The data utilized in this analysis included all animals from the previous analyses, with the exclusion of animals from Cohort 1 who had received thalamic injection of mCherry whose emission spectrum significantly overlaps with Alexa Fluor 647's spectrum.

2.4.4 Stroke Characterization

Using NIH's FIJI program, a blind observer drew masks for each stroked section delineating the stroke cavity as assessed by a total absence of NeuN+ nuclei; these masks where then combined for each animal and transformed into volumetric data. In addition, the overview images of the cranial windows collected prior to IOS imaging at the T28 imaging

session were visually assessed to create a 2D maps of each stroke's final location relative to the hindlimb and forelimb somatosensory representations' locations obtained at the baseline imaging session to determine the percentage of the final infarct core's overlap with the original forelimb and hindlimb somatosensory representations. Since the position of the hindlimb somatosensory map is highly consistent across animals, these estimates were also used to obtain the absolute xy coordinate of the stroke core, which were then combined with the depth data obtained from the immunohistochemical analysis of the stroke cavity and projected onto brain atlases for better visualization using custom-code written in Python. In addition, these 2D stroke masks obtained from the cranial window overview images were used to assess the distance between each imaging site and the final infarct cavity, such that the final imaging site distance reported reflects the average of the smallest 50 distances between the further corner of the imaging site and the infarct cavity location nearest to this corner.

2.4.5 Quantificaiton of Myelin Markers

Cell counts for PDGFRalpha analysis and intensity measures for MBP analysis from each image were quantified using custom-made automated analysis in Python. Auto-thresholding was used to remove any portions of the image outside of the brain slice itself, and for the analysis of the MBP stain the mean intensity of the rest of the image was quantified. For the analysis of the PDGFRa+ cell densities, after the exclusion of the non-tissue parts of the image, the median of the remaining image was calculated and its value multiplied by 0.001 and used as a self-referential threshold for calculating the Laplachian of Gaussian of the image with a minimum sigma of 10 and a maximum sigma of 11 to identify blob-like features in the image. The blobs were then filtered, and any blob that was smaller than pixel size 20 or larger than pixel size 800 or had a major to minor axis ratio greater than 3 was excluded. Measures from underneath the infarct core were averaged together for each animal, as well as measures from areas lateral and medial to the stroke into one measure representative of superficial cortical layers.

2.5 Quetiapine Administration

Animals who had received a photothrombotic stroke were randomized to either a quetiapine treatment of a vehicle treatment after stroke administration. Quetiapine was mixed in with the drinking water starting immediately after the induction of the photothrombotic stroke. The desired target dosage was set at 10 mg/kg/day. Given that mice drink on average 250 ml/kg/day, quetiapine was mixed in with the drinking water at a concentration of 8 mg/200 mL. The quetiapine-dissolved drinking water was changed every 2 days for each cage to prevent the degradation of quetiapine.

2.6 Experimental Timeline

The timeline of the full experiment is summarized on fig. 2.1. The implantation of the cranial window along with the contralesional cortical injection of the eGFP-coding virus were carried out 21 days before the baseline imaging and behavioral testing session. 3 days prior to the baseline data acquisition, training on the pole task was conducted, and at 1 day prior to the baseline data acquisition an additional baseline session for the cylinder test was recorded. During baseline data acquisition, the pole test was administered first, followed by the cylinder test, IOS imaging, eGFP imaging and finally SCORE imaging. Immediate after animals were randomized to either receive a sham surgery or a photothrombotic stroke targeted to the IOS-delineated forelimb somatosensory representation. Upon recovery, animals who were given strokes were randomized to a quetiapine treatment or a vehicle treatment group and quetiapine administration was began immediately. The same set of procedures, excepting the administration of a photothrombotic stroke, were carried at each of days 2, 4, 7, 10, 14, 21 and 28 after the baseline session. Animals were euthanized on day 28 and their brain extracted and processed for immunohistochemical analysis as described above.

2.7 Statistical Analysis

All statistical analysis and graphs were generated using R, and are described in detail throughout the results section as the particular analysis applied across the various types of

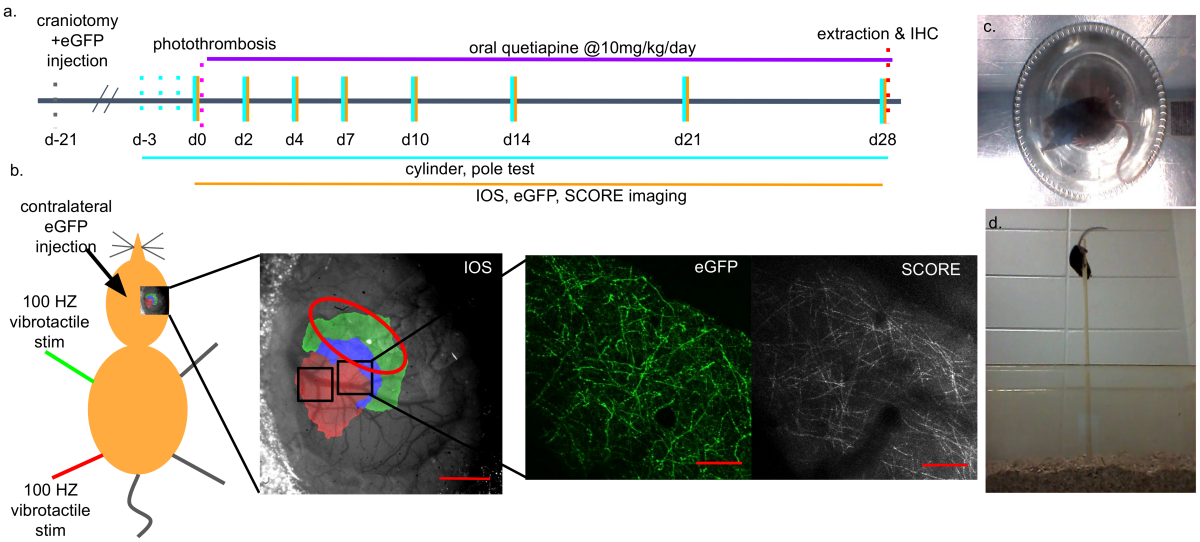

Figure 2.1: Panel (a) shows the experimental timeline employed in this study. Cranial window implantation and contralateral eGFP injection were done 3 weeks before baseline data collection, with behavior pre-training occurring for up to 3 days prior to the baseline session. Immediately following baseline data collection, photothrombotic stroke was administered and a subset of stroked animals started receiving quetiapine mixed in with their drinking water at a dosage of 10 mg/kg/day. Post-stroke data collection occurred on post-stroke days 2, 4, 7, 10, 14, 21 and 28, at which point brains were extracted and processed for immunohistochemical analysis of stroke volumes and myelin markers. The imaging modalities used in study are summarized in panel (b) and included intrinsic optical signal imaging of cortical activity following vibrotactile stimulus delivered to the fore or hindlimb from which maps of forelimb and hindlimb somatosensory representations were generated (scalebar = 1 mm). Photothrombotic stroke was specifically targeted to the IOS-delineated forelimb representation and two peri-lesional imaging sites were picked for the longitudinal imaging of GFP-expressing contralateral crossing fiber, and cortical myelinated fibers imaged using Spectral Confocal Reflectance Microscopy (SCORE) (scalebars = 100 uM). Two behavioral tests were also administered concurrent to each imaging session to track behavioral recovery, namely the cylinder test (c) and the pole test (d).

data were quite variable and better described in close proximity to their results. The main packages used included robustbase for robust mixed linear modelling, car for hypothesis testing following linear modelling, and ggpubr, lattice and ggeffects for graphing. All analysis included assumption testing that then guided the particular choice of statistical test applied. To control the false discovery rate at 0.10 across the entire study, Benjamini-Hochberg procedure was applied over all p-values communicated in this report.

Chapter 3

Results

3.1 Subject Dropout and Data Exclusions

Significant dropout was observed across all groups due to a variety of causes: 5 animals died due to difficulty breathing following prolonged, repeated isoflurane anaesthesia, 3 animals died due to misplaced IP injections, 2 animals were euthanized following the detachment of their headmounts, 4 animals were excluded due to spontaneous cortical damage, and 23 animals' windows deteriorated to differing extents at various timepoints throughout the 28 day imaging period. Overall, 5 sham, 5 stroke and 6 quetiapine animals had the full complement of data out of 52 animals that were originally included in the study, or about $\sim$31%. However, animals with only partial data across time were included in subsequent regression analyses, so long as their brains were extracted at T28 to avoid confounding the estimated effect of stroke volume. Accordingly, a total of 5 sham, 7 stroke and 8 quetiapine animals were included in all analysis.

3.2 Stroke Characteristics and Imaging Locations

Infarct size and location were quantified based on immunohistochemical staining of coronal sections collected 28 days after stroke (fig. 3.1, panel (b)). Based on visual assessment, infarct location was judged to be largely on-target - positioned primarily over the forelimb somatosensory cortex with comparable coverage across both the stroke and quetiapine groups (panel (a)). Stroke volumes between the groups did not differ (p=0.39, Wilcoxon test), suggesting quetiapine likely had no significant neuroprotective effect (panel (c)).

The percentage of the original forelimb and hindlimb somatosensory representations that overlapped with the final infarct at T28 were also quantified, and showed no significant differences across the treatment groups (p=0.50, Student's t-test (panel (d)) and p=0.77, Wilcoxon test (panel (e)), respectively). On average, around 45% of the forelimb map was stroked, compared to around 10% of the hindlimb map, indicating that indeed the stroke primarily targeted the forelimb somatosensory representation. The average distance from the stroke core to the two imaging locations that were assessed for their SCORE-imageable myelinated fiber and GFP+ contralateral crossing fiber content were likewise no different across treatment groups (p=0.92, Student's t-test (panel (f))) and averaged around 1000 uM from the stroke core.

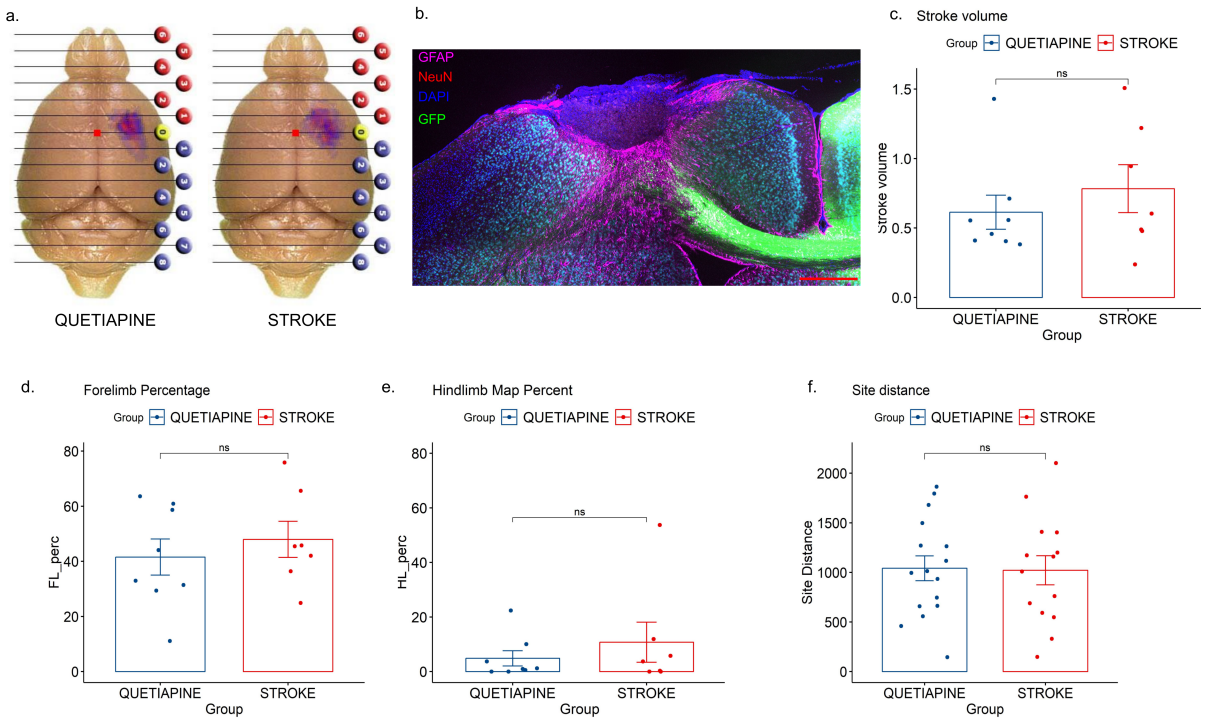

Figure 3.1: Stroke size and position were highly similar across treatment groups and located primarily within the forelimb somatosensory cortex (a). Stroke location and volume were determined based on stained coronal sections 28 days after the initial injury, at which timepoint the infarcts were characterized by a cavity absent any NeuN+ cells or contralateral crossing GFP+ fibers and surrounded by a highly immunoreactive GFAP+ border (b; scale bar = 500 uM). There was no significant difference in stroke volumes between the quetiapine and stroke groups (c) or between the percentages of the original forelimb (d) or hindlimb (e) representations that overlapped with the final infarct core, indicating that indeed the characteristics of the strokes received by the two treatment groups were highly similar. The average distance between the final infarct core and the specific imaging sites from where cortical myelin and contralateral fiber densities were assessed were also very similar across the treatment groups (f). All error bars SE.

3.3 GFP and SCORE Imaging

2-photon imaging of GFP-expressing fibers originating in the contralateral homotopic M1/FL-SS cortex and SCORE imaging of superficial cortical fibers to visualize and quantify myelination was assessed to be a feasible and reliable technique for the longitudinal tracking of these structures. In sham animals, the same imaging area could be identified across timepoints with relative ease, and even single myelinated or GFP-expressing fibers could be stably tracked across the 28 day span of the study fig. 3.2, panel (a)). Due to the initial edema and mass effect, as well as the extensive vascular remapping of the cortex following ischemic injury, the appearance of the imaging sites in the stroke animals (in both the untreated and quetiapine-treated groups) changed considerably with time, but the absolute position of the site itself was kept relatively consistent by referencing stable landmarks around the imaging windows.

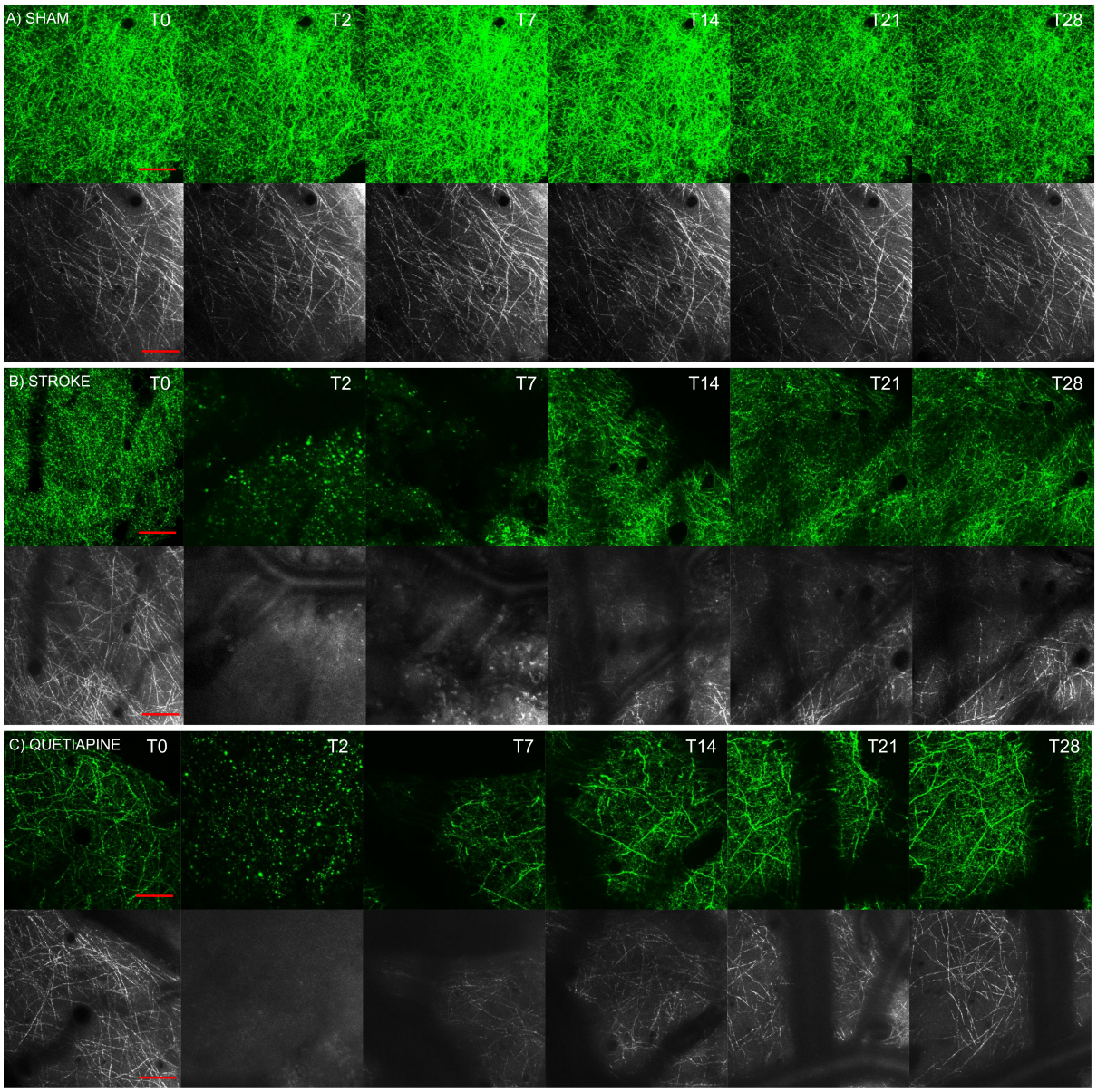

Figure 3.2: Sample images from sham, untreated naive stroke and quetiapine-treated stroke animals across various imaging timepoints collected near the infarct core, on average from $\sim$ 600 uMs away. Images show a 10 uM thick maximum projection from $\sim$ depth 40-50 uM below the cortical surface in the same animals collected from same imaging locations over a period of 28 days. In the sham animal (a), both the density and configuration of GFP+ and SCORE-imaged myelinated fibers remained stable throughout the imaging period, and individual fibers could be stably tracked. In both quetiapine-treated (c) and untreated stroke (b) animals, both GFP+ and SCORE-fibers were absent at 2 days after ischemic injury, with steady recovery in both types of fibers occurring over a period of weeks. Post-ischemic treatment with quetiapine appeared to accelerate the recovery of both GFP+ and myelinated fibers, and boost the overall extent of myelinated fiber recovery. Scalebar = 50 uM.

3.3.1 Visual Assessment

Overall, GFP and SCORE imaging revealed similar patterns of ischemia-induced injury and recovery to both contralateral crossing fibers and myelinated fibers, in both the near

and far imaging sites. In the near site specifically, whose average maximum distance to the stroke core was ∼600 uM, both GFP+ and SCORE-imaged fibers were virtually absent at 2 days post-injury in both treatment groups (fig. 3.2, panels (b) and (c)). GFP imaging at this timepoint instead showed only bright, blebbed structures. Recovery in both types of fibers occurred over the course of the following weeks, with a gradual increase in the number of GFP+ and myelinated fibers visible. Though the initial loss of fibers seemed comparable across treatment groups, the re-appearance of both types of fibers in the quetiapine-treated animals seemed to outpace their untreated counterparts, especially the quantity of SCORE-imageable myelinated fibers.

Images collected at the imaging site further from the ischemic core whose average maximum distance to the stroke core was ∼1400 uM, showed a similar trend in recovery; though here, the initial deficit observed 2 days after injury was generally not as severe, particularly in the quetiapine-treated animals' GFP+ fiber densities (fig. 3.3). Similarly, recovery of both SCORE-imaged and GFP+ fibers here seemed to precede and, in the case of myelinated fibers especially, exceed the quantity of recovered fibers imaged nearer the infarct core. Here again, the GFP+ fiber and SCORE-imaged myelinated fiber recovery in the quetiapine group seemed slightly accelerated as compared to the untreated group.

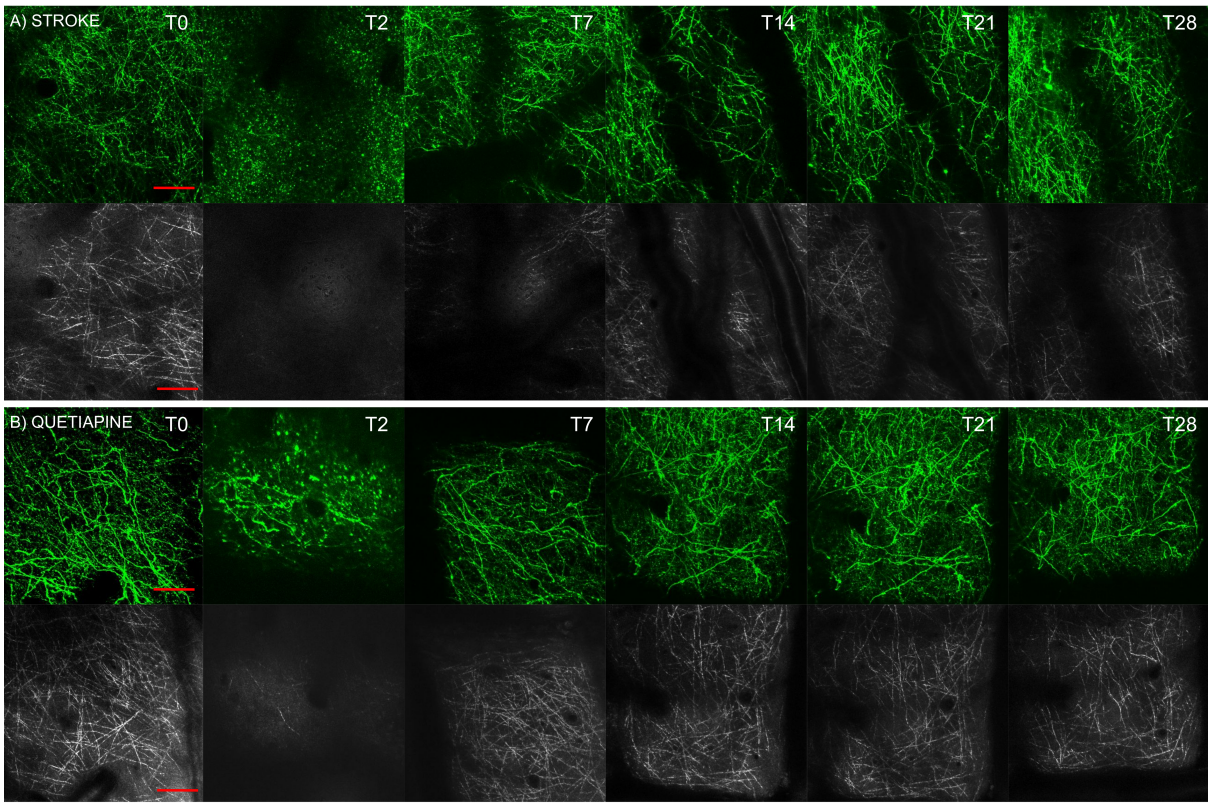

Figure 3.3: Sample images from untreated naive stroke and quetiapine-treated stroke animals across various imaging timepoints collected further away from the infarct core, on average from $\sim$ 1400 uMs away. Images show a 10 uM thick maximum projection from $\sim$ depth 40-50 uM below the cortical surface in the same animals collected from same imaging locations over a period of 28 days. There was a substantial reduction in both GFP+ and SCORE-imageable myelinated fiber densities 2 days after the ischemic injury in both naive stroke (a) and quetiapine-treated (b) stroke animals, with significant recovery occurring along both parameteres in the following week. This recovery again seemed slightly accelerated in quetiapine-treated animals as compared to their untreated counterparts. Scalebar = 50 uM.

In the subset of cases where a particular tissue location could be consistently tracked across time - at imaging sites further from the ischemic core - the vast majority of myelinated fibers that reappeared at later timepoints could be reliably identified as the same fibers imaged at baseline that disappeared at earlier timepoints. The pace of recovery across the individual fibers, however, was not uniform, with some fibers re-appearing earlier than others (fig. 3.4 panel (b)). Amongst the GFP+ fibers, the re-appearance of fibers appeared slightly more dynamic with only some of the fibers imaged at baseline re-appearing after the initial blebbing observed at earlier timepoints (fig. 3.4 panel (a)), and many new fibers appearing over time. Often these the newly appearing fibers were thicker and brighter than the original fibers, who were also sometimes more blebby in appearance - this is particularly evident in fig. 3.3 panel (a). Because specific tissue loca-

tions could not be reliably identified nearer to the infarct core, whether SCORE-imaged myelin recovery occurred on the same fibers as were imaged at baseline could not be determined. However, once the newly established vascularization pattern stabilized and tissue location could be consistently identified, newly appearing fibers were largely stable across imaging timepoints, particularly in SCORE-imageable myelinated fibers (data not shown). Interestingly, the GFP-labelled contralateral crossing fibers did not appear to overlap with the SCORE-imageable myelinated fibers, at any of the timepoints observed (fig. 3.4 panel (c)).

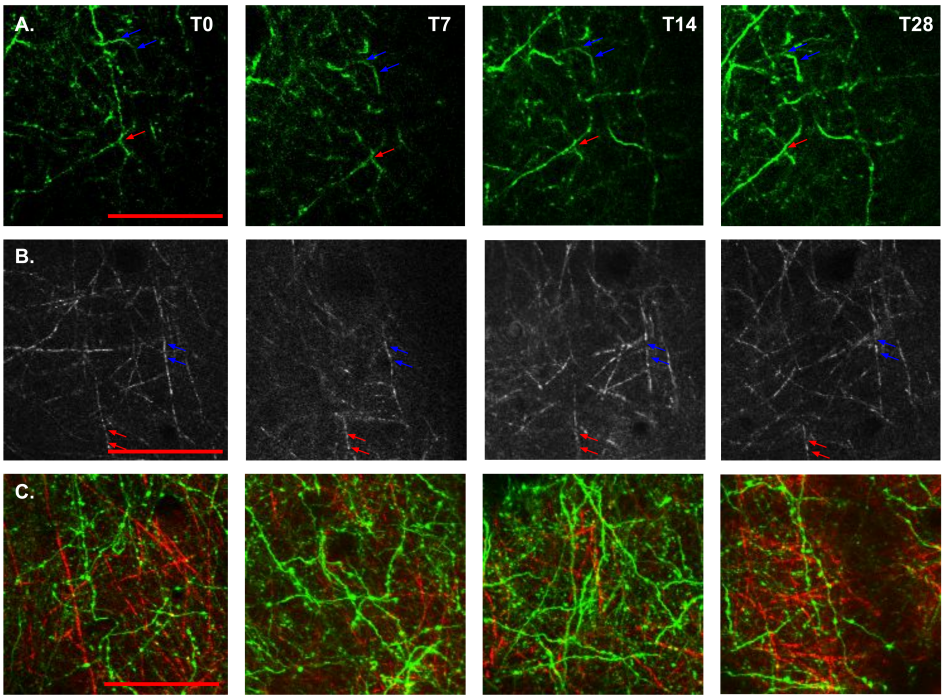

Figure 3.4: In areas of the cortex where vasculature stayed relatively stable after stroke (∼1500 uM from the ischemic core), the same set of fibers as were visible at baseline often reappeared - as indicated by blue and red arrows. Across the SCORE-visible myelinated fibers, the timeline of this gradual reappearance was quite variable across the specific fibers (panel (b)), whereas in the GFP-expressing crossing contralateral fibers, this process appears slightly more dynamic, with a few new fibers being formed and old ones never reappearing (panel (a)). Once a new fiber became visible, however, it invariably remained stable throughout the rest of the imaging sessions. Panel (c) shows the co-localization of the GFP-expressing fibers and the SCORE-imaged myelinated fibers - at no timepoint did there appear to be any significant colocalization of these two fiber types. Scalebar = 50 uM.

3.3.2 Quantification

Upon quantification, the stability of both imaging techniques was evident, with the sham groups showing little overall movement in their fiber density scores. As it was observed visually, the quantification also demonstrated that ischemic stroke itself (whether treated

with quetiapine or untreated) significantly decrease fiber density in both contralateral crossing and cortical myelinated fibers. Though pattern of results in injury-induced deficit and recovery of the myelinated fibers imaged via SCORE showed a similar trend to the recovery of GFP fibers, both the magnitude and pace of recovery in these types of fibers appeared less (see fig. 3.5 panel (a)). Though this was true for both treatment groups, this deficit was much more pronounced in the untreated, stroke-only group. Here, myelinated fibers failed to recover to baseline levels throughout the 28 day period of the study, reaching a peak of around 45% of their pre-stroke levels. This was in comparison to the quetiapine treated animals, whose myelin density on average recovered to levels close to sham animals' by T10. Indeed, in both treatment groups, most of the recovery occurred in the first 10 days after the initial ischemic insult. Quetiapine's effect on the post-stroke myelin recovery then is best characterized as increasing both the rate and extent of SCORE-imaged myelin reappearance.

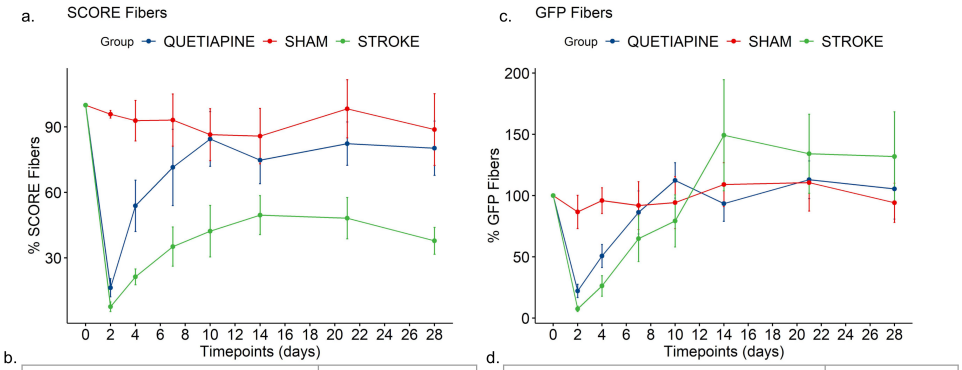

b.

SCORE	p
Treatment	1.008e-09*
Treatment*Time	0.163
Treatment*Site distance	0.039*

d.

GFP	p
Treatment	0.00012*
Treatment*Time	0.717
Treatment*Site distance	0.981

Figure 3.5: Quantification results of GFP+ and SCORE fiber densities, normalized to each animal's own baseline measurements. Data from both imaging sites were pooled for this analysis. Ischemia produces a substantial decrease in myelinated fibers density, followed by a period of recovery particularly concentrated in the first 2 weeks after the initial injury; though in the untreated animals a substantial persistent myelin density deficit is observed even 4 weeks after the initial injury, which is significantly alleviated by quetiapine treatment (a). Stroke produces a similarly significant decrease in GFP+ fiber densities at T2 after the initial injury, though slightly less so in the quetiapine-treated animals, who also show consistently slightly greater GFP+ fiber densities until around T10-T14, from when on robust recovery to control-levels is evident in both treatment groups (c). A robust mixed linear regression model was fit to the quetiapie+stroke and stroke only groups in both datasets and Wald Chi Square tests were conducted to evaluate the effect of treatment with quetiapine. The relevant results of the Wald Chi Square tests in the SCORE-imaged myelinated fiber data is summarized in panel (b) and shows a significant main effect of quetiapine treatment that interacts significantly with site distance, such that with increasing site distance, the effect of treatment reduced - indicating that the most severe deficit in untreated animals occurred near the infarct core in comparison to the quetiapine-treated animals. The relevant results of the Wald Chi Square tests in the GFP+ fiber data is summarized in panel (d) and shows a significant main effect of quetiapine treatment - indicating treatment with quetiapine enhanced GFP+ fiber densities. All scalebars SE.

The treatment's effect of GFP+ fiber density was, in comparison, less pronounced (see fig. 3.5 panel (c)). Though a significant initial deficit in GFP+ fibers was observed at 2 days post-stroke in both groups, this initial decrease in contralateral crossing fibers appeared slightly less with quetiapine treatment. Because the rate of the GFP+ fiber recovery was very similar across both treatment groups, this small difference persisted during the timeperiod through which most of the GFP+ fiber density recovery was occurring - or until around T10-T14. Beyond this timepoint, GFP+ fiber density in both treatment groups was, on average, equal to that seen in the SHAM group. Occasionally, GFP+ fiber densities in animals with ischemic insults surpassed their pre-injury levels - this was likely due to the effect noted earlier whereby initially faint and blebby GFP-labelled fibers sometimes became thicker and bolder following ischemia. Overall,

quetiapine's effect on GFP+ fiber recovery is best characterized as either slightly accelerating the reappearance of crossing fibers during the initial period of recovery or perhaps slightly ameliorating the initial injury-induced deficit in these types of fibers, with both treatment groups eventually showing similarly complete reappearance of GFP-labelled contralateral crossing fibers.

3.3.3 Statistical Analysis

To statistically evaluate differences across the treatment groups in the recovery of GFP+ and SCORE-imaged fiber densities, a robust mixed linear model was fitted to data obtained from the stroke and stroke+quetiapine groups, which specified imaging site distance, as well as stroke volume, and their interactions with each other and time as covariates of the model in order to control for any potential effect systematic difference in these parameters might have had on the aggregate group data. Based on preliminary observations of the data, the interaction between quetiapine and site distance was also estimated, and visualized. The model fitted was

$$Fibers = Treatment + Time + Site\ distance + Stroke\ volume + Treatment : Time +$$
$$Treatment : Site\ distance + Time : Site\ distance + Time : Stroke\ volume +$$
$$Site\ distance : Stroke\ volume + 1|subject.$$

Wald Chi-Squared Tests were then used to assess the significance of each fixed effect in the fitted model. The results from for the SCORE fiber density data are summarized in the table below.

	Df	Chisq	Pr(>Chisq)	BH adj. sig.
Treatment	1	37.31	0.0000	*
Time	1	49.67	0.0000	*
Site distance	1	87.44	0.0000	*
Stroke volume	1	28.28	0.0000	*
Treatment:Time	1	1.95	0.1626	ns
Treatment:Site distance	1	4.26	0.0391	*
Time:Site distance	1	0.16	0.6879	ns
Time:Stroke volume	1	0.20	0.6586	ns
Site distance:Stroke volume	1	0.02	0.8750	ns

Table 3.1: Wald Chi Square Test of fixed effects predicting SCORE fiber density.

These results provide strong evidence that quetiapine enhances SCORE-imageable myelinated fiber recovery, boosting the extent of overall myelin density - yet this treatment effect appears to interact significantly with the imaging site distance, with the quetiapine's pro-myelinating effect waning with increasing imaging site distance.. Time, stroke volume and site distance are all evaluated to be significant predictors as well, but they do not appear to significantly modulate each other's effects. Estimates for the mean effects of each of these parameters were obtained from the models, with all other variables held at their mean values. The estimates are as follows:

- For every increase of 1 mm^3 in stroke volume, fiber percentage changes by **-11.08%**.
- For every increase of 1 mm in imaging site distance from the infarct core in the quetiapine-treated animals fiber percentage changes by **+9.21%** and in the untreated animals by **+20.01%**.
- For every increase of 1 day in time in the quetiapine-treated animals fiber percentage changes by **+1.09%** and in the untreated animals by **+0.65%**.
- The overall average SCORE fiber density in the quetiapine-treated animals is estimated to be **+90.11%** and in the untreated animals to be **+56.82%**.

These estimates demonstrate that, as expected, with increasing stroke volume the per-

centage of SCORE-imageable fiber densities decreases - this is the opposite pattern to that seen with increasing imaging site distance and timepoints, though as mentioned above, the effect of site distance is significantly greater in the untreated animals as compared to the quetiapine-treated animals. This difference is driven by a substantially lower SCORE fiber density in the untreated animals closer to the stroke core as compared to the treated animals, with both groups showing comparable SCORE fiber densities across later timepoints at imaging sites further from the ischemic core (∼1500 uM). Conversely, quetiapine-treated animals are estimated to have slightly faster recovery in their myelinated fiber densities, though this difference is not significant. Indeed, even 1 month after the initial injury, the SCORE-imaged myelinated fiber density in the untreated animals has recovered only to ∼57% of their pre-ischemic levels, whereas with quetiapine treatment this value jumps to ∼90%.

The same set of tests were conduced on the GFP+ fiber density data; the results of the Wald Chi-Squared Tests on the relevant fixed effects across both timespans are summarized in the tables below.

	Df	Chisq	Pr(>Chisq)	BH adj. sig.
Treatment	1	14.80	0.0001	*
Time	1	75.18	0.0000	*
Site distance	1	62.54	0.0000	*
Stroke volume	1	8.12	0.0044	*
Treatment:Time	1	0.13	0.7168	ns
Treatment:Site distance	1	0.00	0.9809	ns
Time:Site distance	1	0.11	0.7394	ns
Time:Stroke volume	1	1.04	0.3074	ns
Site distance:Stroke volume	1	3.05	0.0808	ns

Table 3.2: Wald Chi Square Test of fixed effects predicting GFP+ fiber density.

The results suggest that quetiapine treatment had a significant positive effect on GFP+ fibers as well, in addition to its significant pro-myelinating effect, though the specific characteristic of its boosting effect here are slightly different than its effects on SCORE-

imageable myelinated fiber densities. For example, though as before time, site distance and stroke volume are all significant predictors of GFP+ fiber density in contrast to their interactions which are not, here, site distance does not appear to significantly modulate quetiapine's effects on GFP+ fiber densities. To better highlight this point, estimates for the mean effects of each of these parameters were obtained from the models, with all other variables held at their mean values. The estimates are as follows:

- For every increase of 1 mm^3 in stroke volume, fiber percentage changes by **-3.15%**.
- For every increase of 1 mm in imaging site distance from the infarct core in the quetiapine-treated animals fiber percentage changes by **+14.28%** and in the untreated animals by **+14.44%**.
- For every increase of 1 day in time in the quetiapine-treated animals fiber percentage changes by **+1.58%** and in the untreated animals by **+1.82%**.
- The overall average GFP fiber density in the quetiapine-treated animals is estimated to be **+130.38%** and in the untreated animals to be **+113.09%**.

In contrast to the SCORE data, here the effect of increasing stroke volume, though still significant, was estimated to be much smaller, indicating perhaps that myelinated fiber density is more sensitive to increasing injury size than the density of contralateral crossing fibers. As mentioned above, the effect of imaging site distance was very similar across the two treatment groups and estimated to be around the same as the average across the two treatment groups in the SCORE data. Interestingly, untreated animals appeared to have a slightly accelerated GFP+ fiber density recovery as compared to the treated animals, though this difference was not evaluated to be statistically significant, but nevertheless suggests perhaps some early neuroprotection of GFP+ fibers induced by quetiapine treatment, that could theoretically drive the main effect of quetiapine observed. Indeed, by the last imaging timepoint a month from the initial injury both treated and untreated groups are predicted to have recovered their contralateral crossing fiber densities completely, though again, quetiapine treated animals to a slightly greater extent than their untreated counterparts. This is quite different than the pattern that

emerged in the SCORE-imaged myelinated fiber density data, where neither group showed to-baseline levels of myelinated fiber recovery, though quetiapine-treated animals came near.

To better visualize the exact pattern of SCORE and GFP+ fiber density recovery in the naive stroke and quetiapine-treated groups, the fitted robust mixed linear models specified above were mapped onto heatmaps illustrating the estimated models at range of timepoints and site distances, shown in fig. 3.6 - all estimates were made with the stroke volume held near its average at 0.6 mm^3. These diagrams demonstrate clearly tendency in both treatment groups of increasing SCORE and GFP+ fiber densities with increasing time and imaging site distances from the infarct core as described above. The effect of quetiapine treatment is also clear, though its pattern varies across the CNS structural components imaged. In fig. 3.6 panel (a), for example, post-ischemic treatment with quetiapine appears to induce a more robust and earlier re-appearance of SCORE-visible myelinated fibers across all imaging sites, but the most evident gap in myelination emerges at imaging sites nearer the stroke core, where untreated naive stroke animals demonstrate a persistent deficit in myelin density as opposed to quetiapine-treated animals who even here show close to baseline levels of myelin density at the latest timepoints considered. In contrast, in the GFP+ data, visualized in fig. 3.6 panel (b), no such difference across site distances in the two treatment groups are observed. Indeed, both groups show very similar trends of recovery across time and imaging site distance, though quetiapine animals appear to generally have more GFP-expressing contralateral crossing fibers as compared untreated animals. To underscore this differing pattern seen across the SCORE and GFP+ fiber densities in the treatment groups, the ratio of predicted SCORE:GFP+ fiber density was calculated across all timepoints and site distances previously visualized in both groups. The results are shown in fig. 3.6 panel (c), and well-illustrate the divergent pattern of SCORE:GFP+ fiber density ratios across the two treatment groups. Though both groups show a persistent myelin density deficit as compared to GFP+ fiber densities, with quetiapine treatment this deficit is evaluated to be quite small and extremely stable across all imaging sites and timepoints evaluated. Without quetiapine

treatment, conversely, myelin density is significantly lower than GFP+ fiber density, particularly when evaluating fiber densities at imaging sites nearer the stroke core, again, illustrating a sizeable lag in the recovery of myelinated fibers following ischemic injury in the immediate vicinity of the stroke core when calculated in relation to the rate of recovery of contralateral homotopic transcallosal fibers - a deficit that is alleviated by treatment with quetiapine.

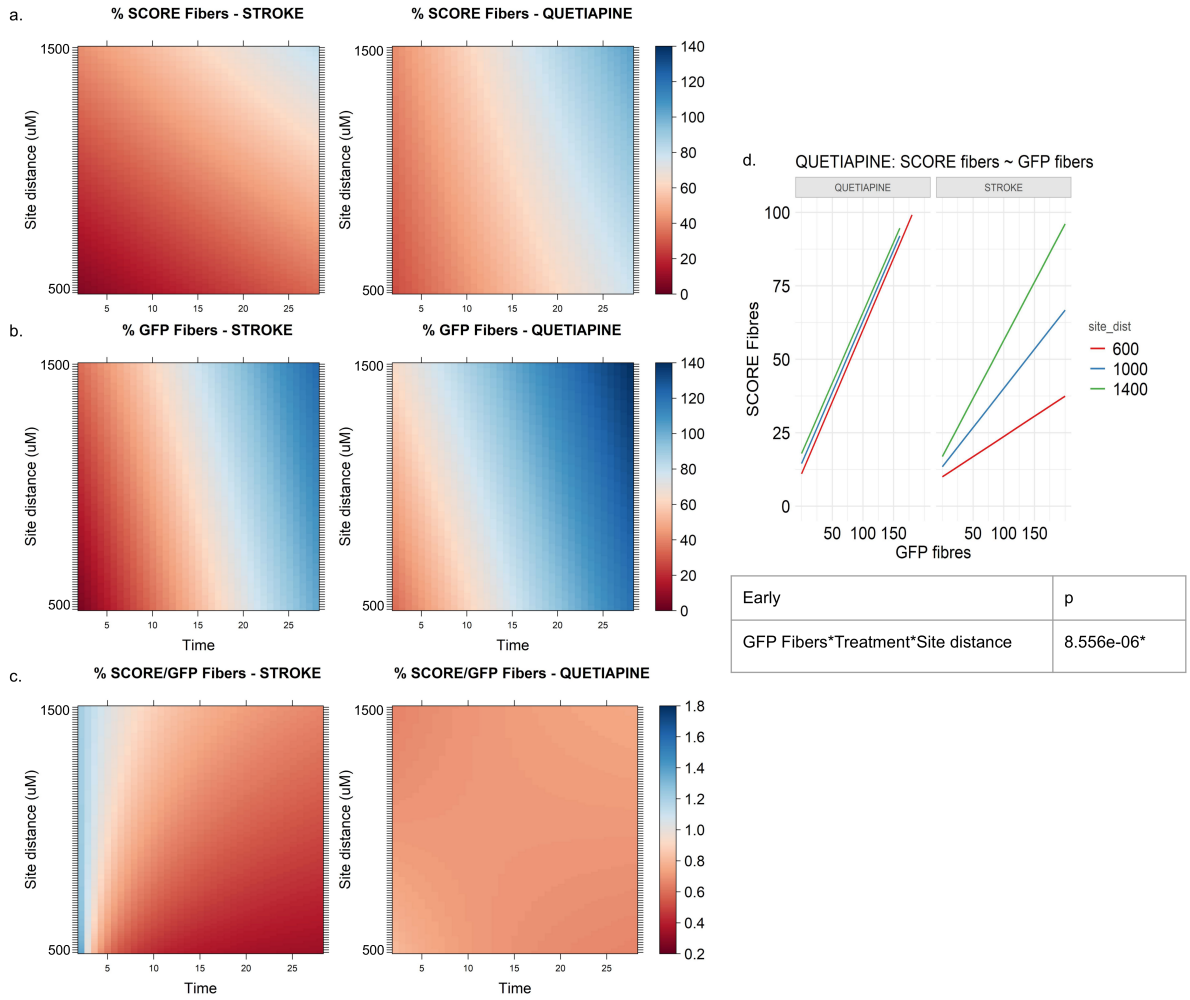

Early	p
GFP Fibers*Treatment*Site distance	8.556e-06*

Figure 3.6: The mixed linear models fit to the SCORE and GFP datasets from the quetiapine-treated and untreated animals are visualized in panels (a) and (b), respectively and demonstrate how fiber densities changed across time in the two treatment groups at various imaging site distances from the ischemic core. In the SCORE data (a), quetiapine's pro-myelinating effect is evident across all timepoints and particularly at imaging sites near the infarct core, where untreated animals show a persistent myelin density deficit even at 4 weeks post-stroke. In the GFP+ data (b), quetiapine more strongly seems to alleviate the initial deficit in GFP+ fiber densities observed, with both treated and untreated groups projected to have robust fiber density recovery occurring across all imaging sites by around 2-3 weeks post-stroke. Given that quetiapine appeared to boost both GFP+ and SCORE-imaged fiber densities, we wanted to evaluate how the size of each of these effects compared and how the relationship between GFP+ fiber densities and SCORE-imaged myelinated fiber densities changed with treatment with quetiapine. As such, panel (c) visualizes the ratio of SCORE-fiber densities to GFP+ fiber densities across both treatment groups. It shows that though both treated and untreated groups are predicted to have consistently less baseline-normalized SCORE fiber densities than baseline-normalized GFP fiber densities, this deficit in myelinated fibers is particularly large in the untreated group at later timepoint and at imaging sites nearer the infarct core. To statistically evaluate this observed trend, another robust mixed linear regression model was fit, that specified GFP+ fiber density as the predictor and SCORE fiber density as the predicted variable, the predictions of this model are summarized visually in panel (d) and statistically in panel (e) and bear out the relationship described above that indicates that though quetiapine treatment increased both GFP+ and SCORE-myelinated fiber densities, its most significant effect was increasing myelinated fiber density near the stroke core.

To further investigate this relationship between GFP+ contralateral crossing fiber

density and SCORE-imaged myelinated fiber density, the robust mixed linear regression model

$$SCORE\ density = Treatment + GFP\ density + Site\ distance + Stroke\ volume +$$
$$GFP\ density : Site\ distance + GFP\ density : Stroke\ volume +$$
$$Treatment : GFP\ density : Site\ distance + 1|subject$$

was fit across all timepoints. The predicted model is visualized in fig. 3.6 panels (d) - all estimates were made with the stroke volume held near its average at 0.6 mm^3. The Wald Chi Square tests are summarized in the table below.

	Df	Chisq	Pr(>Chisq)	BH adj. sig.
Treatment	1	20.25	0.0000	*
GFP density	1	166.43	0.0000	*
Site distance	1	78.30	0.0000	*
Stroke volume	1	33.41	0.0000	*
Group:GFP density	1	3.11	0.0776	ns
GFP density:Site distance	1	30.31	0.0000	*
GFP density:Stroke volume	1	2.14	0.1437	ns
Treatment:GFP density:Site distance	1	20.42	0.0000	*

Table 3.3: Wald Chi Square Test of the relevant fixed effects evaluating SCORE fiber density as a function of GFP+ fiber density.

Interestingly, stroke volume in this analysis again emerged as a significant predictor of SCORE-imageable myelinated fiber density, even with GFP+ fiber density as a predictor, suggesting, as observed before, that the effect of the severity of the initial injury influences these two fiber density measures in slightly different ways. Stroke volume, however, did not significantly modulate GFP+ fiber density's relationship to SCORE fiber density. There was a significant three-way interaction observed between site distance, GFP+ fiber density and treatment with quetiapine, as expected from the heatmaps shown in fig. 3.6 panel (c), that illustrated clearly the pattern outlined above, wherein both treatment

groups show a very similar relationship between GFP+ and SCORE-imaged myelinated fiber densities at imaging sites more distal to the infarct core ($\sim$ 1500 uM), but whereas this same relationship persists across all imaging sites measures in the quetiapine-treated animals, in the untreated naive stroke animals there is a growing myelin deficit observed as imaging site distance from the stroke core decreases. This analysis is particularly important, since quetiapine was demonstrated earlier to have a significant positive effect on both myelinated and contralateral crossing fiber densities - here we see that though it increases both fiber types, it has a proportionally larger effect on the recovery of SCORE-imaged fiber densities at imaging sites near the infarct core than it does enhancing the recovery of GFP+ fiber densities. In other words, though quetiapine is estimated to somewhat boosts GFP+ fiber densities as compared to untreated animals, it boosts the recovery of SCORE-imaged myelinated fiber densities even more when its effects are evaluated close to the infarct core.

3.4 IOS Imaging

3.4.1 Visual Assessment

Cortical activation patterns in response to vibratory limb stimulation under light anaesthesia were investigated using Intrinsic Optical Signal imaging. In animals without cortical injury, hindlimb and forelimb somatosensory maps imaged this way remained relatively stable throughout the 28-day imaging period (fig. 3.7 panel (a)). Following a targeted forelimb somatosensory infarct, cortical activation patterns were significantly altered, with - as expected - different patterns of injury and recovery observed across the hindlimb and forelimb somatosensory responses.

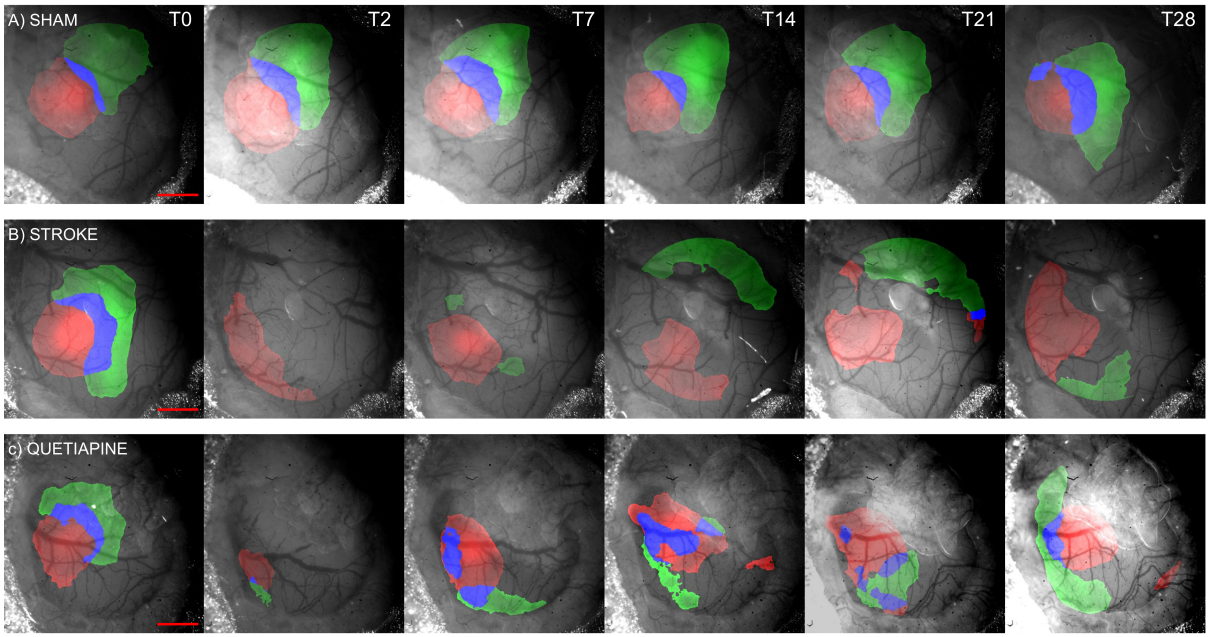

Figure 3.7: Sample images showing the results of intrinsic optical signal imaging in response to forelimb (green) and hindlimb (red) somatosensory stimulation across a period of weeks in a sham (a), stroke (b) and quetiapine (c) animal (scalebar = 1 mm). The results show the stability of somatosensory representations in uninjured animals across the 4-week period of study. In contrast, both the naive stroke and quetiapine-treated stroke animals' somatosensory representation are significantly disrupted for a period time following the initial insult. Since the photothrombotic stroke was targeted specifically at the forelimb somatosensory representation, the disturbance to the hindlimb somatosensory map was recovered from more quickly compared to the forelimb somatosensory map. The spatial configuration of the forelimb map also shifted significantly more than that of the hindlimb map as cortical activation in response to incoming forelimb somatosensory information remapped to uninjured areas of the cortex.

The hindlimb somatosensory map, which was not the primary target of the cortical injury, nevertheless experienced a temporary disruption of its functioning, with the cortex often becoming completely unresponsive to hindlimb or forelimb stimuli in the day following the initial injury. This was likely due to a variety of ischemia-induced mechanisms that cause widespread changes in cortex responsivity and not just in the areas of disrupted blood flow such as edema, cortical depression and remote diaschisis due to disrupted electrical signalling. However, these changes were transient, and hindlimb somatosensory maps were re-established in the weeks following the initial insult to closely resemble their original configurations, with no salient differences observed across quetiapine-treated and naive stroke animals.

The cortical response to forelimb stimulation, in comparison, was more severely impaired at earlier timepoints, with some recovery occurring over the following weeks, but, unlike in the hindlimb somatosensory maps, the forelimb maps never recovered to their

original configuration. In most cases, forelimb responsivity shifted to uninjured regions of the cortex spatially close to the original forelimb somatosensory maps - in most cases, this ended up being the region directly lateral to the hindlimb somatosensory map, an area previously processing sensory information from the shoulder region. However, these newly established patterns of responses to forelimb stimulation were often unstable across the imaging timepoints investigated, even 28 days after injury. Treatment with quetiapine, again, had no observable effect of the pattern or timeline of this recovery (fig. 3.7 panels (b) and (c)).

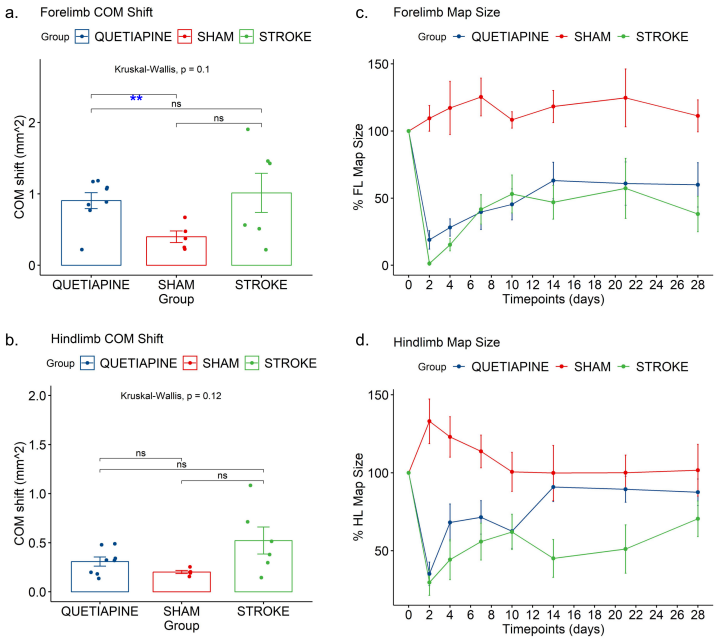

e.

FL Map Size	p	HL Map Size	p
Treatment Treatment*Time	0.90 0.71	Treatment Treatment*Time	0.53 0.71

Figure 3.8: Summary of the results following quantification of the intrinsic optical signal imaging data obtained following forelimb and hindlimb somatosensory stimulation. The center of mass of each available somatosensory map from T14, T21 and T28 was compared to the center of mass of each animal's baseline maps and averaged. Kruskal-Wallis tests comparing all three groups across both the forelimb (a) and hindlimb (b) data revealed no significant overall differences in COM shift values across the three groups, but follow-up non-paired Wilcoxon tests showed that the quetiapine group's COM shift in its forelimb somatosensory representation was significantly greater than the sham group's. Though untreated stroke group had a comparable average COM shift to the quetiapine group, and was not statistically significantly different than the quetiapine group's, due to increased variability it was also not statistically significantly different than the COM shift calculated across the sham group's forelimb representation. Given that the stroke was targeted to the forelimb somatosensory representation, it is not surprising that the average COM shift in the forelimb representation was significantly greater than the average COM shift in the hindlimb representation. The area of the cortex responding to the incoming somatosensory stimuli was also quantified: the results are shown in (c) and (d). The size of both forelimb and hindlimb somatosensory maps decreased immediately after ischemic injury, and recover gradually over a period of weeks - though the size of the initial deficit in the forelimb was considerably larger, and subsequently, unlike in the hindlimb, forelimb map size did not recover to baseline levels even at T28. As before, robust mixed linear regression models were fit to the untreated and treated stroke groups to evaluate the effect of quetiapine. Results show that quetiapine had no significant effect on the recovery curve of either fore- or hindlimb somatosensation across the timespan evaluated (e). All scalebars SE.

3.4.2 Center of Mass of Somatosensory Representations

Group differences in the normalized COM estimates were evaluated by averaging the normalized COM values from T14, T21 and T28 for each animal and calculated a one-way Kruskal-Wallis test across the groups, followed by post-hoc nonpaired Wilcoxon tests. The results of these comparisons are summarized in fig. 3.8 panels (a) and (b). In

the forelimb, the Kruskal-Wallis showed a weak trend towards a group-wide difference in COM shifts (p=0.10), but only the stroke+quetiapine (p=0.034*) group had significantly higher shifts in the center of mass values of their forelimb somatosensory representations than the sham group at the averages of timepoints T14, T21 and T28. Though the stroke group had a very comparable average COM shift as the quetiapine group, the estimates shifts here were more variable across animals and thus were deemed not significantly different from the sham groups' values (p=0.17). The difference between the quetiapine and stroke groups were also non-significant (p=0.85). In the hindlimb data, the overall Kruskal-Wallis showed no group-wide differences in COM shifts (p=0.12), and none of the post-hoc contrasts were significant (sham-stroke p=0.08, sham-quetiapine p=0.27, quetiapine-stroke p=0.22).

Overall, the distance that the somatosensory representation maps shifted following ischemic stroke above and beyond the shift in the sham group averaged around 550 uM in the forelimb, which was significantly higher than the average shift relative to the sham group in the hindlimb representation, which was estimated to be around 200 uM (paired samples t-test, t=3.49, p=0.00398*, df = 13). This pattern is consistent with the idea that the area of the cortex responsive to forelimb stimulation had to remap significantly further from its original location compared to the area of the cortex responsive to hindlimb stimulation.

3.4.3 Map Size of Somatosensory Representations

The area of the cortex responding to forelimb somatosensory stimulation remained relatively stable in the sham group throughout the entirety of the study period, but was significantly reduced after ischemic injury to the forelimb somatosensory representation, with some limited recovery occurring over the weeks following. This was mostly concentrated in the first 2 weeks; however, a substantial, deficit persisted even 28 days after the initial insult, in both quetiapine treated and untreated groups. In fact, no differences amongst the two treatment groups were evident at any point during the study (data shown in fig. 3.8 panels (c)). The area of the cortex responding to hindlimb stimulation in the sham group actually showed slight increase in the first week of study, but

remained stable at all other imaging timepoints; this was in comparison to the treated and untreated stroke groups, whose cortical responsitivity was moderately reduced in the days following the initial insult, and showed a gradual, steady recovery to sham-levels by the end of the imaging period (data shown in fig. 3.8 panel (d)). This overall patterns of results from the forelimb and hindlimb data generally corroborates the conclusions of the COM shift analysis and is in line with an injury targeting primarily the forelimb representation, with the ischemia's impact being more pronounced and enduring to the forelimb as compared to the hindlimb somatosensory maps. In the hindlimb, however, and in contrast to the forelimb data, quetiapine animals seemed to show greater recovery of hindlimb somatosensory processing at almost all timepoints.

To statistically and precisely evaluate differences across the treatment groups, a robust mixed linear model was fitted to both the forelimb and hindlimb data from the stroke and stroke+quetiapine groups, which specified map percentage and stroke volume as covariates of the model in order to control for any potential effect systematic difference in these parameters might have had on the aggregate group data. Specifically, the model fitted was

$$MapSize = Treatment * Time + Map\,Percentage + Stroke\,volume + 1|subject.$$

Wald Chi-Squared Tests were then used to assess the significance of each fixed effect in the fitted model. The results of the Wald Chi-Squared Tests on the fixed effects in the model fit to the forelimb map size data is summarized below.

	Df	Chisq	Pr(>Chisq)	BH adj. sig.
Treatment	1	0.02	0.8976	ns
Time	1	10.01	0.0016	*
Stroke volume	1	15.19	0.0001	*
FL percentage	1	2.84	0.0918	ns
Treatment:Time	1	0.14	0.7079	ns

Table 3.4: Wald Chi Square Test of fixed effects predicting forelimb somatosensory map size.

These results reinforce earlier observations that treatment with quetiapine had no significant effect on the recovery of cortex responsivity to forelimb stimulation following ischemic injury. There was, however, a significant positive effect of time, with both groups showing a gradual increase in the size of their forelimb somatosensory representations. Also significant was the effect of stroke volume, but interestingly the percentage of the original forelimb somatosensory representation that overlapped with the final infarct area was not a significant predictor of the post-injury size of the cortex responding to forelimb stimulation, though there was a trend towards significance.

The same set of results for the hindlimb map size data are summarized below.

	Df	Chisq	Pr(>Chisq)	BH adj. sig.
Treatment	1	0.40	0.5260	ns
Time	1	22.24	0.0000	*
Hindlimb map percentage	1	69.73	0.0000	*
Stroke volume	1	14.32	0.0002	*
Treatment:Time	1	0.14	0.7100	ns

Table 3.5: Wald Chi Square Test of fixed effects predicting hindlimb somatosensory map size.

The pattern of results here resemble those seen in the forelimb somatosensory data, with no significant effect of quetiapine resolved, despite earlier observations about a potential accelerant effect of quetiapine. Likely the stroke-only group had slightly greater HL somatosensory overlap in its stroke targeting, and though this difference was not statistically significant, as shown in fig. 3.1 panel (e), it was large enough to cause a systemic difference in the recovery curve of the hindlimb somatosensory map size between the treatment groups, which did show a significant effect of Treatment even with stroke volume but not the hindlimb map stroked percentage controlled for (p=0.014*). Here too, time had a significant positive effect on the recovery of hindlimb map size and increasing stroke volume a significantly negative effect. However here, as opposed to the forelimb somatosensory data, the percentage of the original hindlimb map that overlapped with the final infarct location was very significantly predictive of the subsequent size of the cortex that responded to hindlimb stimulation. This was perhaps due to the fact that

most of the strokes were correctly targeted to the forelimb somatosensory representation, meaning in the forelimb data, much of the variability in the recovery of the forelimb map size was captured by stroke volume, rather than the percentage of the original forelimb map infarcted, whereas in the hindlimb data, where the majority of the strokes did not significantly impact the original hindlimb representation, but a few did, the percentage of the original hindlimb map stroked remained a significant predictor as the stroke volume estimate captured less of the variability in the hindlimb map size variable.

To investigate how SCORE-imageable myelinated fiber density and GFP-expressing contralateral crossing fiber density influenced the recovery of the fore- and hindlimb somatosensory representations, the mixed robust regression model

$$Map\,Size = Map\,percentage + Stroke\,volume + Fibers + Stroke\,volume : Fibers + 1|subject$$

was fit to both the forelimb and hindlimb map size data, for both SCORE and GFP fibers. Stroke volume was allowed to interact with fiber density to account for potentially differing effects of fibers density in different sized strokes. Wald Chi Square Tests were used to assess the significance of each relevant fixed effect. The results for forelimb maps are summarized below, and the fitted models are visualized in fig. 3.9 panels (a) and (b).

	Df	Chisq	Pr(>Chisq)	BH. adj. sig
FL percentage	1	4.84	0.0278	*
Stroke Volume	1	17.42	0.0000	*
SCORE fibers	1	29.63	0.0000	*
SCORE fibers:Stroke volume	1	0.39	0.5328	ns

Table 3.6: Wald Chi Square Test of the fixed effects of SCORE fibers predicting forelimb somatosensory map size.

	Df	Chisq	Pr(>Chisq)	BH adj. sig.
FL percentage	1	6.16	0.0130	*
Stroke volume	1	22.50	0.0000	*
GFP fibers	1	10.65	0.0011	*
GFP fibers:Stroke volume	1	0.87	0.3520	ns

Table 3.7: Wald Chi Square Test of the fixed effects of GFP fibers predicting forelimb somatosensory map size.

The results show a very similar pattern in the predictive trends of GFP+ and SCORE+ fibers, which is not surprising given the close correlation between these measures. In both analyses stroke volume and forelimb percentage were significantly predictive of the area of the cortex responsive to forelimb somatosensory stimulation, in the direction excepted such that with increasing stroke volume and forelimb map percentage, the size of cortical activation in response forelimb stimulation decreases. The densities of SCORE-imaged cortical myelinated fibers and GFP-expressing contralateral crossing fibers likewise emerged as significant predictors of forelimb map size, indicating that the timelines of recovery between the structural microscale fiber density measures and the functional outcome of forelimb somatosensation are strongly correlated. These effects are visualized in fig. 3.9 panels (a) and (b).

To further explore this relationship, all relevant datasets were de-trended relative to time: this involved a transformation such that at each timepoint, the mean value of all animals within that timepoint was subtracted from every animal's individual datapoint. Using this analysis method, we aimed to investigate whether the same relationships described above held once the general trend of improvement over time was removed from the variables being considered. In other words, we investigated whether at each timepoint animals that showed greater SCORE-imaged and GFP+ fiber densities also tended to have better recovery in their forelimb somatosensory responsiveness. This summary of the Wald Chi Square tests on the relevant fixed effects are summarized below.

	Df	Chisq	Pr(>Chisq)	BH. adj. sig
Stroke volume	1	27.59	0.0000	*
FL percentage	1	12.63	0.0004	*
detrended SCORE fibers	1	4.34	0.0372	*
detrended SCORE fibers:Stroke volume	1	1.87	0.1716	ns

Table 3.8: Wald Chi Square Test of the fixed effects of time-detrended SCORE fibers predicting time-detrended forelimb somatosensory map size.

In this analysis, again, stroke volume and forelimb map percentage remained significant predictors of forelimb somatosensory map size, in the same direction as calculated before. Myelinated fiber density remained a significant positive predictor of forelimb somatosensory map size even after all common variation across time was removed the datasets. The effect of stroke volume on this relationship - though it could not be estimated with enough certainty to be considered a significant modulator - seemed to indicate that with increasing stroke size, the relationship between SCORE fiber density and forelimb somatosensory map size tended to become more positive with greater SCORE-imaged myelinated fiber densities above the mean of the group predicting greater gains in forelimb map size above the mean of the group.

The results of the Wald Chi Squared tests on the relevant fixed effects in the GFP+ fiber density analysis are summarized below.

	Df	Chisq	Pr(>Chisq)	BH. adj. sig
Stroke volume	1	32.24	0.0000	*
FL percentage	1	11.50	0.0007	*
detrended GFP fibers	1	0.22	0.6397	ns
detrended GFP fibers:Stroke volume	1	0.03	0.8607	ns

Table 3.9: Wald Chi Square Test of the fixed effects of time-detrended GFP fibers predicting time-detrended forelimb somatosensory map size.

This analysis showed again the expected pattern of main effects with regard to stroke volume and forelimb map percentage; however the main effect of GFP fiber density no longer emerged as a significant predictor of the size of the cortical area responding to forelimb stimulation, which is significantly different than the pattern seen across the

non-detrended analysis and the SCORE-imaged myelinated fiber density data. This suggests that the earlier significant positive relationship observed between these variable likely resulted from their common variance over time with both measures increasing significantly over time, such that when this common variance was removed, increased GFP+ fiber density no longer significantly predicted forelimb somatosensory map size. The estimated models in the time-detrended analysis are summarized in fig. 3.9 panels (c) and (d).

Exploring the same set of relationships in the hindlimb map size data yielded the pattern of results summarized below.

	Df	Chisq	Pr(>Chisq)	BH. adj. sig
HL percentage	1	138.47	0.0000	*
Stroke volume	1	32.08	0.0000	*
SCORE fibers	1	31.59	0.0000	*
SCORE fibers: Stroke volume	1	10.08	0.0015	*

Table 3.10: Wald Chi Square Test of the fixed effects of SCORE fibers predicting hindlimb somatosensory map size.

	Df	Chisq	Pr(>Chisq)	BH adj. sig.
HL percentage	1	198.25	0.0000	*
Stroke volume	1	51.86	0.0000	*
GFP fibers	1	12.28	0.0005	*
GFP fibers:Stroke volume	1	5.33	0.0210	*

Table 3.11: Wald Chi Square Test of the fixed effects of GFP fibers predicting hindlimb somatosensory map size.

Here again, GFP+ and SCORE+ fibers exhibit very similar patterns of results. The percentage of the original hindlimb map that overlapped with the final infarct area as well as the stroke volume are both evaluated to be significant predictors of the size of the cortex activated in response to a hindlimb stimulus, in the expected direction such that increasing size of injury predicts increased deficits in hindlimb somatosensory processing. Though here the two types of fibers densities are also significantly positively related to the hindlimb map size, both of their effects are significantly modulated by stroke volume. In

particular, the relationship between fiber densities and hindlimb map size becomes more positive with increasing stroke volumes, suggesting that myelin and contralateral crossing fiber density and integrity and more important indicators of recovery with increasing injury sizes. These effects are best visualized in fig. 3.9 panels (e) and (f).

This dataset was also detrended relative to time to investigate whether there was a time-invariant effect of fiber density on the recovery of the hindlimb somatosensory map size. The results of the Wald Chi Square tests of the relevant fixed effects are summarized below.

	Df	Chisq	Pr(>Chisq)	BH. adj. sig
Stroke volume	1	15.60	0.0001	*
HL percentage	1	77.40	0.0000	*
detrended SCORE fibers	1	11.95	0.0005	*
detrended SCORE fibers:Stroke volume	1	4.14	0.0418	*

Table 3.12: Wald Chi Square Test of the fixed effects of time-detrended SCORE fibers predicting time-detrended hindlimb somatosensory map size.

	Df	Chisq	Pr(>Chisq)	BH. adj. sig
Stroke volume	1	31.11	0.0000	*
HL percentage	1	99.76	0.0000	*
detrended GFP fibers	1	0.26	0.6113	ns
detrended GFP fibers:Stroke volume	1	4.51	0.0337	*

Table 3.13: Wald Chi Square Test of the fixed effects of time-detrended GFP fibers predicting time-detrended hindlimb somatosensory map size.

The detrended analysis here showed a results similar to the non-detrended regressions, though the main effect of GFP+ fiber density was no longer significant after the common variation across time in GFP+ fiber densities of hindlimb somatosensory map size were removed. However, both fiber density measures' interaction with stroke volume was evaluated to be in the same direction as before (namely the effect of increasing fiber densities becoming more positively predictive with increasing stroke volumes) and were still calculated to be significantly different than the null hypothesis. These model estimates are visualized in fig. 3.9 panels (g) and (h).

Interestingly, in the recovery of both the forelimb and hindlimb somatosensory representations, animals with greater SCORE fiber densities reliably had greater cortical responsitivity to incoming forelimb and hindlimb somatosensory stimuli, and in the case of predicting hindlimb somatosensory map sizes particularly in animals with greater stroke sizes. In comparison, increasing GFP+ fiber density had divergent effects in predicting forelimb and hindlimb map size recovery, particularly in larger strokes, such that animals with greater GFP+ fiber densities tended to have larger hindlimb somatosensory representations, but the size of their forelimb somatosensory representations were no greater than animals who had less GFP+ fiber densities. This discrepancy seen in the pattern of results across GFP+ fiber densities in predicting forelimb versus hindlimb map size supports the notion that the structural mechanisms underlying the re-establishment of cortical responsitivity to limb stimulation potentially differ in the forelimb and hindlimb somatosensory representations following a targeted forelimb-stroke. Additionally, the divergence seen across the role of contralateral crossing fibers and cortical myelinated fibers in predicting the recovery of forelimb somatosensation highlight the differential role various structural plasticity mechanisms may play in functional recovery.

Based on this pattern of results, the absence of a group-level effect of quetiapine in both the fore- and hindlimb map size data is surprising given the correlations presented above. One plausible explanation is that the effect of quetiapine in increasing myelinated and GFP+ fiber density above levels seen in naive (drug-free) recovery is possibly not large enough to detect a significant shift in the recovery curve of the size of the cortex responding to somatosensory stimulation at this sample size. Given that somatosensory recovery is likely governed by a whole host of physiological mechanisms aside from myelination and contralateral crossing fiber patterns, this explanation seems likely.

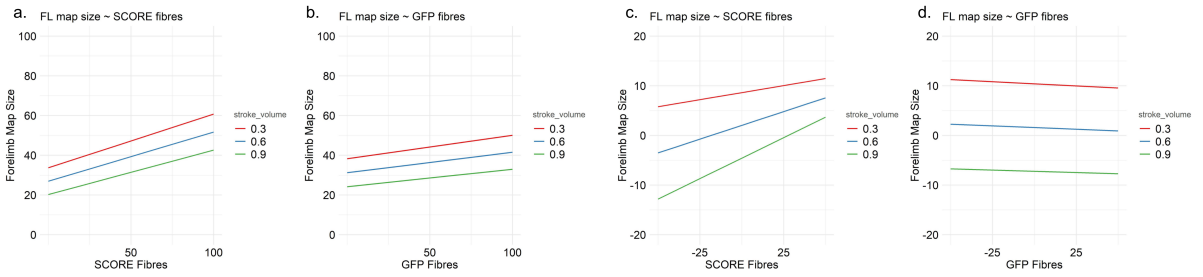

FL Map Size	p	FL Map Size	p
Stroke volume	2.99e-05*	Stroke volume	2.106e-06*
FL percentage	0.028*	FL percentage	0.0130*
SCORE	5.24e-08*	GFP	0.00110*
SCORE:Stroke volume	0.53	GFP:Stroke volume	0.351

Detrend FL Map Size	p	Detrend FL Map Size	p
Stroke volume	1.49e-07*	Stroke volume	1.35e-08*
FL percentage	0.00038*	FL percentage	0.00069*
SCORE	0.03716*	GFP	0.639
SCORE:Stroke volume	0.17163	GFP:Stroke volume	0.860

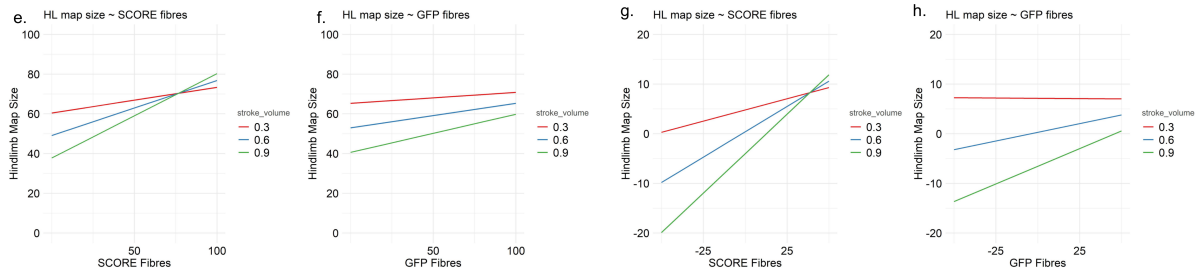

HL Map Size	p	HL Map Size	p
Stroke volume	1.48e-08*	Stroke volume	5.96e-13*
HL percentage	< 2e-16*	HL percentage	< 2e-16*
SCORE	1.90e-08*	GFP	0.00045*
SCORE:Stroke volume	0.0015*	GFP:Stroke volume	0.021*

Detrend HL Map Size	p	Detrend HL Map Size	p
Stroke volume	7.81e-05*	Stroke volume	2.43e-08*
HL percentage	< 2e-16*	HL percentage	< 2e-16*
SCORE	0.00054*	GFP	0.6112
SCORE:Stroke volume	0.0418*	GFP:Stroke volume	0.03368*

Figure 3.9: The relationships between map size and SCORE-imaged myelinated fibers and GFP+ contralateral crossing fibers was investigated in both the forelimb and hindlimb. Both GFP+ contralateral crossing fiber density and SCORE-imaged myelin fiber density was significantly predictive of both forelimb and hindlimb map sizes (a, b, e and f), though both fiber densities' effects were significantly modulated by stroke volume in predicting hindlimb map sizes. This indicates that a strong temporal relationship exists between the recovery of somatosensory processing and the recovery of myelinated fiber densities and contralateral crossing fiber densities. To evaluate whether fiber densities remained a significant predictor of map sizes even after their common variation across time was removed, all datasets were de-trended relative to time and new regression models fitted. The results of these models are visualized in panels (c, d, g, and h). Both fiber density's relationship to hindlimb map size remained essentially unaltered even after time-detrending. In the forelimb, SCORE-imaged myelinated fiber density remained significantly predictive of map size, however, GFP+ fiber density was no longer deemed a significant predictor.

3.5 Behavioral Tests

3.5.1 Cylinder Test

Two behavioral tests were administered throughout the study to evaluate the recovery of sensorimotor behavior; namely, the cylinder test and the pole test. In the cylinder test, there indeed appeared to be a tendency for animals to slightly alter their limb preferences after a cortical infarct targeted to the forelimb somatosensory area to the uninjured limb.

This switching behavior appeared to occur somewhat earlier in the quetiapine-treated animals and perhaps more stably as compared to the untreated animals, but was generally sustained throughout the duration of the study in both groups of animals. In the animals who did not receive a photothrombotic stroke, limb preference overall tended to stay similar to baseline measures (fig. 3.10 panel (a)).

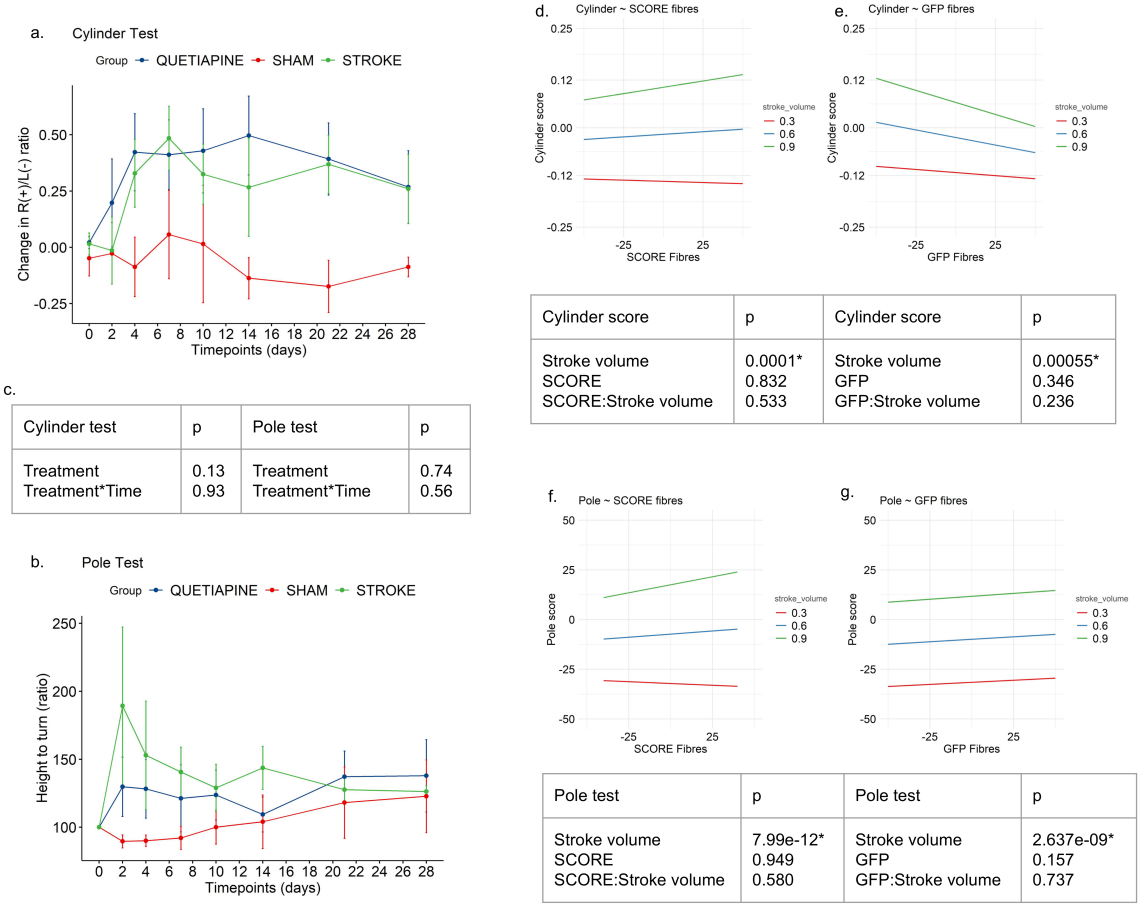

c.

Cylinder test	p	Pole test	p
Treatment Treatment*Time	0.13 0.93	Treatment Treatment*Time	0.74 0.56

Cylinder score	p	Cylinder score	p
Stroke volume SCORE SCORE:Stroke volume	0.0001* 0.832 0.533	Stroke volume GFP GFP:Stroke volume	0.00055* 0.346 0.236

Pole test	p	Pole test	p
Stroke volume SCORE SCORE:Stroke volume	7.99e-12* 0.949 0.580	Stroke volume GFP GFP:Stroke volume	2.637e-09* 0.157 0.737

Figure 3.10: Summary of the results following quantification of performance on the cylinder and pole tests. Stroke, whether coupled to treatment quetiapine or not, resulted in statistically significant alterations in limb preference in spontaneous use as indicated by the cylinder test, an alteration that persisted throughout the entire period of study investigated (a). Similarly, a statistically significant impairment in the ability to perform turns on the pole was also evident and likewise persisted throughout the duration of the study (b), though this impairment was more variable across animals, especially within the untreated group. A robust mixed linear regression was fit to the stroke groups in both datasets to evaluate any effect quetiapine may have had on behavioral recovery, but no significant effect of quetiapine was found on either test (c). In addition, we investigated whether the time-detrended GFP+ and SCORE fiber densities were significant predictive of performance, but found no significant effect of either fiber density on either behavioral outcomes (d-g). All scalebars SE.

To statistically evaluate whether quetiapine treatment alters limb switching behavior,

the robust mixed linear model

$$Cylinder\ score = Treatment * Time + Stroke\ volume + 1|subject$$

was fit to all timepoints with the exclusion of T2 to preserve linearity along the time variable in the stroke and stroke+quetiapine groups. Wald Chi Square tests were then conducted to evaluate the significance of each fixed effect in the model. The results of these test are summarized in the table below.

	Df	Chisq	Pr(>Chisq)	BH adj. sig.
Treatment	1	2.29	0.1301	ns
Time	1	0.28	0.593	ns
Stroke volume	1	12.48	0.0004	*
Treatment:Time	1	0.01	0.9315	ns

Table 3.14: Wald Chi Square Test of fixed effects predicting cylinder score.

The results show that the effect of stroke volume was the only factor considered that was strongly predictive of the shift in spontaneous limb preference, with greater strokes producing greater shifts. Across these timepoints, interestingly, these was no significant effect of time, indicating no recovery towards baseline limb preference over the period of the study and no significant effect of treatment, indicating quetiapine did not significantly alter this behavior.

To investigate whether SCORE fiber density and GFP+ fiber density were predictive of cylinder scores, all datasets were detrended relative to time according to the procedure described above. The robust mixed linear regression model

$$Cylinder\ Score = Stroke\ volume + Fibers + Stroke\ volume : Fibers + 1|subject$$

was then fit using both sets of data, to cylinder test scores from T4 onwards. Wald Chi Square tests were then used to evaluate the effects of fiber density; the results are summarized below.

	Df	Chisq	Pr(>Chisq)	BH adj. sig.
Stroke volume	1	14.25	0.0002	*
detrended SCORE fibers	1	0.04	0.8326	ns
detrended SCORE fibers:Stroke volume	1	0.39	0.5331	ns

Table 3.15: Wald Chi Square Test of the fixed effects of time-detrended SCORE fibers predicting detrended cylinder score.

	Df	Chisq	Pr(>Chisq)	BH adj. sig.
Stroke volume	1	11.94	0.0006	*
detrended GFP fibers	1	0.89	0.3467	ns
detrended GFP fibers:Stroke volume	1	1.40	0.2368	ns

Table 3.16: Wald Chi Square Test of the fixed effects of time-detrended GFP fibers predicting detrended cylinder score.

These results show that the only significant predictor of cylinder score was stroke volume, with greater size of stroke predicting greater limb switching behaviors, as visualized in fig. 3.10 panel (d) and (e), and as was apparent in the analysis prior. Neither the density of intact cortical myelin nor the density of homotopic contralesionally originating transcallossal fibers seems to predict this behavioral outcome, suggesting altered limb preference after a cortical injury functions independent of these particular structural measures of post-stroke recovery.

3.5.2 Pole test

The results of the pole test also seem to show some deficits in the animals whose forelimb somatosensory representation was targeted by photothrombotic infarct, but the variability across this test was quite high - especially in the groups who received strokes (see fig. 3.10 panel (b). Further complicating the interpretation of the results is that perhaps the 3 day training period on the pole test was not sufficiently long for a significant portion of animals - indeed, 12 out of the original 52 animals (23%) were excluded based on the criterion that at the baseline testing session they had to be able to turn at or above 50% of the full height of the pole. Amongst the remaining animals, however, performance on the pole test worsened slightly immediately after stroke, with some potential improvement in

performance over the following weeks in untreated animals. Amongst quetiapine-treated animals, in contrast, performance was steadily worse across the study period, though the magnitude of this change was smaller than that initially observed in the untreated stroke animals.

To statistically evaluate whether quetiapine treatment had any effect of performance on the pole test the robust mixed linear regression model

$$Pole\ score = Treatment * Time + Stroke\ volume + 1|subject$$

was fit to both the stroke and stroke+quetiapine datasets. Note that because of the exclusion of animals who were not able to satisfactorily perform the pole test at the baseline testing session, the dataset used in this analysis was significantly reduced compared to the datasets used in all previous analysis of quetiapine's effects. Though with 63 observations and 4 regressors, the model is still not considered overfit, because there were only 2 observations in the stroke groups at later timepoints the results of these tests should be interpreted with caution. The Wald Chi Square tests performed on the fixed effects of the model are summarized below.

	Df	Chisq	Pr(>Chisq)	BH adj. sig.
Treatment	1	0.11	0.7425	ns
Time	1	0.02	0.8807	ns
Stroke volume	1	10.19	0.0014	*
Treatment:Time	1	0.33	0.5628	ns

Table 3.17: Wald Chi Square Test of fixed effects predicting pole score.

Interestingly, the only significant effect in the analysis was stroke volume, with animals with larger strokes exhibiting an increased height to turn on the pole test. Time, however, did not significantly predict performance, suggesting no marked recovery in either treatment group for the duration of the study - similar to what was observed in the cylinder test. Also similar to the results of the cylinder test, treatment with quetiapine ultimately did not significantly alter performance on the pole test after stroke volume was properly controlled for.

To further investigate how SCORE and GFP+ fiber density may have influenced performance on the pole test, the robust mixed linear regression model

$$Pole\ Score = Stroke\ volume + Fibers + Stroke\ volume : Fibers + 1|subject$$

was fit to the time-detrended datasets. The results of the Wald Chi Square tests for each relevant fixed effect are summarized below.

	Df	Chisq	Pr(>Chisq)	BH adj. sig.
Stroke volume	1	46.77	0.0000	*
detrended SCORE fibers	1	0.00	0.9498	ns
detrended SCORE fibers:Stroke volume	1	0.31	0.5801	ns

Table 3.18: Wald Chi Square Test of the fixed effects of time-detrended SCORE fibers predicting detrended pole score.

	Df	Chisq	Pr(>Chisq)	BH adj. sig.
Stroke volume	1	35.43	0.0000	*
detrended GFP fibers	1	2.00	0.1576	ns
detrended GFP fibers:Stroke volume	1	0.11	0.7379	ns

Table 3.19: Wald Chi Square Test of the fixed effects of time-detrended GFP fibers predicting detrended pole score.

This pattern of results essentially replicates that observed in the cylinder test, with the only significant predictor of the ability to turn successfully and early on the vertical pole being stroke volume, with greater sizes of injury predicting greater deficits on the task. This is visualized in fig. 3.10 panels (f) and (g). Neither the SCORE-imaged myelinated fiber density nor the GFP-expressing contralaterally originating axonal densities in the peri-infarct area significantly predicted performance on this behavioral task, suggesting that though the task itself is sensitive to cortical injury, the ability to perform well on it depends on mechanisms other than the structural measures of the types of fiber densities assessed.

3.6 Immunohistochemistry

Two myelin-related immunomarkers were assessed after brain extraction at 4 weeks after stroke, namely MBP and PDGFR-alpha. One way ANOVAs were conducted to determine overall group differences in all immunomarkers at all locations imaged with post-hoc unpaired two samples t-tests to evaluate differences in all contrast pairings. The results of these tests are summarized in fig. 3.11.

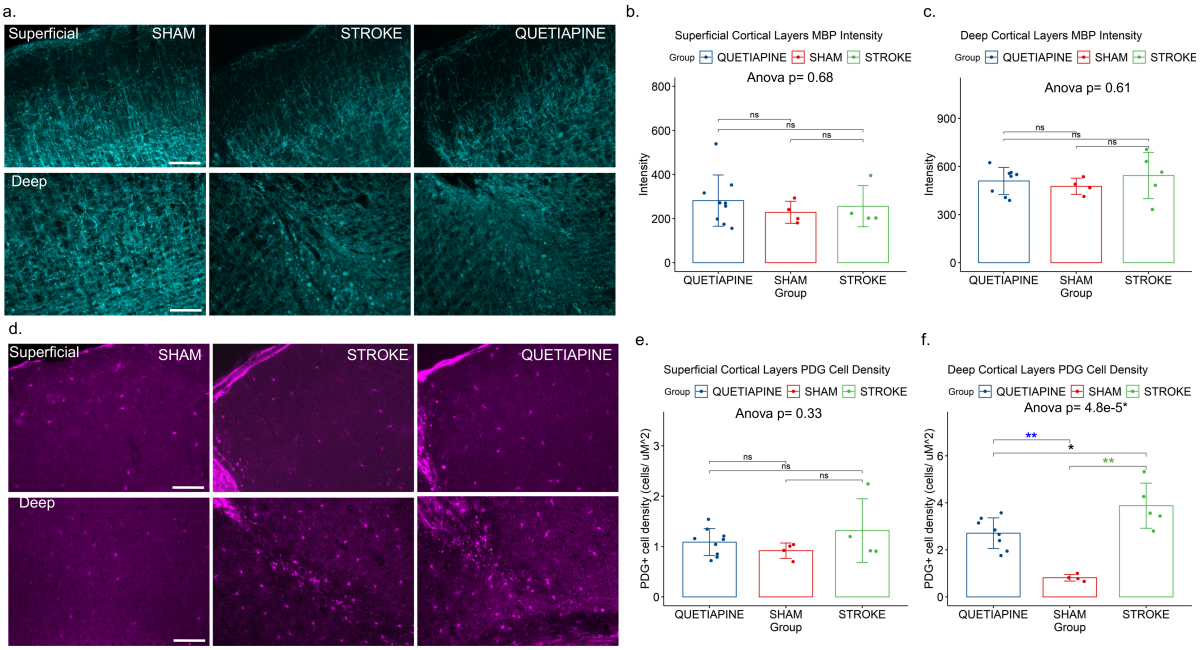

Figure 3.11: Immunohistochemical analysis of two different myelin-related proteins was conducted. One-way anova tests were used to assess the main effect of group, with post-hoc t-tests to evaluate the difference across every possible pairing. Panel (a) shows representative images of MBP immunostaining from all three groups at both superficial and deep cortical layers. No significant differences in the mean intensity of MBP staining are found across any of the groups at either the superficial (b) or deep (c) imaging locations. Representative images of PDGFRalpha+ stains are shown in panel (d) and subsequent analysis again reveals no significant differences across groups in more superficial cortical layers (e), but shows a significant overall difference in PDGFRalpha cell densities, driven by an increase in both quetiapine-treated and untreated stroke groups as compared to sham groups. Additionally, the untreated stroke group also showed a trend towards higher density of PDGFRalpha cells as compared to the quetiapine-treated group. All scalebars SE.

3.6.1 MBP Intensity

In evaluating the mean intensity of MBP immunostaining in the three groups, no significant group differences were detected at either more superficial (F=0.40, df=(2,14), p=0.68) or deeper cortical layers (F=0.51, df=(2,14), p=0.61). No post-hoc contrasts across any set of two groups were significant either. This is surprising, given the par-

tial myelin deficit that was observed using SCORE imaging, especially in the untreated stroke group. One possible reason for this discrepancy could be a location specific effect - whereby myelin density is differentially impacted through the different cortical layers, and because SCORE imaging visualizes myelinated fibers only throughout layer I&II cortex, whereas the majority of the image intensity in the MBP images is concentrated to deeper cortical layers, MBP+ image intensity is likely measuring a different outcome than SCORE imaging. Another potential explanation may be the fact that SCORE imaging could potentially be more sensitive to smaller, configurational changes in myelin sheaths than MBP immunostaining. Indeed, particularly in the deeper cortical layers, the MBP-stained myelin in the stroked animals appears significantly abnormal as compared to the sham animal, yet still shows the same overall intensity of the MBP stain. These results of this group of analyses are summarized on fig. 3.11 panels (a), (b) and (c).

3.6.2 PDGFRalpha+ Cell Density

Secondly, PDGFRalpha+ cell densities were evaluated, which is considered to be an OPC marker. There were no significant group differences (F=1.22, df=(2,14), p=0.33) or significant differences across the individual post-hocs comparisons in superficial cortical layers (quetiapine-sham p=0.18; quetiapine-stroke p=0.53; stroke-sham p=0.30). In deeper cortical layers, however, there was a significant group effect (F=22.0, df=(2,14), p=4.8e-05*), driven by significant increases in PDGFRalpha+ cell densities in both the quetiapine treated (p=0.00004*) and untreated (p=0.0018*) stroke groups as compared to the sham groups. A significant difference was also detected between the quetiapine treated and naive stroke groups (p=0.05), though upon controlling for the false discovery rate, this contrast was no longer significant. Nevertheless, there was a strong trend towards higher PDGFRalpha+ cell densities in the untreated stroke group as compared to the quetiapine treated group. These results of these group of analyses are summarized on fig. 3.11 panels (d), (e) and (f).

Chapter 4

Discussion

4.1 GFP+ and SCORE-imaged fiber densities

4.1.1 Summary

In this investigation, we explored the utility of a novel in vivo imaging technique named Spectral Confocal Reflectance Microscopy (SCORE) to track superficial cortical myelination patterns after a targeted photothrombotic stroke and characterized the changing patterns of myelin density within a border zone of ∼1.5 mm surrounding the infarct core over a period of 28 days following the initial injury. Concurrently, we tracked similar changes in the density of fibers originating in the contralesional homotopic cortical area projecting transcallossaly to the peri-lesional cortex, using a viral vector encoding eGFP. We showed photothrombotic ischemia results in an immediate and severe reductions in the densities of both myelinated and contralateral crossing fiber, but that robust recovery occurs over the following weeks - predominantly concentrated in the first 10 days after the initial insult and occurring sooner across cortical areas further from the stroke core. In GFP-expressing contralaterally originating axons, in fact, full recovery to pre-stroke levels of fiber density was observed, in comparison to SCORE-imaged myelinated fibers, where a persistent deficit of fiber density was observed particularly near the infarct core. Treatment with the atypical antipsychotic drug quetiapine appeared to alleviate this persistent deficit, accelerating the recovery of myelinated fibers across all imaging sites to reach close to baseline levels by 28 days after the initial injury. Quetiapine also seemed to attenuate the initial deficit in GFP+ fiber densities, and demonstrated over-

all consistently greater levels of contralateral crossing fiber densities across all imaging sites investigated in the immediate cortical areas surrounding the infarct core, though comparatively quetiapine's effect as a pro-myelinating agent was calculated to be greater than its enhancement of the recovery of contralateral crossing fibers.

4.1.2 Cortical Myelinated Fibers

This is the first study to demonstrate the viability of using SCORE imaging to track changes in superficial myelination patterns following an ischemic insult. As demonstrated earlier by [229], SCORE imaging through a cranial window in sham animals was completely stable throughout the 28-day imaging period. In animals who had received an ischemic injury, in contrast, by 48 hours following ischemia, the density of myelinated fibers visible to this imaging technique was almost completely obliterated especially near the core of the infarct. This fast disappearance of myelin is similar to the rapid disruption in the conformation of myelin sheaths observed using electron microscopy that starts to occur within hours of ischemic onset in the white matter[186, 187, 189], but similar trends in myelin disruption have not been investigated using EM in grey matter. Some of these EM studies, however, report a differential timeline of myelination changes in the immediate peri-infarct zone versus further away from the infarct core, such that whereas in the peri-infarct region myelin disruption is immediate and lessens in severity over the course of the first week, the exact opposite pattern is observed further away from the infarct core with disruption of myelination only becoming evident at 1 week after the initial insult, suggestive of an slowly expanding radius of damage [187]. These finding, however, may be unique to the ET-1 induced stroke model, which does not induce immediate substantial disruption of the blood brain barrier similar to that observed in photothrombotic strokes - indeed, following a subcortical photothrombotic stroke, though site specific effects were not specifically investigated in the particular study, the most significant damage to myelin sheaths was observed within the first 24 hours after the initial impact, with myelin sheath integrity entering its recovery phase by 4 days post-stroke and continuing over the next 3 weeks [189]. Even 21 days after the initial injury, however, a substantial deficit in myelin sheath density and thickness was reported. This is very similar to what was observed

in this study, with recovery of the initial decrease observed in myelinated fiber density evident at 4 days post-injury and continuing to around 14 days. At this point, however, recovery appeared to plateau until the end of the imaging period - an observation not previously reported - despite recovery to only around 50% of pre-stroke values, though most of the lasting deficit was concentrated around imaging sites nearest the stroke core with sites >1.5 mm demonstrating almost complete recovery of myelinated fiber densities. No delayed decrease in SCORE-imageable myelinated fiber density was observed at imaging sites further from the stroke core at any timepoint, suggesting that a slowly expanding core of damage is not a pathophysiological feature of this type of cortical infarct, a finding consistent with previous characterizations of photothrombotic stroke [17].

The substantial and rapid disappearance of myelinated fibers visible to the SCORE technique, however, is a substantially different pattern of results than that observed in the post-stroke brain using immunohistochemical assessments of antibodies raised against myelin-associated proteins such as MBP and PLP or the quantifications of their specific mRNA sequences. A number of such studies demonstrate either a delayed onset of deficits [179], a minimal extent of deficits [174, 175], or even significant increases in myelin density in the peri-infarct region in the weeks following the initial ischemia [173, 184]. Other studies using the same techniques on the other hand report findings more similar to what was observed here with a rapid initial decrease followed by a period of recovery in the days-weeks following, though the extent of the recovery again varies significantly across investigations [177, 178], with only a few reporting persistent deficits at 28 days post-stroke [176, 183]. McIver et al., 2010 [185] for example, followed the fate of individual myelinating OLs expressing GFP in the corpus callosum following tMCAO and showed an immediate blebbing within 24 hours of the OL's myelinating processes with complete to-baseline recovery of the number of processes within 1 week after the initial insult. Comparatively, this study showed a much more persistent myelin density deficit apparent even at 28 days after the initial injury, demonstrating that perhaps SCORE imaging is more sensitive to smaller conformation changes in myelin sheaths not necessarily reflected in immunohistochemical stains or the density of OL processes. Indeed, assessing myelin

density post-stroke using antibodies raised against MBP in this investigation also failed to show a persistent deficit at T28 in stroke animals as compared to sham animals - possibly due to the fact that MBP staining is not as sensitive to myelin integrity as SCORE imaging. Also possibly contributing to these discrepancies may be the particular imaging location accessible to SCORE imaging, which is necessarily limited to ∼150 uM depth, or specifically cortical layer I and II, while other investigations have generally considered all cortical layers or specifically white matter tracts. Layer I axons, in contrast to axons throughout deeper cortical layers and especially in white matter tracts, show sparse myelination of specific axonal segments [124]. In the present investigation, at imaging sites further from the stroke core where vascularization patterns after ischemic injury remained stable enough for reliable single-fiber tracking, we showed the gradual reappearance of the same set of myelinated cortical fibers that were imaged at baseline timepoints, further supporting the idea that SCORE imaging may be sensitive to smaller conformational changes to myelin sheaths that normalize over the weeks following an initial injury. However, since the stable identification of single myelinated fibres nearer the stroke core was not feasible in the present study, to what extent pattern of myelination after ischemic injury near the stroke core resemble their original configuration could not be determined, but could very well be significantly different than the stable pattern observed further from the stroke core, just as the most striking axonal repatterning occurs in immediate vicinity of the ischemic core [83].

Layer I contains few neuronal cell bodies which are exclusively GABAergic interneurons it seems [237], but is primarily composed of association fibres originating in layer 2/3 of the neocortex as well as the apical tufts of pyramidal cells [238]. Just recently, Rubio et al., 2009 [239] showed that contrary to popular belief, large numbers and subtypes of thalamic neurons also converge directly in layer I cortex, suggesting this pathway may provide a good anatomical candidate for feedback interactions between various cortical areas and the thalamus. fMRI imaging in the visual cortex appears to support this hypothesis, with contextual feedback information processing showing peak activity throughout the more superficial cortical layers [240]. Information integration across the extensive

apical dendritic arborizations of pyramidal cells, including its layer I inputs, has likewise been suggested to underlie much of the computation complexity of the brain [241]; these observations highlight the likely key functional contributions to information processing occurring in the molecular layer (layer I), which, this study demonstrates, suffers from chronic demyelination following an ischemic injury. This could, in turn, potentially result in serious disruptions of information flow due to the disorganization in the timing of action potentials. To further explore the effects of myelin disruptions, we administered the atypical antipsychotic quetiapine to a subset of the animals receiving photothrombotic strokes. Quetiapine is a known pro-myelinating agent, especially well characterized in the cuprizone induced model of demyelination, but its myelin-related effects in ischemic stroke have never been explored [207, 208]. Here we showed that quetiapine accelerated the rate and boosted the overall extent of post-stroke myelin density, to some extent alleviating the persistent myelin deficit observed in the immediate surround of the ischemic core. It's mechanism of action in this setting, however, is uncertain - typically, quetiapine is thought to enhance myelination through promoting the differentiation of OPCs into myelinating OLs [209], but it's unclear to what extent OL cell death and subsequent OPC differentiation and remyelination contributed to the results observed here, especially considering SCORE imaging is likely additionally sensitive to mere disruptions of myelin sheaths. Immunohistochemical analysis for the OPC marker PDGFRalpha done at 28 days after the initial injury still showed a significantly greater density of OPCs underneath the stroke cavity throughout the deeper cortical layers, but not superficially, as compared to uninjured sham animals, possibly reflective of the migration of SVZ-derived OPCs along the RMS to the site of injury, as has been observed elsewhere [140]. Interestingly, we showed a trend towards decreased PDGFRalpha+ cell density throughout the deeper cortical layers in the quetiapine-treated animals as compared to their untreated counterparts, similar to results obtained during the remyelinating phase of the cuprizone model where quetiapine's pro-myelinating effect was attributed to its driving OPC differenatiation resulting in overall decreased OPC cell densities [208].

4.1.3 Contralateral Crossing Fibers

In addition to its pro-myelinating effect, however, in the current investigation quetiapine was also shown to significantly boost the density of axonal fibers originating in the contralesional homotopic areas imaged in the ipsilesional peri-infarct cortex. Unlike in the cortical myelinated fiber density analysis however, even in the untreated animals the density of these contralateral crossing fibers eventually recovered to baseline levels at all imaging sites assessed, though again this recovery occurred significantly more quickly in areas further from the stroke core. Immediately after the initial injury, severe blebbing in almost all GFP-expressing crossing fibers was observed, but at imaging sites further from the ischemic core this blebbing often resolved and a significant portion of the fibers previously observed reappeared, though here this process was more dynamic with the emergence of new fibers and the lasting disappearance of others. Nearer the infarct core, though the tracking of individual GFP-expressing fibers was not feasible, initially blebbed regions either went on to recover an abundance of visually intact contralateral crossing fibers or the bright GFP blebs gradually disappeared with a dark cavity to mark the borders of the infarct core. This initial blebbing then may more appropriately reflect ongoing axonal injury rather than complete axonal disintegration, that may resolve within days to weeks following the initial injury depending on the severity of the ongoing pathophysiological processes, or lead to the eventual death of the GFP-expressing axon that may then be phagocytosed in the post-stroke inflammatory response [17]. Interestingly, none of the GFP-expressing contralaterally originating fibers appeared to co-register with SCORE-imaged myelinated cortical segments at any timepoint; unfortunately layer I myelination has not been investigated in enough detail to reveal whether this was a unique feature of SCORE imaging depth localization or a normal feature of brain anatomy. Evolving axonal injury following ischemic injury has been reported using APP and SMI32 antibodies in a number of stroke models where rapid accumulation of these damage-related proteins have been detected within hours of ischemia onset [242–244], similar to the early axonal damage observed using EM [187]. Long term EM imaging following subcortical ischemia has shown swelling in axons lasting as long as 21 days post ischemia [189]. Yet ultimate

fate of initially damaged axons and the long term timecourse of their subsequent demise or recovery have, to our knowledge, never been resolved. In addition, the pathophysiology, timecourse and extent of damage specifically in contralaterally originating axons may differ significantly from locally originating ones, as their cell bodies are located very remote to the primary site of ischemia.

The mechanism of action through which quetiapine limited the overall damage observed to the contralateral crossing fibers is unclear - indeed, this was a surprising result, but may be explicable by additional effects of quetiapine that have previously been reported. Amongst these, quetiapine has been shown to be a potent immunomodulator, reducing T-cell infiltration into demyelinating lesions [214] and reducing the microglial release of both NO and TNF-alpha [211]. Since peak immunological activation in photothrombosis occurs as late as around 4 days after the initial insult [17] it is thought to be an important contributor to ongoing neurodegeneration, and consequently possibly axonal damage occurring in the days following the initial ischemia [16]. Quetiapine also helps curb the production of reactive oxygen species, which again likely plays a key role in ongoing oxidative damage inducing continuing apoptotic cell death and whose short-term antagonism has been shown to be significantly neuroprotective specifically in photothrombosis [27]. Indeed, pretreatment with quetiapine in focal ischemia results in decreased apoptotic cell death, as observed days after the injury in the penumbral regions [227]. Though in this study quetiapine administration began immediately after the induction of photothrombotic stroke, through its effects outlined above that unfold over days following the initial insult, quetiapine's reported protective effect in limiting the extent of the axonal injury observed following ischemia is an entirely feasible outcome.

Interestingly, the overall rate of contralateral crossing fiber recovery was quite similar across the treatment groups at all imaging sites assessed, despite the earlier and more robust myelin reappearance observed in the quetiapine-treated group, particularly closer to the ischemic core. This indicates the increased quantities of intact myelin do not appear to be significantly antagonistic to axonal reorganization in the peri-infarct region, despite a multitude of studies demonstrating the potently inhibitory effects of

myelin-associated proteins to axonal regeneration [151, 153], and conversely enhanced axonal plasticity following their blockade [158]. Such inhibitory effects following other pro-myelinating treatments in focal ischemia have yet to be reported. Indeed others that have specifically assessed the quantity of the myelin-associated protein NoGo-A following ischemic injury with the administration of a myelin boosting treatment have either found either no significant concomitant increases in NoGo-A to the increased myelin quantity reported [199], or have found a significant decrease in the quantity of NoGo-A [200], suggesting newly forming myelin after an injury with certain pro-myelinating agents may be structurally distinct from established myelin in its inhibitory profile. In addition, quetiapine specifically has been shown to form part of the receptor complex to both NoGo and MAG, and ultimately limit the downstream activation of Rho-kinase and hence curb the growth-inhibitory effects of these myelin-associated proteins on axonal regeneration [223] - a possible mechanism for the pattern of results observed here. Nevertheless, it is possible that the majority of the axonal reappearance imaged was not driven by axonal plasticity, but rather by the gradual attenuation of the initial axonal injury that resulted in blebbing, thereby masking the true inhibitory effect of myelin density on axonal plasticity.

4.2 Functional Outcomes

4.2.1 Summary

Concurrent to tracking the micro-scale structural changes occurring in the peri-lesional cortex, a number of functional outcomes were also assessed. IOS imaging was used to track the extent of cortical responsitivity to incoming somatosensory stimuli to the fore- and hindlimb, and the cylinder test and pole test were administered to gauge the extent of behavioral recovery. We demonstrated a gradual re-emergence of cortical activation in response to incoming somatosensory stimuli to the fore- and hindlimb after a forelimb-targeted photothromobotic stroke: The area of the cortex processing hindlimb stimulation showed complete recovery by around 3-4 weeks after the initial injury, significantly faster and more complete than the area of the cortex processing forelimb stimulation which was substantially reduced as compared to its baseline size even 4 weeks after the initial injury

- a pattern consistent with the targeting of the infarct to the forelimb representation. Additionally, we showed that the movement in the center of mass of the forelimb representation in stroked animals relative the movement assessed in the sham animals was significantly more than the movement observed in the center of mass of the hindlimb representation, suggesting the primarily targeted forelimb representation reemerged further from its original cortical location than the relatively uninjured hindlimb somatosensory map. Performance on both the pole and cylinder tests were significantly worsened by the ischemic injury and showed minimal recovery throughout the 28 days investigation. Quetiapine administration throughout the post-stroke recovery period did not significantly affect any of the functional outcomes measures, despite its significant positive effect on the densities of both cortical myelinated and contralesionally originating transcallossal fibers.

4.2.2 Somatosensory Processing

Though a number of studies have reported significant spontaneous functional remapping of somatosensory and motor processing cortical networks after an injury [42–44] - and have amply demonstrated the functional significance of this plasticity process [51–53], few have assessed the precise timeline of these changes following a targeted injury to a specific functional network. Our results demonstrate a gradual reemergence of growing cortical activation responding to incoming sensory stimuli in response to both hind- and forelimb vibrations, very similar to what was observed by Clarkson et al., 2013 [45] who showed a steady increase in the area of the cortex processing somatosensory information, but also demonstrated lasting map size deficits in the fore- and hindlimb maps even at 56 days post-stroke following a mixed somatosensory photothrombotic injury. In other investigations however, severe cortical inactivity was reported in a targeted forelimb injury model in response to forelimb stimulation as late as 2 weeks after stroke, with re-emergence of the forelimb somatosensory map observed by 4 weeks localized partially such that it overlapped significantly with the location of the hindlimb somatosensory map [43]. Yet others, using the same targeted injury, report re-emergence more medial and anterior to the original forelimb representation in partial overlap with the primary motor cortex that

occurs only around 6-8 weeks following initial injury [42, 44]. Indeed, ongoing changes to the particular dynamics of the induced cortical response may evolve well past the the first 4 weeks with stable functional remapping of the somatosensory response occurring beyond the first month after stroke [43].

Though we demonstrated a gradual reinstatement of the cortical response to forelimb stimulation over the period of 4 weeks investigated, map location was often unstable across trials, even near the end of the 28 days of study and overall map size remained significantly impaired even at later timepoints, perhaps indicative of ongoing remapping that this investigation failed to capture. The initial disappearance of the hindlimb somatosensory map, though not specifically investigated on such a timescale elsewhere, was however in line with other work reporting deficits in hindlimb responsitivity following forelimb targeted strokes at 1 week post-stroke [42], with almost complete reinstatement in a similar location particularly in the quetiapine group by around 2 weeks [43]. This initial non-responsiveness despite no direct ischemic injury could be attributed to continuing pathophysiological cascades at play in the days following the initial injury such as ongoing edema, electrical disturbances, immune infiltration, and even delayed neurodegeneration [16, 17, 36, 37]. The delay in hindlimb reappearance in the untreated animals appears to have been an artefact of imprecise stroke targeting - when this confound was controlled for statistically, however, untreated animals showed remarkably similar recovery curves in their hindlimb somatosensation to treated animals'. Indeed treatment with quetiapine had no significant neuroprotective or neuroplastic effect on this particular mesoscale assessement of somatosensory functioning. The location in which the primarily targeted forelimb map re-emerged was variable across animals and indeed occurred both more posterior and anterior to the original representation, though more commonly posterior, presumably depending on the precise extent of the infarct with most remapping occurring preferentially across networks previously processing forelimb stimuli that survived the original insult [43]. The remapped location of the forelimb somatosensory map was indeed further from its original location than the re-emerging cortical map responding to hindlimb stimulation, in line with expectations in a forelimb-targeted injury model.

Though treatment with quetiapine did not result in any significant alteration of the recovery of either fore- or hindlimb mesoscale somatosensory processing, we demonstrated that both SCORE-imaged cortical myelinated fiber density and the density of contralesionally originating transcallosal axons are significantly predictive of the size of the cortex responding to both forelimb and hindlimb somatosensory stimulation even after controlling for confounding variables, indicative of strongly correlated timelines of recovery amongst these structural and functional plasticity measures. In predicting the recovery of hindlimb somatosensation, we additionally observed a significant interaction of both fiber densities with stroke volume, such that lower fiber densities in larger strokes predicted relatively worse hindlimb somatosensory map sizes than comparably low fiber densities in smaller strokes - perhaps signalling a heightened sensitivity of somatosensory processing in networks experiencing secondary evolving damage to structural perturbations under conditions of greater injury. Additionally, we applied a time-detrending transformation to the data such that any additional correlations observed would be independent of a coincident timeline of recovery across the outcomes measures. Using this technique we demonstrated that myelin and contralateral crossing fiber density remained significant predictors of the area of the cortex activated in response to a hindlimb stimulus, in the same pattern as observed before detrending - namely both fiber densities were again significantly modulated by stroke volume. This result strongly reinforces the idea that cortical myelinated fiber integrity and axonal integrity of the contralateral crossing fibers in the peri-infarct region surrounding the infarct core are functionally relevant to the ongoing recovery of somatosensation-induced cortical activity. Similarly in the forelimb data, SCORE-imaged cortical myelination remained a significant predictor of forelimb map size even after time-detrending; contralateral crossing fiber density, however, lost its predictive power in the detrended analysis, suggesting that the underlying mechanisms governing the recovery of somatosensory responsitivity across primarily injured cortical networks may be different than those in secondarily injured networks. Note however, that the functional interpretation of the density measure of the contralateral crossing fibers may be ambiguous: on one hand it may partly reflect general axonal integrity in the peri-lesional cortex, indicative of ongoing axonal injury and hence presumably positively

correlated to the extent of functionally intact cortical networks capable of supporting information processing; on the other hand, however, it may reflect increasing contralesional innervation of the ipsilesional cortex, which may itself be a form of maladaptive plasticity that ultimately serves to boost the imbalance in interhemispheric inhibition that is sometimes observed following a unilateral stroke and is purported to dampen peri-lesional plasticity mechanisms and ultimately lead to worse functional outcomes [58, 92, 93, 97–100]. This study provides no resolution between these potentially conflicting interpretations of the functional relevance of GFP-expressing fiber densities, and consequently any conclusion drawn should be interpreted with caution.

4.2.3 Behavioral Recovery

Lastly, we have shown that post-stroke treatment with quetiapine had no significant effect on behavioral recovery as assessed by the height to turn on the pole test and the preferential use of the uninjured forelimb compared to the injured forelimb as assessed by the cylinder test. Both behavioral measures showed a significant deficit following stroke as compared to the sham group (data not presented), and performance on them was shown to be strongly predicted by the size of the final stroke volume, indicating that they are indeed sensitive measures of cortical injury. In this study, however, neither outcome showed significant improvements over time - though similar results have been reported in the cylinder test in rats, where the cylinder test is thought to be a highly sensitive measure of even small cortical injuries and behavioral deficits [245], the literature on the use of the cylinder test in mice is rather mixed with some studies showing transient deficits in spontaneous limb use [236], others reporting minimal to no noticeable changes [234] and still other showing lasting deficits following unilateral cortical injury [246]. Deficits assessed via the pole test have likewise been variable, with some groups reporting significantly increased scores for up to 3 weeks after ischemia [247, 248], and others showing minimal sensitivity of this particular behavior to cortical injury [249, 250]. Note however that most studies utilizing the pole test assess time to turn and time to descend the length of the pole whereas we chose to measure distance to turn based on preliminary evidence indicating it may be a more sensitive measure of behavioral deficit

in our stroke model. Indeed, such discrepancies across studies may be readily explained by differences in the relative size, targeting and mode of injuries across studies that may govern the extent of ongoing functional plasticity capable of supporting the normalization of these complex behaviors. We further analyzed whether performance on these behavioral tasks was significantly predicted by either SCORE-imaged cortical myelin density or contralateral crossing fiber densities and found no significant relationship across any of the proposed pairings, indicating that their recovery is likely governed by mechanisms other than the specific structural markers assessed.

Though improved behavioral recovery with pro-myelinating treatments have been demonstrated elsewhere [196–198], in this investigation we failed to observe a group-level effect of a pro-myelinating agent. Note, however, that both this study and the others cited above reporting improved functional outcomes concurrent to an increase in myelination have so far failed to control for potentially off-target effects of their pro-myelinating agent, potentially seriously confounding their conclusions. Indeed, even here we observed a significant off-target effect of quetiapine in boosting post-stroke crossing fiber axonal integrity in the peri-lesional cortex, which we showed is significantly predictive of the size of the cortical area responsive to a hindlimb somatosensory stimulus, just as we showed that SCORE-imaged fiber density is significantly predictive of both the fore- and hindlimb map sizes. Our lack of a group level effect may then be explained by the relatively small effects of both the pro-myelinating quality of quetiapine as well as effect of myelin fiber density on fore- and hindlimb map sizes. This suggests functional recovery after ischemic injury as assessed by both behavioral measures and functional imaging of somatosensory processing may be governed by a complex amalgamation of multiple neuroplastic and regenerative pathways, myelin density and contralateral crossing fiber integrity and density being just one of them, with possibly limited influence. Potentially further contributing to the observed lack of a significant treatment effect of quetiapine in our functional outcome measures may be that though quetiapine boosted both the overall density of SCORE-visible myelinated fibers and GFP-expressing contralateral fibers, these artificially driven increases may have been implemented suboptimally without the functional

guidance of behavioral rehabilitation. Indeed, a number of studies have demonstrated only limited to moderate spontaneous recovery and in particular functional remapping without rehabilitative training, even in the presence of pro-plasticity treatments [51, 65, 79], suggesting that the re-establishment of maximally functional cortical networks may be dependent on the repeated practice of the injured behaviors. Additionally, in the absence of directed behavioral training even the limited spontaneous remapping that occurs may reflect compensatory patterns of behavior, rather than true behavioral recovery [90], further underlining the idea that rehab may be necessary for driving truly functional patterns of rewiring. This may be particularly true for myelination, where a preponderance of studies demonstrate that myelination patterns are strongly regulated by the intensity of ongoing cortical activity, with highly active axons experiencing preferential myelination [118–120, 127] - given this functional dependence, we suggest rehab-driven cortical activation may be necessary to exploit the full potential of pro-myelinating therapies such as quetiapine.

4.3 Limitations and Further Work

Though we demonstrated the utility and feasibility of utilizing SCORE imaging for the stable tracking of post-ischemic cortical myelination changes, significant gaps in knowledge remain, in particular about the requisite conditions of myelin sheaths required for them to visible to this type of microscopy. Though Schain, Hill & Grutzendler 2014 [229] demonstrated the co-registration of SCORE-imaged myelinated fibers with Fluoromyelin stained myelinated sheaths, they showed SCORE-imaging may in fact localize the myelin slightly differently than the widely-utilized myelin label but the exact optics of this discrepancy remain unresolved. Additionally, they limited their exploration to healthy brain tissue and to our knowledge, no one has yet investigated what effect small conformational changes in myelin sheaths may have on SCORE-imageability - a question worth pursuing given the potentially far reaching applications of this imaging technology given its clear feasibility in high resolution in vivo tracking of single cortical myelinated fibers over a period of time. As it stands however, we could not in the current investigation ascertain the precise extent of the myelin damage that was observed using SCORE.

Note moreover, that the depth penetration of SCORE imaging in our hands was necessarily limited to cortical layers I and II: additionally characterizing changing patterns of myelinated throughout the deeper cortical layers using transgenic lines might provide valuable insight into larger-scale network reorganization and functional recovery following ischemia. Further work to elucidate the precise functional contribution of contralesionally originating transcallosal fibers passing through or terminating in peri-lesional areas should be additionally undertaken, given that the current investigation could not resolve its functional relevance due to the confounding effect of this measure additionally potentially encoding general axonal injury and integrity. Concurrent in vivo tracking of ipsilesionally originating axon integrity may help resolve this issue and clarify the exact role the density of contralesional projections into the ipsilesional hemisphere may play in post-stroke recovery.

The sensitivity of functional measures of recovery employed here could also be improved, for example by utilizing calcium responsive fluorescent transgenic lines for more precise measurements of cortical activation patterns [251], and the improvement of pretraining protocols for use in the pole test. An extended timeline of imaging and behavioral tracking may also be warranted to capture potentially ongoing neuroplasticity and functional reorganization in the post-stoke brain. Further comparisons of quetiapine to the effects of other atypical antipsychotics following stroke would also be of interest to help clarify the specificity of its pro-myelinating effect and its functional significance. Lastly, investigating the combined effect of coupling quetiapine treatment with a rehabilitative training program on cortical myelination pattern may be a particularly fruitful endeavor, and could potentially help elucidate the mechanisms underlying the limited functional success currently observed of this particular pro-myelinating treatment.

Chapter 5

Conclusion

In summary, we utilized a novel in vivo imaging technique to characterize both the time-course and spatial distribution of myelination across the superficial cortex surrounding the central ischemic cavity produced by a targeted photothrombotic stroke and showed though some recovery in myelin density occurs, mostly concentrated within the first 2 weeks after the initial injury, a persistent myelin deficit is evident within a band of $\sim<1$ mm around the infarct core even 4 weeks after stroke. In addition, we demonstrated that treatment with the atypical antipsychotic quetiapine helps alleviate this myelination deficit to some extent. We also showed the feasability of longitudinally tracking the integrity and density of homotopically, contralaterally originating axons expressing eGFP concurrent to tracking myelination patterns, and showed that despite an initially severe blebbing observed across these axons their densities robustly recover to their pre-stroke levels within $\sim$2 weeks after the initial injury, and that in addition to its pro-myelinating effect, quetiapine may help boost this contralateral crossing fiber density to some extent. Concurrent to this micro-scale structural imaging, we also tracked the timeline and spatial distribution of changes to the area of the cortex activated by an external somatosensory stimulus to either the hind- or forelimb and showed that a targeted forelimb photothrombotic stroke disrupts processing of both hindlimb and forelimb stimuli, and though hindlimb somatosensory processing ultimately recovers to patterns very similar to those observed at baseline, the recovery of forelimb somatosensation occurs much more slowly, is still incomplete 4 weeks after the injury, and shows greater overall spatial movement over time. Despite its pro-myelinating effect, treatment with quetiapine did not alter

the recovery of the area of the cortex responding to incoming somatosensory stimulus to either the forelimb or hindlimb, despite myelin density being a demonstrably significant predictor of both hindlimb and forelimb somatosensory map sizes. This suggests that perhaps myelination plays a relatively minor role in the recovery of somatosensation-induced cortical activity after ischemic injury, or perhaps that simply increasing myelin density without training ongoing functional patterns of activity across cortical networks to guide its precise localization is not sufficient to significantly enhance functional recovery. Lastly we demonstrated a persistent deficit on both the pole and cylinder tests using this targeted photothrombotic stroke model, but failed to show any association between performance on these behavioral tasks and either contralateral crossing fiber density or myelin density.

Bibliography

[1] R. Brouns and P. P. De Deyn, "The complexity of neurobiological processes in acute ischemic stroke," *Clinical Neurology and Neurosurgery*, vol. 111, no. 6, pp. 483–495, Jul. 2009, ISSN: 1872-6968. DOI: 10.1016/j.clineuro.2009.04.001.

[2] U. Dirnagl, C. Iadecola, and M. A. Moskowitz, "Pathobiology of ischaemic stroke: An integrated view," *Trends in Neurosciences*, vol. 22, no. 9, pp. 391–397, Sep. 1999, ISSN: 0166-2236. DOI: 10.1016/s0166-2236(99)01401-0.

[3] D. Dewar, P. Yam, and J. McCulloch, "Drug development for stroke: Importance of protecting cerebral white matter," *European Journal of Pharmacology*, vol. 375, no. 1, pp. 41–50, Jun. 30, 1999, ISSN: 0014-2999. DOI: 10.1016/s0014-2999(99)00280-0.

[4] Public Health Agency of Canada, "Tracking heart disease and stroke in canada," Tech. Rep., 2009.

[5] H. Krueger, J. Koot, R. E. Hall, C. O'Callaghan, M. Bayley, and D. Corbett, "Prevalence of individuals experiencing the effects of stroke in canada: Trends and projections," *Stroke*, vol. 46, no. 8, pp. 2226–2231, Aug. 2015, ISSN: 1524-4628. DOI: 10.1161/STROKEAHA.115.009616.

[6] (Nov. 14, 2019). Types of stroke | cdc.gov, [Online]. Available: https://www.cdc.gov/stroke/types_of_stroke.htm.

[7] U.S. Food and Drug Administration, "Altepase Product Approval Information - Licensing Action 6/18/96," Tech. Rep., 1996.

[8] J. Mann, "Truths about the NINDS study: Setting the record straight," *The Western Journal of Medicine*, vol. 176, no. 3, pp. 192–194, May 2002, ISSN: 0093-0415. DOI: 10.1136/ewjm.176.3.192.

[9] M. G. Lansberg, E. Bluhmki, and V. N. Thijs, "Efficacy and safety of tissue plasminogen activator 3 to 4.5 hours after acute ischemic stroke: A metaanalysis," *Stroke*, vol. 40, no. 7, pp. 2438–2441, Jul. 2009, ISSN: 1524-4628. DOI: 10.1161/STROKEAHA.109.552547.

[10] S.-y. Xu and S.-y. Pan, "The failure of animal models of neuroprotection in acute ischemic stroke to translate to clinical efficacy," *Medical Science Monitor Basic Research*, vol. 19, pp. 37–45, Jan. 28, 2013, ISSN: 2325-4394. DOI: 10.12659/MSMBR.883750. [Online]. Available: https://www.ncbi.nlm.nih.gov/pmc/articles/PMC3638705/.

[11] A. G. Dyker and K. R. Lees, "Duration of neuroprotective treatment for ischemic stroke," *Stroke*, vol. 29, no. 2, pp. 535–542, Feb. 1998, ISSN: 0039-2499. DOI: 10.1161/01.str.29.2.535.

[12] S. C. Cramer and J. D. Riley, "Neuroplasticity and brain repair after stroke," *Current Opinion in Neurology*, vol. 21, no. 1, p. 76, Feb. 2008, ISSN: 1350-7540. DOI: 10.1097/WCO.0b013e3282f36cb6. [Online]. Available: http://journals.lww.com/co-neurology/Fulltext/2008/02000/Neuroplasticity_and_brain_repair_after_stroke.13.aspx.

[13] S. T. Carmichael, "Rodent models of focal stroke: Size, mechanism, and purpose," *NeuroRx*, vol. 2, no. 3, pp. 396–409, Jul. 2005, ISSN: 1545-5343. [Online]. Available: https://www.ncbi.nlm.nih.gov/pmc/articles/PMC1144484/.

[14] A. Durukan and T. Tatlisumak, "Acute ischemic stroke: Overview of major experimental rodent models, pathophysiology, and therapy of focal cerebral ischemia," *Pharmacology Biochemistry and Behavior*, vol. 87, no. 1, pp. 179–197, May 1, 2007, ISSN: 0091-3057. DOI: 10.1016/j.pbb.2007.04.015. [Online]. Available: http://www.sciencedirect.com/science/article/pii/S0091305707001372.

[15] B. D. Watson, W. D. Dietrich, R. Busto, M. S. Wachtel, and M. D. Ginsberg, "Induction of reproducible brain infarction by photochemically initiated thrombosis," *Annals of Neurology*, vol. 17, no. 5, pp. 497–504, 1985, ISSN: 1531-8249. DOI: 10.1002/ana.410170513. [Online]. Available: http://dx.doi.org/10.1002/ana.410170513.

[16] J. S. Braun, S. Jander, M. Schroeter, O. W. Witte, and G. Stoll, "Spatiotemporal relationship of apoptotic cell death to lymphomonocytic infiltration in photochemically induced focal ischemia of the rat cerebral cortex," *Acta Neuropathologica*, vol. 92, no. 3, pp. 255–263, Aug. 1, 1996, ISSN: 1432-0533. DOI: 10.1007/s004010050516. [Online]. Available: https://doi.org/10.1007/s004010050516.

[17] H. Li, N. Zhang, H.-Y. Lin, Y. Yu, Q.-Y. Cai, L. Ma, and S. Ding, "Histological, cellular and behavioral assessments of stroke outcomes after photothrombosis-induced ischemia in adult mice," *BMC Neuroscience*, vol. 15, no. 1, p. 58, May 2, 2014, ISSN: 1471-2202. DOI: 10.1186/1471-2202-15-58. [Online]. Available: https://doi.org/10.1186/1471-2202-15-58.

[18] H. J Bidmon, V Jancsik, A Schleicher, G Hagemann, O. W Witte, P Woodhams, and K Zilles, "Structural alterations and changes in cytoskeletal proteins and proteoglycans after focal cortical ischemia," *Neuroscience*, vol. 82, no. 2, pp. 397–420, Oct. 17, 1997, ISSN: 0306-4522. DOI: 10.1016/S0306-4522(97)00289-3. [Online]. Available: http://www.sciencedirect.com/science/article/pii/S0306452297002893.

[19] M. Nour, F. Scalzo, and D. S. Liebeskind, "Ischemia-reperfusion injury in stroke," *Interventional Neurology*, vol. 1, no. 3, pp. 185–199, 2012, ISSN: 1664-9737, 1664-5545. DOI: 10.1159/000353125. [Online]. Available: https://www.karger.com/Article/FullText/353125.

[20] Warach Steven and Latour Lawrence L., "Evidence of reperfusion injury, exacerbated by thrombolytic therapy, in human focal brain ischemia using a novel imaging marker of early blood–brain barrier disruption," *Stroke*, vol. 35, no. 11, pp. 2659–2661, Nov. 1, 2004. DOI: 10.1161/01.STR.0000144051.32131.09. [Online]. Available: https://www.ahajournals.org/doi/full/10.1161/01.STR.0000144051.32131.09.

[21] C. E. Brown, C. Wong, and T. H. Murphy, "Rapid morphologic plasticity of peri-infarct dendritic spines after focal ischemic stroke," *Stroke*, vol. 39, no. 4, pp. 1286–1291, Apr. 2008, ISSN: 1524-4628. DOI: 10.1161/STROKEAHA.107.498238.

[22] C. E. Brown, P. Li, J. D. Boyd, K. R. Delaney, and T. H. Murphy, "Extensive turnover of dendritic spines and vascular remodeling in cortical tissues recovering from stroke," *The Journal of Neuroscience: The Official Journal of the Society for Neuroscience*, vol. 27, no. 15, pp. 4101–4109, Apr. 11, 2007, ISSN: 1529-2401. DOI: 10.1523/JNEUROSCI.4295-06.2007.

[23] N. van Bruggen, B. M. Cullen, M. D. King, M. Doran, S. R. Williams, D. G. Gadian, and J. E. Cremer, "T2- and diffusion-weighted magnetic resonance imaging of a focal ischemic lesion in rat brain," *Stroke*, vol. 23, no. 4, pp. 576–582, Apr. 1992, ISSN: 0039-2499. DOI: 10.1161/01.str.23.4.576.

[24] Lee Vee Meng, Burdett Newman G., Carpenter T. Adrian, Hall Laurance D., Pambakian Perouz S., Patel Sara, Wood Nigel I., and James Michael F., "Evolution of photochemically induced focal cerebral ischemia in the rat," *Stroke*, vol. 27, no. 11, pp. 2110–2119, Nov. 1, 1996. DOI: 10.1161/01.STR.27.11.2110. [Online]. Available: https://www.ahajournals.org/doi/10.1161/01.STR.27.11.2110.

[25] J. M. Provenzale, R. Jahan, T. P. Naidich, and A. J. Fox, "Assessment of the patient with hyperacute stroke: Imaging and therapy," *Radiology*, vol. 229, no. 2, pp. 347–359, Nov. 2003, ISSN: 0033-8419. DOI: 10.1148/radiol.2292020402.

[26] Kaufmann Anthony M., Firlik Andrew D., Fukui Melanie B., Wechsler Lawrence R., Jungries Charles A., and Yonas Howard, "Ischemic core and penumbra in human stroke," *Stroke*, vol. 30, no. 1, pp. 93–99, Jan. 1, 1999. DOI: 10.1161/01.STR.30.1.93. [Online]. Available: https://www.ahajournals.org/doi/full/10.1161/01.str.30.1.93.

[27] K. Schoknecht, O. Prager, U. Vazana, L. Kamintsky, D. Harhausen, M. Zille, L. Figge, Y. Chassidim, E. Schellenberger, R. Kovács, U. Heinemann, and A. Friedman, "Monitoring stroke progression: In vivo imaging of cortical perfusion, blood–brain barrier permeability and cellular damage in the rat photothrombosis model," *Journal of Cerebral Blood Flow & Metabolism*, vol. 34, no. 11, pp. 1791–1801, Nov. 2014, ISSN: 0271-678X. DOI: 10.1038/jcbfm.2014.147. [Online]. Available: https://www.ncbi.nlm.nih.gov/pmc/articles/PMC4269756/.

[28] H. Benveniste, J. Drejer, A. Schousboe, and N. H. Diemer, "Elevation of the extracellular concentrations of glutamate and aspartate in rat hippocampus during transient cerebral ischemia monitored by intracerebral microdialysis," *Journal of Neurochemistry*, vol. 43, no. 5, pp. 1369–1374, Nov. 1984, ISSN: 0022-3042. DOI: 10.1111/j.1471-4159.1984.tb05396.x.

[29] R. Bullock, A. Zauner, J. Woodward, and H. F. Young, "Massive persistent release of excitatory amino acids following human occlusive stroke," *Stroke*, vol. 26, no. 11, pp. 2187–2189, Nov. 1995, ISSN: 0039-2499. DOI: 10.1161/01.str.26.11.2187.

[30] Dávalos Antoni, Castillo José, Serena Joaquín, and Noya Manuel, "Duration of glutamate release after acute ischemic stroke," *Stroke*, vol. 28, no. 4, pp. 708–710, Apr. 1, 1997. DOI: 10.1161/01.STR.28.4.708. [Online]. Available: https://www.ahajournals.org/doi/10.1161/01.STR.28.4.708.

[31] C. Grewer, A. Gameiro, Z. Zhang, Z. Tao, S. Braams, and T. Rauen, "Glutamate forward and reverse transport: From molecular mechanism to transporter-mediated release after ischemia," *IUBMB life*, vol. 60, no. 9, pp. 609–619, Sep. 2008, ISSN: 1521-6543. DOI: 10.1002/iub.98. [Online]. Available: https://www.ncbi.nlm.nih.gov/pmc/articles/PMC2632779/.

[32] Q. J. Wu and M. Tymianski, "Targeting NMDA receptors in stroke: New hope in neuroprotection," *Molecular Brain*, vol. 11, no. 1, p. 15, Mar. 13, 2018, ISSN: 1756-6606. DOI: 10.1186/s13041-018-0357-8. [Online]. Available: https://doi.org/10.1186/s13041-018-0357-8.

[33] B. H. Juurlink, S. K. Thorburne, and L. Hertz, "Peroxide-scavenging deficit underlies oligodendrocyte susceptibility to oxidative stress," *Glia*, vol. 22, no. 4, pp. 371–378, Apr. 1998, ISSN: 0894-1491. DOI: 10.1002/(sici)1098-1136(199804)22:4⟨371::aid-glia6⟩3.0.co;2-6.

[34] S. Love, "Oxidative stress in brain ischemia," *Brain Pathology*, vol. 9, no. 1, pp. 119–131, Jan. 1, 1999, ISSN: 1015-6305. DOI: 10.1111/j.1750-3639.1999.tb00214.x. [Online]. Available: https://onlinelibrary.wiley.com/doi/abs/10.1111/j.1750-3639.1999.tb00214.x.

[35] D. Amantea, G. Nappi, G. Bernardi, G. Bagetta, and M. T. Corasaniti, "Post-ischemic brain damage: Pathophysiology and role of inflammatory mediators," *The FEBS Journal*, vol. 276, no. 1, pp. 13–26, 2009, ISSN: 1742-4658. DOI: 10.1111/j.1742-4658.2008.06766.x. [Online]. Available: https://febs.onlinelibrary.wiley.com/doi/abs/10.1111/j.1742-4658.2008.06766.x.

[36] M. Kawabori and M. A. Yenari, "Inflammatory responses in brain ischemia," *Current medicinal chemistry*, vol. 22, no. 10, pp. 1258–1277, 2015, ISSN: 0929-8673. [Online]. Available: https://www.ncbi.nlm.nih.gov/pmc/articles/PMC5568039/.

[37] M. Duering and R. Schmidt, "Remote changes after ischaemic infarcts: A distant target for therapy?" *Brain*, vol. 140, no. 7, pp. 1818–1820, Jul. 1, 2017, ISSN: 0006-8950. DOI: 10.1093/brain/awx135. [Online]. Available: https://academic.oup.com/brain/article/140/7/1818/3892696.

[38] T. H. Murphy and D. Corbett, "Plasticity during stroke recovery: From synapse to behaviour," *Nature Reviews. Neuroscience*, vol. 10, no. 12, pp. 861–872, Dec. 2009, ISSN: 1471-0048. DOI: 10.1038/nrn2735.

[39] I. R. Winship and T. H. Murphy, "Remapping the somatosensory cortex after stroke: Insight from imaging the synapse to network," *The Neuroscientist: A Review Journal Bringing Neurobiology, Neurology and Psychiatry*, vol. 15, no. 5, pp. 507–524, Oct. 2009, ISSN: 1089-4098. DOI: 10.1177/1073858409333076.

[40] C. Alia, C. Spalletti, S. Lai, A. Panarese, G. Lamola, F. Bertolucci, F. Vallone, A. Di Garbo, C. Chisari, S. Micera, and M. Caleo, "Neuroplastic changes following brain ischemia and their contribution to stroke recovery: Novel approaches in neurorehabilitation," *Frontiers in Cellular Neuroscience*, vol. 11, Mar. 16, 2017, ISSN: 1662-5102. DOI: 10.3389/fncel.2017.00076. [Online]. Available: https://www.ncbi.nlm.nih.gov/pmc/articles/PMC5352696/.

[41] A. Zepeda, C. Arias, and F. Sengpiel, "Optical imaging of intrinsic signals: Recent developments in the methodology and its applications," *Journal of Neuroscience Methods*, vol. 136, no. 1, pp. 1–21, Jun. 15, 2004, ISSN: 0165-0270. DOI: 10.1016/j.jneumeth.2004.02.025.

[42] C. E. Brown, K. Aminoltejari, H. Erb, I. R. Winship, and T. H. Murphy, "In vivo voltage-sensitive dye imaging in adult mice reveals that somatosensory maps lost to stroke are replaced over weeks by new structural and functional circuits with prolonged modes of activation within both the peri-infarct zone and distant sites," *The Journal of Neuroscience: The Official Journal of the Society for Neuroscience*, vol. 29, no. 6, pp. 1719–1734, Feb. 11, 2009, ISSN: 1529-2401. DOI: 10.1523/JNEUROSCI.4249-08.2009.

[43] I. R. Winship and T. H. Murphy, "In vivo calcium imaging reveals functional rewiring of single somatosensory neurons after stroke," *The Journal of Neuroscience*, vol. 28, no. 26, pp. 6592–6606, Jun. 25, 2008, ISSN: 0270-6474. DOI: 10.1523/JNEUROSCI.0622-08.2008. [Online]. Available: https://www.ncbi.nlm.nih.gov/pmc/articles/PMC6670410/.

[44] T. C. Harrison, G. Silasi, J. D. Boyd, and T. H. Murphy, "Displacement of sensory maps and disorganization of motor cortex after targeted stroke in mice," *Stroke*, vol. 44, no. 8, pp. 2300–2306, Aug. 1, 2013, ISSN: 0039-2499, 1524-4628. DOI: 10.1161/STROKEAHA.113.001272. [Online]. Available: http://stroke.ahajournals.org/content/44/8/2300.

[45] A. N. Clarkson, H. E. López-Valdés, J. J. Overman, A. C. Charles, K. C. Brennan, and S Thomas Carmichael, "Multimodal examination of structural and functional remapping in the mouse photothrombotic stroke model," *Journal of Cerebral Blood Flow & Metabolism*, vol. 33, no. 5, pp. 716–723, May 2013, ISSN: 0271-678X. DOI: 10.1038/jcbfm.2013.7. [Online]. Available: https://www.ncbi.nlm.nih.gov/pmc/articles/PMC3652691/.

[46] T. Keck, T. D. Mrsic-Flogel, M. V. Afonso, U. T. Eysel, T. Bonhoeffer, and M. Hübener, "Massive restructuring of neuronal circuits during functional reorganization of adult visual cortex," *Nature Neuroscience*, vol. 11, no. 10, pp. 1162–1167, Oct. 2008, ISSN: 1546-1726. DOI: 10.1038/nn.2181. [Online]. Available: https://www.nature.com/articles/nn.2181.

[47] J. A. Jablonka, K. Burnat, O. W. Witte, and M. Kossut, "Remapping of the somatosensory cortex after a photothrombotic stroke: Dynamics of the compensatory reorganization," *Neuroscience*, vol. 165, no. 1, pp. 90–100, Jan. 13, 2010, ISSN: 1873-7544. DOI: 10.1016/j.neuroscience.2009.09.074.

[48] G. S. Doetsch, K. W. Johnston, and C. J. Hannan, "Physiological changes in the somatosensory forepaw cerebral cortex of adult raccoons following lesions of a single cortical digit representation," *Experimental Neurology*, vol. 108, no. 2, pp. 162–175, May 1, 1990, ISSN: 0014-4886. DOI: 10.1016/0014-4886(90)90024-M. [Online]. Available: http://www.sciencedirect.com/science/article/pii/001448869090024M.

[49] W. M. Jenkins and M. M. Merzenich, "Chapter 21 reorganization of neocortical representations after brain injury: A neurophysiological model of the bases of recovery from stroke," in *Progress in Brain Research*, ser. Neural Regeneration, F. J. Seil, E. Herbert, and B. M. Carlson, Eds., vol. 71, Elsevier, Jan. 1, 1987, pp. 249–266. DOI: 10.1016/S0079-6123(08)61829-4. [Online]. Available: http://www.sciencedirect.com/science/article/pii/S0079612308618294.

[50] C. Xerri, M. M. Merzenich, B. E. Peterson, and W. Jenkins, "Plasticity of primary somatosensory cortex paralleling sensorimotor skill recovery from stroke in adult monkeys," *Journal of Neurophysiology*, vol. 79, no. 4, pp. 2119–2148, Apr. 1, 1998, ISSN: 0022-3077, 1522-1598. [Online]. Available: http://jn.physiology.org/content/79/4/2119.

[51] M. A. Castro-Alamancos and J. Borrell, "Functional recovery of forelimb response capacity after forelimb primary motor cortex damage in the rat is due to the reorganization of adjacent areas of cortex," *Neuroscience*, vol. 68, no. 3, pp. 793–805, Oct. 1, 1995, ISSN: 0306-4522. DOI: 10.1016/0306-4522(95)00178-L. [Online]. Available: http://www.sciencedirect.com/science/article/pii/030645229500178L.

[52] Y. Liu and E. M. Rouiller, "Mechanisms of recovery of dexterity following unilateral lesion of the sensorimotor cortex in adult monkeys," *Experimental Brain Research*, vol. 128, no. 1, pp. 149–159, Sep. 1, 1999, ISSN: 1432-1106. DOI: 10.1007/s002210050830. [Online]. Available: https://doi.org/10.1007/s002210050830.

[53] R. M. Dijkhuizen, A. B. Singhal, J. B. Mandeville, O. Wu, E. F. Halpern, S. P. Finklestein, B. R. Rosen, and E. H. Lo, "Correlation between brain reorganization, ischemic damage, and neurologic status after transient focal cerebral ischemia in rats: A functional magnetic resonance imaging study," *The Journal of Neuroscience: The Official Journal of the Society for Neuroscience*, vol. 23, no. 2, pp. 510–517, Jan. 15, 2003, ISSN: 1529-2401.

[54] C. Weiller, S. C. Ramsay, R. J. Wise, K. J. Friston, and R. S. Frackowiak, "Individual patterns of functional reorganization in the human cerebral cortex after capsular infarction," *Annals of Neurology*, vol. 33, no. 2, pp. 181–189, Feb. 1993, ISSN: 0364-5134. DOI: 10.1002/ana.410330208.

[55] F. Chollet, V. DiPiero, R. J. Wise, D. J. Brooks, R. J. Dolan, and R. S. Frackowiak, "The functional anatomy of motor recovery after stroke in humans: A study with positron emission tomography," *Annals of Neurology*, vol. 29, no. 1, pp. 63–71, Jan. 1991, ISSN: 0364-5134. DOI: 10.1002/ana.410290112.

[56] S. C. Cramer, G. Nelles, R. R. Benson, J. D. Kaplan, R. A. Parker, K. K. Kwong, D. N. Kennedy, S. P. Finklestein, and B. R. Rosen, "A functional MRI study of subjects recovered from hemiparetic stroke," *Stroke*, vol. 28, no. 12, pp. 2518–2527, Dec. 1997, ISSN: 0039-2499. DOI: 10.1161/01.str.28.12.2518.

[57] J. D. Schaechter, C. I. Moore, B. D. Connell, B. R. Rosen, and R. M. Dijkhuizen, "Structural and functional plasticity in the somatosensory cortex of chronic stroke patients," *Brain: A Journal of Neurology*, vol. 129, pp. 2722–2733, Pt 10 Oct. 2006, ISSN: 1460-2156. DOI: 10.1093/brain/awl214.

[58] N. S. Ward, M. M. Brown, A. J. Thompson, and R. S. J. Frackowiak, "Neural correlates of motor recovery after stroke: A longitudinal fMRI study," *Brain: A Journal of Neurology*, vol. 126, pp. 2476–2496, Pt 11 Nov. 2003, ISSN: 0006-8950. DOI: 10.1093/brain/awg245.

[59] P. Cicinelli, R. Traversa, and P. M. Rossini, "Post-stroke reorganization of brain motor output to the hand: A 2-4 month follow-up with focal magnetic transcranial stimulation," *Electroencephalography and Clinical Neurophysiology*, vol. 105, no. 6, pp. 438–450, Dec. 1997, ISSN: 0013-4694. DOI: 10.1016/s0924-980x(97)00052-0.

[60] G. Nelles, G. Spiekermann, M. Jueptner, G. Leonhardt, S. Müller, H. Gerhard, and H. C. Diener, "Evolution of functional reorganization in hemiplegic stroke: A serial positron emission tomographic activation study," *Annals of Neurology*, vol. 46, no. 6, pp. 901–909, 1999, ISSN: 1531-8249. DOI: 10.1002/1531-8249(199912)46:6⟨901::AID-ANA13⟩3.0.CO;2-7. [Online]. Available: https://onlinelibrary.wiley.com/doi/abs/10.1002/1531-8249%28199912%2946%3A6%3C901%3A%3AAID-ANA13%3E3.0.CO%3B2-7.

[61] J. R. Carey, T. J. Kimberley, S. M. Lewis, E. J. Auerbach, L. Dorsey, P. Rundquist, and K. Ugurbil, "Analysis of fMRI and finger tracking training in subjects with chronic stroke," *Brain: A Journal of Neurology*, vol. 125, pp. 773–788, Pt 4 Apr. 2002, ISSN: 0006-8950. DOI: 10.1093/brain/awf091.

[62] A. Jaillard, C. D. Martin, K. Garambois, J. F. Lebas, and M. Hommel, "Vicarious function within the human primary motor cortex? a longitudinal fMRI stroke study," *Brain: A Journal of Neurology*, vol. 128, pp. 1122–1138, Pt 5 May 2005, ISSN: 1460-2156. DOI: 10.1093/brain/awh456.

[63] H. Johansen-Berg, H. Dawes, C. Guy, S. M. Smith, D. T. Wade, and P. M. Matthews, "Correlation between motor improvements and altered fMRI activity after rehabilitative therapy," *Brain: A Journal of Neurology*, vol. 125, pp. 2731–2742, Pt 12 Dec. 2002, ISSN: 0006-8950. DOI: 10.1093/brain/awf282.

[64] J. Liepert, H. Bauder, H. R. Wolfgang, W. H. Miltner, E. Taub, and C. Weiller, "Treatment-induced cortical reorganization after stroke in humans," *Stroke*, vol. 31, no. 6, pp. 1210–1216, Jun. 2000, ISSN: 0039-2499. DOI: 10.1161/01.str.31.6.1210.

[65] R. J. Nudo, B. M. Wise, F. SiFuentes, and G. W. Milliken, "Neural substrates for the effects of rehabilitative training on motor recovery after ischemic infarct," *Science (New York, N.Y.)*, vol. 272, no. 5269, pp. 1791–1794, Jun. 21, 1996, ISSN: 0036-8075. DOI: 10.1126/science.272.5269.1791.

[66] K. M. Jacobs and J. P. Donoghue, "Reshaping the cortical motor map by unmasking latent intracortical connections," *Science (New York, N.Y.)*, vol. 251, no. 4996, pp. 944–947, Feb. 22, 1991, ISSN: 0036-8075. DOI: 10.1126/science.2000496.

[67] M. Hallett, "Plasticity of the human motor cortex and recovery from stroke," *Brain Research. Brain Research Reviews*, vol. 36, no. 2, pp. 169–174, Oct. 2001. DOI: 10.1016/s0165-0173(01)00092-3.

[68] I. Ferezou, F. Haiss, L. J. Gentet, R. Aronoff, B. Weber, and C. C. H. Petersen, "Spatiotemporal dynamics of cortical sensorimotor integration in behaving mice," *Neuron*, vol. 56, no. 5, pp. 907–923, Dec. 6, 2007, ISSN: 0896-6273. DOI: 10.1016/j.neuron.2007.10.007.

[69] C. Stosiek, O. Garaschuk, K. Holthoff, and A. Konnerth, "In vivo two-photon calcium imaging of neuronal networks," *Proceedings of the National Academy of Sciences*, vol. 100, no. 12, pp. 7319–7324, Jun. 10, 2003, ISSN: 0027-8424, 1091-6490. DOI: 10.1073/pnas.1232232100. [Online]. Available: https://www.pnas.org/content/100/12/7319.

[70] T. R. Sato, N. W. Gray, Z. F. Mainen, and K. Svoboda, "The functional microarchitecture of the mouse barrel cortex," *PLOS Biology*, vol. 5, no. 7, e189, Jul. 10, 2007, ISSN: 1545-7885. DOI: 10.1371/journal.pbio.0050189. [Online]. Available: https://journals.plos.org/plosbiology/article?id=10.1371/journal.pbio.0050189.

[71] T. Berger, A. Borgdorff, S. Crochet, F. B. Neubauer, S. Lefort, B. Fauvet, I. Ferezou, A. Carleton, H.-R. Lüscher, and C. C. H. Petersen, "Combined voltage and calcium epifluorescence imaging in vitro and in vivo reveals subthreshold and suprathreshold dynamics of mouse barrel cortex," *Journal of Neurophysiology*, vol. 97, no. 5, pp. 3751–3762, May 2007, ISSN: 0022-3077. DOI: 10.1152/jn.01178.2006.

[72] C. C. H. Petersen, A. Grinvald, and B. Sakmann, "Spatiotemporal dynamics of sensory responses in layer 2/3 of rat barrel cortex measured in vivo by voltage-sensitive dye imaging combined with whole-cell voltage recordings and neuron reconstructions," *The Journal of Neuroscience: The Official Journal of the Society for Neuroscience*, vol. 23, no. 4, pp. 1298–1309, Feb. 15, 2003, ISSN: 1529-2401.

[73] S. Thomas Carmichael, L. Wei, C. M. Rovainen, and T. A. Woolsey, "New patterns of intracortical projections after focal cortical stroke," *Neurobiology of Disease*, vol. 8, no. 5, pp. 910–922, Oct. 2001, ISSN: 0969-9961. DOI: 10.1006/nbdi.2001.0425. [Online]. Available: http://www.sciencedirect.com/science/article/pii/S0969996101904255.

[74] J. J. Overman, A. N. Clarkson, I. B. Wanner, W. T. Overman, I. Eckstein, J. L. Maguire, I. D. Dinov, A. W. Toga, and S. T. Carmichael, "A role for ephrin-a5 in axonal sprouting, recovery, and activity-dependent plasticity after stroke," *Proceedings of the National Academy of Sciences of the United States of America*, vol. 109, no. 33, E2230–2239, Aug. 14, 2012, ISSN: 1091-6490. DOI: 10.1073/pnas.1204386109.

[75] S. Li, E. H. Nie, Y. Yin, L. I. Benowitz, S. Tung, H. V. Vinters, F. R. Bahjat, M. P. Stenzel-Poore, R. Kawaguchi, G. Coppola, and S. T. Carmichael, "GDF10 is a signal for axonal sprouting and functional recovery after stroke," *Nature Neuroscience*, vol. 18, no. 12, pp. 1737–1745, Dec. 2015, ISSN: 1546-1726. DOI: 10.1038/nn.4146. [Online]. Available: https://www.nature.com/articles/nn.4146.

[76] N. Dancause, S. Barbay, S. B. Frost, E. J. Plautz, D. Chen, E. V. Zoubina, A. M. Stowe, and R. J. Nudo, "Extensive cortical rewiring after brain injury," *The Journal of Neuroscience: The Official Journal of the Society for Neuroscience*, vol. 25, no. 44, pp. 10 167–10 179, Nov. 2, 2005, ISSN: 1529-2401. DOI: 10.1523/JNEUROSCI.3256-05.2005.

[77] N. T. Lindau, B. J. Bänninger, M. Gullo, N. A. Good, L. C. Bachmann, M. L. Starkey, and M. E. Schwab, "Rewiring of the corticospinal tract in the adult rat after unilateral stroke and anti-nogo-a therapy," *Brain: A Journal of Neurology*, vol. 137, pp. 739–756, Pt 3 Mar. 2014, ISSN: 1460-2156. DOI: 10.1093/brain/awt336.

[78] V. Riban and M.-F. Chesselet, "Region-specific sprouting of crossed corticofugal fibers after unilateral cortical lesions in adult mice," *Experimental Neurology*, vol. 197, no. 2, pp. 451–457, Feb. 2006, ISSN: 0014-4886. DOI: 10.1016/j.expneurol.2005.10.026.

[79] A. M. Wiersma, K. Fouad, and I. R. Winship, "Enhancing spinal plasticity amplifies the benefits of rehabilitative training and improves recovery from stroke," *Journal of Neuroscience*, vol. 37, no. 45, pp. 10 983–10 997, Nov. 8, 2017, ISSN: 0270-6474, 1529-2401. DOI: 10.1523/JNEUROSCI.0770-17.2017. [Online]. Available: https://www.jneurosci.org/content/37/45/10983.

[80] K. A. Tennant, S. L. Taylor, E. R. White, and C. E. Brown, "Optogenetic rewiring of thalamocortical circuits to restore function in the stroke injured brain," *Nature Communications*, vol. 8, no. 1, pp. 1–14, Jun. 23, 2017, ISSN: 2041-1723. DOI: 10.1038/ncomms15879. [Online]. Available: https://www.nature.com/articles/ncomms15879.

[81] R. P. Stroemer, T. A. Kent, and C. E. Hulsebosch, "Increase in synaptophysin immunoreactivity following cortical infarction," *Neuroscience Letters*, vol. 147, no. 1, pp. 21–24, Nov. 23, 1992, ISSN: 0304-3940. DOI: 10.1016/0304-3940(92)90765-Y. [Online]. Available: http://www.sciencedirect.com/science/article/pii/030439409290765Y.

[82] R. Mostany, T. G. Chowdhury, D. G. Johnston, S. A. Portonovo, S. T. Carmichael, and C. Portera-Cailliau, "Local hemodynamics dictate long-term dendritic plasticity in peri-infarct cortex," *The Journal of Neuroscience: The Official Journal of the Society for Neuroscience*, vol. 30, no. 42, pp. 14 116–14 126, Oct. 20, 2010, ISSN: 1529-2401. DOI: 10.1523/JNEUROSCI.3908-10.2010.

[83] S. T. Carmichael, I. Archibeque, L. Luke, T. Nolan, J. Momiy, and S. Li, "Growth-associated gene expression after stroke: Evidence for a growth-promoting region in peri-infarct cortex," *Experimental Neurology*, vol. 193, no. 2, pp. 291–311, Jun. 2005, ISSN: 0014-4886. DOI: 10.1016/j.expneurol.2005.01.004. [Online]. Available: http://www.sciencedirect.com/science/article/pii/S0014488605000105.

[84] S. Li and S. T. Carmichael, "Growth-associated gene and protein expression in the region of axonal sprouting in the aged brain after stroke," *Neurobiology of Disease*, vol. 23, no. 2, pp. 362–373, Aug. 1, 2006, ISSN: 0969-9961. DOI: 10.1016/j.nbd.2006.03.011. [Online]. Available: http://www.sciencedirect.com/science/article/pii/S096999610600074X.

[85] J.-K. Lee, J.-E. Kim, M. Sivula, and S. M. Strittmatter, "Nogo receptor antagonism promotes stroke recovery by enhancing axonal plasticity," *Journal of Neuroscience*, vol. 24, no. 27, pp. 6209–6217, Jul. 7, 2004, ISSN: 0270-6474, 1529-2401. DOI: 10.1523/JNEUROSCI.1643-04.2004. [Online]. Available: https://www.jneurosci.org/content/24/27/6209.

[86] Tsai Shih-Yen, Papadopoulos Catherine M., Schwab Martin E., and Kartje Gwendolyn L., "Delayed anti-nogo-a therapy improves function after chronic stroke in adult rats," *Stroke*, vol. 42, no. 1, pp. 186–190, Jan. 1, 2011. DOI: 10.1161/STROKEAHA.110.590083. [Online]. Available: https://www.ahajournals.org/doi/full/10.1161/STROKEAHA.110.590083.

[87] J. J. Hill, K. Jin, X. O. Mao, L. Xie, and D. A. Greenberg, "Intracerebral chondroitinase ABC and heparan sulfate proteoglycan glypican improve outcome from chronic stroke in rats," *Proceedings of the National Academy of Sciences*, vol. 109, no. 23, pp. 9155–9160, Jun. 5, 2012, ISSN: 0027-8424, 1091-6490. DOI: 10.1073/pnas.1205697109. [Online]. Available: https://www.pnas.org/content/109/23/9155.

[88] S. Soleman, P. K. Yip, D. A. Duricki, and L. D. F. Moon, "Delayed treatment with chondroitinase ABC promotes sensorimotor recovery and plasticity after stroke in aged rats," *Brain*, vol. 135, no. 4, pp. 1210–1223, Apr. 1, 2012, ISSN: 0006-8950. DOI: 10.1093/brain/aws027. [Online]. Available: https://academic.oup.com/brain/article/135/4/1210/359507.

[89] L. Gherardini, M. Gennaro, and T. Pizzorusso, "Perilesional treatment with chondroitinase ABC and motor training promote functional recovery after stroke in rats," *Cerebral Cortex*, vol. 25, no. 1, pp. 202–212, Jan. 1, 2015, ISSN: 1047-3211. DOI: 10.1093/cercor/bht217. [Online]. Available: https://academic.oup.com/cercor/article/25/1/202/370179.

[90] M. Nishibe, S. Barbay, D. Guggenmos, and R. J. Nudo, "Reorganization of motor cortex after controlled cortical impact in rats and implications for functional recovery," *Journal of Neurotrauma*, vol. 27, no. 12, pp. 2221–2232, Dec. 2010, ISSN: 1557-9042. DOI: 10.1089/neu.2010.1456.

[91] M. H. Mohajerani, K. Aminoltejari, and T. H. Murphy, "Targeted mini-strokes produce changes in interhemispheric sensory signal processing that are indicative of disinhibition within minutes," *Proceedings of the National Academy of Sciences*, vol. 108, no. 22, E183–E191, May 31, 2011, ISSN: 0027-8424, 1091-6490. DOI: 10.1073/pnas.1101914108. [Online]. Available: http://www.pnas.org/content/108/22/E183.

[92] P. Talelli, R. J. Greenwood, and J. C. Rothwell, "Arm function after stroke: Neurophysiological correlates and recovery mechanisms assessed by transcranial magnetic stimulation," *Clinical Neurophysiology: Official Journal of the International Federation of Clinical Neurophysiology*, vol. 117, no. 8, pp. 1641–1659, Aug. 2006, ISSN: 1388-2457. DOI: 10.1016/j.clinph.2006.01.016.

[93] N. S. Ward, J. M. Newton, O. B. C. Swayne, L. Lee, A. J. Thompson, R. J. Greenwood, J. C. Rothwell, and R. S. J. Frackowiak, "Motor system activation after subcortical stroke depends on corticospinal system integrity," *Brain: A Journal of Neurology*, vol. 129, pp. 809–819, Pt 3 Mar. 2006, ISSN: 1460-2156. DOI: 10.1093/brain/awl002.

[94] V. Rema and F. F. Ebner, "Lesions of mature barrel field cortex interfere with sensory processing and plasticity in connected areas of the contralateral hemisphere," *Journal of Neuroscience*, vol. 23, no. 32, pp. 10 378–10 387, Nov. 12, 2003, ISSN: 0270-6474, 1529-2401. DOI: 10.1523/JNEUROSCI.23-32-10378.2003. [Online]. Available: https://www.jneurosci.org/content/23/32/10378.

[95] D. G. Johnston, M. Denizet, R. Mostany, and C. Portera-Cailliau, "Chronic in vivo imaging shows no evidence of dendritic plasticity or functional remapping in the contralesional cortex after stroke," *Cerebral Cortex*, vol. 23, no. 4, pp. 751–762, Apr. 1, 2013, ISSN: 1047-3211. DOI: 10.1093/cercor/bhs092. [Online]. Available: https://academic.oup.com/cercor/article/23/4/751/347764.

[96] A Ferbert, A Priori, J. C. Rothwell, B. L. Day, J. G. Colebatch, and C. D. Marsden, "Interhemispheric inhibition of the human motor cortex.," *The Journal of Physiology*, vol. 453, pp. 525–546, 1992, ISSN: 0022-3751. [Online]. Available: https://www.ncbi.nlm.nih.gov/pmc/articles/PMC1175572/.

[97] J. Duque, F. Hummel, P. Celnik, N. Murase, R. Mazzocchio, and L. G. Cohen, "Transcallosal inhibition in chronic subcortical stroke," *NeuroImage*, vol. 28, no. 4, pp. 940–946, Dec. 2005, ISSN: 1053-8119. DOI: 10.1016/j.neuroimage.2005.06.033.

[98] N. Murase, J. Duque, R. Mazzocchio, and L. G. Cohen, "Influence of interhemispheric interactions on motor function in chronic stroke," *Annals of Neurology*, vol. 55, no. 3, pp. 400–409, Mar. 2004, ISSN: 0364-5134. DOI: 10.1002/ana.10848.

[99] N. Takeuchi, T. Chuma, Y. Matsuo, I. Watanabe, and K. Ikoma, "Repetitive transcranial magnetic stimulation of contralesional primary motor cortex improves hand function after stroke," *Stroke*, vol. 36, no. 12, pp. 2681–2686, Dec. 2005, ISSN: 1524-4628. DOI: 10.1161/01.STR.0000189658.51972.34.

[100] N. Takeuchi, T. Tada, M. Toshima, T. Chuma, Y. Matsuo, and K. Ikoma, "Inhibition of the unaffected motor cortex by 1 hz repetitive transcranical magnetic stimulation enhances motor performance and training effect of the paretic hand in patients with chronic stroke," *Journal of Rehabilitation Medicine*, vol. 40, no. 4, pp. 298–303, Apr. 2008, ISSN: 1650-1977. DOI: 10.2340/16501977-0181.

[101] L. J. Boddington and J. N. J. Reynolds, "Targeting interhemispheric inhibition with neuromodulation to enhance stroke rehabilitation," *Brain Stimulation*, vol. 10, no. 2, pp. 214–222, Apr. 2017, ISSN: 1876-4754. DOI: 10.1016/j.brs.2017.01.006.

[102] S. Madhavan, L. M. Rogers, and J. W. Stinear, "A paradox: After stroke, the non-lesioned lower limb motor cortex may be maladaptive," *The European Journal of Neuroscience*, vol. 32, no. 6, pp. 1032–1039, Sep. 2010, ISSN: 1460-9568. DOI: 10.1111/j.1460-9568.2010.07364.x.

[103] J. Netz, T. Lammers, and V. Hömberg, "Reorganization of motor output in the non-affected hemisphere after stroke," *Brain: A Journal of Neurology*, vol. 120 (Pt 9), pp. 1579–1586, Sep. 1997, ISSN: 0006-8950. DOI: 10.1093/brain/120.9.1579.

[104] K. J. Werhahn, A. B. Conforto, N. Kadom, M. Hallett, and L. G. Cohen, "Contribution of the ipsilateral motor cortex to recovery after chronic stroke," *Annals of Neurology*, vol. 54, no. 4, pp. 464–472, Oct. 2003, ISSN: 0364-5134. DOI: 10.1002/ana.10686.

[105] A. S. Wahl, W. Omlor, J. C. Rubio, J. L. Chen, H. Zheng, A. Schröter, M. Gullo, O. Weinmann, K. Kobayashi, F. Helmchen, B. Ommer, and M. E. Schwab, "Neuronal repair. asynchronous therapy restores motor control by rewiring of the rat corticospinal tract after stroke," *Science (New York, N.Y.)*, vol. 344, no. 6189, pp. 1250–1255, Jun. 13, 2014, ISSN: 1095-9203. DOI: 10.1126/science.1253050.

[106] L. C. Bachmann, N. T. Lindau, P. Felder, and M. E. Schwab, "Sprouting of brainstem-spinal tracts in response to unilateral motor cortex stroke in mice," *The Journal of Neuroscience: The Official Journal of the Society for Neuroscience*, vol. 34, no. 9, pp. 3378–3389, Feb. 26, 2014, ISSN: 1529-2401. DOI: 10.1523/JNEUROSCI.4384-13.2014.

[107] A. H. Seidl, "Regulation of conduction time along axons," *Neuroscience*, vol. 0, pp. 126–134, Sep. 12, 2014, ISSN: 0306-4522. DOI: 10.1016/j.neuroscience.2013.06.047. [Online]. Available: https://www.ncbi.nlm.nih.gov/pmc/articles/PMC3849146/.

[108] Y. Yamazaki, Y. Hozumi, K. Kaneko, S. Fujii, K. Goto, and H. Kato, "Oligodendrocytes: Facilitating axonal conduction by more than myelination," *The Neuroscientist*, vol. 16, no. 1, pp. 11–18, Feb. 1, 2010, ISSN: 1073-8584. DOI: 10.1177/1073858409334425. [Online]. Available: https://doi.org/10.1177/1073858409334425.

[109] M. S. Kaller, A. Lazari, C. Blanco-Duque, C. Sampaio-Baptista, and H. Johansen-Berg, "Myelin plasticity and behaviour — connecting the dots," *Current Opinion in Neurobiology*, vol. 47, pp. 86–92, Dec. 2017, ISSN: 0959-4388. DOI: 10.1016/j.conb.2017.09.014. [Online]. Available: https://www.ncbi.nlm.nih.gov/pmc/articles/PMC5844949/.

[110] T. Philips and J. D. Rothstein, "Oligodendroglia: Metabolic supporters of neurons," *The Journal of Clinical Investigation*, vol. 127, no. 9, pp. 3271–3280, Sep. 1, 2017, ISSN: 1558-8238. DOI: 10.1172/JCI90610.

[111] T. Czopka, C. Ffrench-Constant, and D. A. Lyons, "Individual oligodendrocytes have only a few hours in which to generate new myelin sheaths in vivo," *Developmental Cell*, vol. 25, no. 6, pp. 599–609, Jun. 24, 2013, ISSN: 1878-1551. DOI: 10.1016/j.devcel.2013.05.013.

[112] N. G. Bauer, C. Richter-Landsberg, and C. Ffrench-Constant, "Role of the oligodendroglial cytoskeleton in differentiation and myelination," *Glia*, vol. 57, no. 16, pp. 1691–1705, Dec. 2009, ISSN: 1098-1136. DOI: 10.1002/glia.20885.

[113] B. Emery, "Regulation of oligodendrocyte differentiation and myelination," *Science*, vol. 330, no. 6005, pp. 779–782, Nov. 5, 2010, ISSN: 0036-8075, 1095-9203. DOI: 10.1126/science.1190927. [Online]. Available: https://science.sciencemag.org/content/330/6005/779.

[114] K. K. Bercury, J. Dai, H. H. Sachs, J. T. Ahrendsen, T. L. Wood, and W. B. Macklin, "Conditional ablation of raptor or rictor has differential impact on oligodendrocyte differentiation and CNS myelination," *The Journal of Neuroscience: The Official Journal of the Society for Neuroscience*, vol. 34, no. 13, pp. 4466–4480, Mar. 26, 2014, ISSN: 1529-2401. DOI: 10.1523/JNEUROSCI.4314-13.2014.

[115] C. Taveggia, P. Thaker, A. Petrylak, G. L. Caporaso, A. Toews, D. L. Falls, S. Einheber, and J. L. Salzer, "Type III neuregulin-1 promotes oligodendrocyte myelination," *Glia*, vol. 56, no. 3, pp. 284–293, Feb. 2008, ISSN: 0894-1491. DOI: 10.1002/glia.20612.

[116] M. S. Y. Yeung, S. Zdunek, O. Bergmann, S. Bernard, M. Salehpour, K. Alkass, S. Perl, J. Tisdale, G. Possnert, L. Brundin, H. Druid, and J. Frisén, "Dynamics of oligodendrocyte generation and myelination in the human brain," *Cell*, vol. 159, no. 4, pp. 766–774, Nov. 6, 2014, ISSN: 1097-4172. DOI: 10.1016/j.cell.2014.10.011.

[117] L. E. Rivers, K. M. Young, M. Rizzi, F. Jamen, K. Psachoulia, A. Wade, N. Kessaris, and W. D. Richardson, "PDGFRA/NG2 glia generate myelinating oligodendrocytes and piriform projection neurons in adult mice," *Nature Neuroscience*, vol. 11, no. 12, pp. 1392–1401, Dec. 2008, ISSN: 1546-1726. DOI: 10.1038/nn.2220. [Online]. Available: https://www.nature.com/articles/nn.2220.

[118] J. Liu, K. Dietz, J. M. DeLoyht, X. Pedre, D. Kelkar, J. Kaur, V. Vialou, M. K. Lobo, D. M. Dietz, E. J. Nestler, J. Dupree, and P. Casaccia, "Impaired adult myelination in the prefrontal cortex of socially isolated mice," *Nature Neuroscience*, vol. 15, no. 12, pp. 1621–1623, Dec. 2012, ISSN: 1546-1726. DOI: 10.1038/nn.3263.

[119] E. M. Gibson, D. Purger, C. W. Mount, A. K. Goldstein, G. L. Lin, L. S. Wood, I. Inema, S. E. Miller, G. Bieri, J. B. Zuchero, B. A. Barres, P. J. Woo, H. Vogel, and M. Monje, "Neuronal activity promotes oligodendrogenesis and adaptive myelination in the mammalian brain," *Science (New York, N.Y.)*, vol. 344, no. 6183, p. 1 252 304, May 2, 2014, ISSN: 1095-9203. DOI: 10.1126/science.1252304.

[120] I. A. McKenzie, D. Ohayon, H. Li, J. P. d. Faria, B. Emery, K. Tohyama, and W. D. Richardson, "Motor skill learning requires active central myelination," *Science*, vol. 346, no. 6207, pp. 318–322, Oct. 17, 2014, ISSN: 0036-8075, 1095-9203. DOI: 10.1126/science.1254960. [Online]. Available: https://science.sciencemag.org/content/346/6207/318.

[121] J. Scholz, M. C. Klein, T. E. Behrens, and H. Johansen-Berg, "Training induces changes in white matter architecture," *Nature neuroscience*, vol. 12, no. 11, pp. 1370–1371, Nov. 2009, ISSN: 1097-6256. DOI: 10.1038/nn.2412. [Online]. Available: https://www.ncbi.nlm.nih.gov/pmc/articles/PMC2770457/.

[122] S. L. Bengtsson, Z. Nagy, S. Skare, L. Forsman, H. Forssberg, and F. Ullén, "Extensive piano practicing has regionally specific effects on white matter development," *Nature Neuroscience*, vol. 8, no. 9, pp. 1148–1150, Sep. 2005, ISSN: 1546-1726. DOI: 10.1038/nn1516. [Online]. Available: https://www.nature.com/articles/nn1516.

[123] A. Etxeberria, K. C. Hokanson, D. Q. Dao, S. R. Mayoral, F. Mei, S. A. Redmond, E. M. Ullian, and J. R. Chan, "Dynamic modulation of myelination in response to visual stimuli alters optic nerve conduction velocity," *The Journal of Neuroscience: The Official Journal of the Society for Neuroscience*, vol. 36, no. 26, pp. 6937–6948, 2016, ISSN: 1529-2401. DOI: 10.1523/JNEUROSCI.0908-16.2016.

[124] G. S. Tomassy, D. R. Berger, H.-H. Chen, N. Kasthuri, K. J. Hayworth, A. Vercelli, H. S. Seung, J. W. Lichtman, and P. Arlotta, "Distinct profiles of myelin distribution along single axons of pyramidal neurons in the neocortex," *Science (New York, N.Y.)*, vol. 344, no. 6181, pp. 319–324, Apr. 18, 2014, ISSN: 1095-9203. DOI: 10.1126/science.1249766.

[125] K. D. Micheva, D. Wolman, B. D. Mensh, E. Pax, J. Buchanan, S. J. Smith, and D. D. Bock, "A large fraction of neocortical myelin ensheathes axons of local inhibitory neurons," *eLife*, vol. 5, 2016, ISSN: 2050-084X. DOI: 10.7554/eLife.15784. [Online]. Available: https://www.ncbi.nlm.nih.gov/pmc/articles/PMC4972537/.

[126] H. N. Nelson, A. J. Treichel, E. N. Eggum, M. R. Martell, A. J. Kaiser, A. G. Trudel, J. R. Gronseth, S. T. Maas, S. Bergen, and J. H. Hines, "Individual neuronal subtypes control initial myelin sheath growth and stabilization," *bioRxiv*, p. 809 996, Oct. 18, 2019. DOI: 10.1101/809996. [Online]. Available: https://www.biorxiv.org/content/10.1101/809996v1.

[127] C Demerens, B Stankoff, M Logak, P Anglade, B Allinquant, F Couraud, B Zalc, and C Lubetzki, "Induction of myelination in the central nervous system by electrical activity.," *Proceedings of the National Academy of Sciences of the United States of America*, vol. 93, no. 18, pp. 9887–9892, Sep. 3, 1996, ISSN: 0027-8424. [Online]. Available: https://www.ncbi.nlm.nih.gov/pmc/articles/PMC38524/.

[128] S. Mensch, M. Baraban, R. Almeida, T. Czopka, J. Ausborn, A. El Manira, and D. A. Lyons, "Synaptic vesicle release regulates myelin sheath number of individual oligodendrocytes in vivo," *Nature Neuroscience*, vol. 18, no. 5, pp. 628–630, May 2015, ISSN: 1546-1726. DOI: 10.1038/nn.3991.

[129] E. Kougioumtzidou, T. Shimizu, N. B. Hamilton, K. Tohyama, R. Sprengel, H. Monyer, D. Attwell, and W. D. Richardson, "Signalling through AMPA receptors on oligodendrocyte precursors promotes myelination by enhancing oligodendrocyte survival," *eLife*, vol. 6, C. A. Mason, Ed., e28080, Jun. 13, 2017, ISSN: 2050-084X. DOI: 10.7554/eLife.28080. [Online]. Available: https://doi.org/10.7554/eLife.28080.

[130] C. Li, L. Xiao, X. Liu, W. Yang, W. Shen, C. Hu, G. Yang, and C. He, "A functional role of NMDA receptor in regulating the differentiation of oligodendrocyte precursor cells and remyelination," *Glia*, vol. 61, no. 5, pp. 732–749, May 2013, ISSN: 1098-1136. DOI: 10.1002/glia.22469.

[131] H. Wake, F. C. Ortiz, D. H. Woo, P. R. Lee, M. C. Angulo, and R. D. Fields, "Nonsynaptic junctions on myelinating glia promote preferential myelination of electrically active axons," *Nature Communications*, vol. 6, p. 7844, Aug. 4, 2015, ISSN: 2041-1723. DOI: 10.1038/ncomms8844.

[132] A. Trevisiol, A. S. Saab, U. Winkler, G. Marx, H. Imamura, W. Möbius, K. Kusch, K.-A. Nave, and J. Hirrlinger, "Monitoring ATP dynamics in electrically active white matter tracts," *eLife*, vol. 6, 2017, ISSN: 2050-084X. DOI: 10.7554/eLife.24241.

[133] A. S. Saab, I. D. Tzvetavona, A. Trevisiol, S. Baltan, P. Dibaj, K. Kusch, W. Möbius, B. Goetze, H. M. Jahn, W. Huang, H. Steffens, E. D. Schomburg, A. Pérez-Samartín, F. Pérez-Cerdá, D. Bakhtiari, C. Matute, S. Löwel, C. Griesinger, J. Hirrlinger, F. Kirchhoff, and K.-A. Nave, "Oligodendroglial NMDA receptors regulate glucose import and axonal energy metabolism," *Neuron*, vol. 91, no. 1, pp. 119–132, 2016, ISSN: 1097-4199. DOI: 10.1016/j.neuron.2016.05.016.

[134] U. Fünfschilling, L. M. Supplie, D. Mahad, S. Boretius, A. S. Saab, J. Edgar, B. G. Brinkmann, C. M. Kassmann, I. D. Tzvetanova, W. Möbius, F. Diaz, D. Meijer, U. Suter, B. Hamprecht, M. W. Sereda, C. T. Moraes, J. Frahm, S. Goebbels, and K.-A. Nave, "Glycolytic oligodendrocytes maintain myelin and long-term axonal integrity," *Nature*, vol. 485, no. 7399, pp. 517–521, May 2012, ISSN: 1476-4687. DOI: 10.1038/nature11007. [Online]. Available: https://www.nature.com/articles/nature11007.

[135] Y. Lee, B. M. Morrison, Y. Li, S. Lengacher, M. H. Farah, P. N. Hoffman, Y. Liu, A. Tsingalia, L. Jin, P.-W. Zhang, L. Pellerin, P. J. Magistretti, and J. D. Rothstein, "Oligodendroglia metabolically support axons and contribute to neurodegeneration," *Nature*, vol. 487, no. 7408, pp. 443–448, Jul. 26, 2012, ISSN: 0028-0836. DOI: 10.1038/nature11314. [Online]. Available: https://www.ncbi.nlm.nih.gov/pmc/articles/PMC3408792/.

[136] J. D. Haines, M. Inglese, and P. Casaccia, "Axonal damage in multiple sclerosis," *The Mount Sinai journal of medicine, New York*, vol. 78, no. 2, pp. 231–243, Mar. 2011, ISSN: 0027-2507. DOI: 10.1002/msj.20246. [Online]. Available: https://www.ncbi.nlm.nih.gov/pmc/articles/PMC3142952/.

[137] W. F. Blakemore and J. A. Murray, "Quantitative examination of internodal length of remyelinated nerve fibres in the central nervous system," *Journal of the Neurological Sciences*, vol. 49, no. 2, pp. 273–284, Feb. 1981, ISSN: 0022-510X. DOI: 10.1016/0022-510x(81)90084-8.

[138] R. F. Gledhill and W. I. McDonald, "Morphological characteristics of central demyelination and remyelination: A single-fiber study," *Annals of Neurology*, vol. 1, no. 6, pp. 552–560, Jun. 1977, ISSN: 0364-5134. DOI: 10.1002/ana.410010607.

[139] B. E. Powers, D. L. Sellers, E. A. Lovelett, W. Cheung, S. P. Aalami, N. Zapertov, D. O. Maris, and P. J. Horner, "Remyelination reporter reveals prolonged refinement of spontaneously regenerated myelin," *Proceedings of the National Academy of Sciences of the United States of America*, vol. 110, no. 10, pp. 4075–4080, Mar. 5, 2013, ISSN: 1091-6490. DOI: 10.1073/pnas.1210293110.

[140] Kishida Natsue, Maki Takakuni, Takagi Yasushi, Yasuda Ken, Kinoshita Hisanori, Ayaki Takashi, Noro Takayuki, Kinoshita Yusuke, Ono Yuichi, Kataoka Hiroharu, Yoshida Kazumichi, Lo Eng H., Arai Ken, Miyamoto Susumu, and Takahashi Ryosuke, "Role of perivascular oligodendrocyte precursor cells in angiogenesis after brain ischemia," *Journal of the American Heart Association*, vol. 8, no. 9, e011824, May 7, 2019. DOI: 10.1161/JAHA.118.011824. [Online]. Available: https://www.ahajournals.org/doi/10.1161/JAHA.118.011824.

[141] X. Zhu, R. A. Hill, and A. Nishiyama, "NG2 cells generate oligodendrocytes and gray matter astrocytes in the spinal cord," *Neuron Glia Biology*, vol. 4, no. 1, pp. 19–26, Feb. 2008, ISSN: 1741-0533. DOI: 10.1017/S1740925X09000015.

[142] L. Dimou, C. Simon, F. Kirchhoff, H. Takebayashi, and M. Götz, "Progeny of olig2-expressing progenitors in the gray and white matter of the adult mouse cerebral cortex," *The Journal of Neuroscience: The Official Journal of the Society for Neuroscience*, vol. 28, no. 41, pp. 10 434–10 442, Oct. 8, 2008, ISSN: 1529-2401. DOI: 10.1523/JNEUROSCI.2831-08.2008.

[143] S. H. Kang, M. Fukaya, J. K. Yang, J. D. Rothstein, and D. E. Bergles, "NG2+ CNS glial progenitors remain committed to the oligodendrocyte lineage in postnatal life and following neurodegeneration," *Neuron*, vol. 68, no. 4, pp. 668–681, Nov. 18, 2010, ISSN: 1097-4199. DOI: 10.1016/j.neuron.2010.09.009.

[144] D. E. Bergles, J. D. Roberts, P. Somogyi, and C. E. Jahr, "Glutamatergic synapses on oligodendrocyte precursor cells in the hippocampus," *Nature*, vol. 405, no. 6783, pp. 187–191, May 11, 2000, ISSN: 0028-0836. DOI: 10.1038/35012083.

[145] S.-c. Lin and D. E. Bergles, "Synaptic signaling between GABAergic interneurons and oligodendrocyte precursor cells in the hippocampus," *Nature Neuroscience*, vol. 7, no. 1, pp. 24–32, Jan. 2004, ISSN: 1546-1726. DOI: 10.1038/nn1162. [Online]. Available: https://www.nature.com/articles/nn1162.

[146] D. Sakry, A. Neitz, J. Singh, R. Frischknecht, D. Marongiu, F. Binamé, S. S. Perera, K. Endres, B. Lutz, K. Radyushkin, J. Trotter, and T. Mittmann, "Oligodendrocyte precursor cells modulate the neuronal network by activity-dependent ectodomain cleavage of glial NG2," *PLOS Biology*, vol. 12, no. 11, e1001993, Nov. 11, 2014, ISSN: 1545-7885. DOI: 10.1371/journal.pbio.1001993. [Online]. Available: https://journals.plos.org/plosbiology/article?id=10.1371/journal.pbio.1001993.

[147] K. E. Rhodes, L. D. F. Moon, and J. W. Fawcett, "Inhibiting cell proliferation during formation of the glial scar: Effects on axon regeneration in the CNS," *Neuroscience*, vol. 120, no. 1, pp. 41–56, 2003, ISSN: 0306-4522. DOI: 10.1016/s0306-4522(03)00285-9.

[148] A. M. Tan, W. Zhang, and J. M. Levine, "NG2: A component of the glial scar that inhibits axon growth," *Journal of Anatomy*, vol. 207, no. 6, pp. 717–725, Dec. 2005, ISSN: 0021-8782. DOI: 10.1111/j.1469-7580.2005.00452.x. [Online]. Available: https://www.ncbi.nlm.nih.gov/pmc/articles/PMC1571583/.

[149] S. Moyon, A. L. Dubessy, M. S. Aigrot, M. Trotter, J. K. Huang, L. Dauphinot, M. C. Potier, C. Kerninon, S. Melik Parsadaniantz, R. J. M. Franklin, and C. Lubetzki, "Demyelination causes adult CNS progenitors to revert to an immature state and express immune cues that support their migration," *The Journal of Neuroscience: The Official Journal of the Society for Neuroscience*, vol. 35, no. 1, pp. 4–20, Jan. 7, 2015, ISSN: 1529-2401. DOI: 10.1523/JNEUROSCI.0849-14.2015.

[150] J. H. Seo, N. Miyamoto, K. Hayakawa, L.-D. D. Pham, T. Maki, C. Ayata, K.-W. Kim, E. H. Lo, and K. Arai, "Oligodendrocyte precursors induce early blood-brain barrier opening after white matter injury," *The Journal of Clinical Investigation*, vol. 123, no. 2, pp. 782–786, Feb. 2013, ISSN: 1558-8238. DOI: 10.1172/JCI65863.

[151] M. E. Schwab and H. Thoenen, "Dissociated neurons regenerate into sciatic but not optic nerve explants in culture irrespective of neurotrophic factors," *The Journal of Neuroscience: The Official Journal of the Society for Neuroscience*, vol. 5, no. 9, pp. 2415–2423, Sep. 1985, ISSN: 0270-6474.

[152] L. Schnell and M. E. Schwab, "Axonal regeneration in the rat spinal cord produced by an antibody against myelin-associated neurite growth inhibitors," *Nature*, vol. 343, no. 6255, pp. 269–272, Jan. 18, 1990, ISSN: 0028-0836. DOI: 10.1038/343269a0.

[153] V. Kottis, P. Thibault, D. Mikol, Z.-C. Xiao, R. Zhang, P. Dergham, and P. E. Braun, "Oligodendrocyte-myelin glycoprotein (OMgp) is an inhibitor of neurite outgrowth," *Journal of Neurochemistry*, vol. 82, no. 6, pp. 1566–1569, Sep. 2002, ISSN: 0022-3042. DOI: 10.1046/j.1471-4159.2002.01146.x.

[154] S. Tang, R. W. Woodhall, Y. J. Shen, M. E. deBellard, J. L. Saffell, P. Doherty, F. S. Walsh, and M. T. Filbin, "Soluble myelin-associated glycoprotein (MAG) found in vivo inhibits axonal regeneration," *Molecular and Cellular Neurosciences*, vol. 9, no. 5, pp. 333–346, 1997, ISSN: 1044-7431. DOI: 10.1006/mcne.1997.0633.

[155] S. Tang, J. Qiu, E. Nikulina, and M. T. Filbin, "Soluble myelin-associated glycoprotein released from damaged white matter inhibits axonal regeneration," *Molecular and Cellular Neurosciences*, vol. 18, no. 3, pp. 259–269, Sep. 2001, ISSN: 1044-7431. DOI: 10.1006/mcne.2001.1020.

[156] K. C. Wang, J. A. Kim, R. Sivasankaran, R. Segal, and Z. He, "P75 interacts with the nogo receptor as a co-receptor for nogo, MAG and OMgp," *Nature*, vol. 420, no. 6911, pp. 74–78, Nov. 7, 2002, ISSN: 0028-0836. DOI: 10.1038/nature01176.

[157] S. Mi, X. Lee, Z. Shao, G. Thill, B. Ji, J. Relton, M. Levesque, N. Allaire, S. Perrin, B. Sands, T. Crowell, R. L. Cate, J. M. McCoy, and R. B. Pepinsky, "LINGO-1 is a component of the nogo-66 receptor/p75 signaling complex," *Nature Neuroscience*, vol. 7, no. 3, pp. 221–228, Mar. 2004, ISSN: 1097-6256. DOI: 10.1038/nn1188.

[158] E. M. Grados-Munro and A. E. Fournier, "Myelin-associated inhibitors of axon regeneration," *Journal of Neuroscience Research*, vol. 74, no. 4, pp. 479–485, 2003, ISSN: 1097-4547. DOI: 10.1002/jnr.10803. [Online]. Available: https://onlinelibrary.wiley.com/doi/abs/10.1002/jnr.10803.

[159] G. Raisman, "Myelin inhibitors: Does NO mean GO?" *Nature Reviews Neuroscience*, vol. 5, no. 2, pp. 157–161, Feb. 2004, ISSN: 1471-003X. DOI: 10.1038/nrn1328. [Online]. Available: http://www.nature.com/nrn/journal/v5/n2/full/nrn1328.html.

[160] D. B. Pettigrew and K. A. Crutcher, "White matter of the CNS supports or inhibits neurite outgrowth in vitro depending on geometry," *Journal of Neuroscience*, vol. 19, no. 19, pp. 8358–8366, Oct. 1, 1999, ISSN: 0270-6474, 1529-2401. [Online]. Available: http://www.jneurosci.org/content/19/19/8358.

[161] D. B. Pettigrew and K. A. Crutcher, "Myelin contributes to the parallel orientation of axonal growth on white matter in vitro," *BMC Neuroscience*, vol. 2, p. 9, May 31, 2001, ISSN: 1471-2202. DOI: 10.1186/1471-2202-2-9. [Online]. Available: http://www.ncbi.nlm.nih.gov/pmc/articles/PMC32297/.

[162] S. J. A. Davies, M. T. Fitch, S. P. Memberg, A. K. Hall, G. Raisman, and J. Silver, "Regeneration of adult axons in white matter tracts of the central nervous system," *Nature*, vol. 390, no. 6661, pp. 680–683, Dec. 18, 1997, ISSN: 0028-0836. DOI: 10.1038/37776. [Online]. Available: http://www.nature.com/nature/journal/v390/n6661/full/390680a0.html.

[163] M. Oubidar, M. Boquillon, C. Marie, L. Schreiber, and J. Bralet, "Ischemia-induced brain iron delocalization: Effect of iron chelators," *Free Radical Biology & Medicine*, vol. 16, no. 6, pp. 861–867, Jun. 1994, ISSN: 0891-5849. DOI: 10.1016/0891-5849(94)90205-4.

[164] M. H. Selim and R. R. Ratan, "The role of iron neurotoxicity in ischemic stroke," *Ageing Research Reviews*, vol. 3, no. 3, pp. 345–353, Jul. 2004, ISSN: 1568-1637. DOI: 10.1016/j.arr.2004.04.001.

[165] M. Bradl and H. Lassmann, "Oligodendrocytes: Biology and pathology," *Acta Neuropathologica*, vol. 119, no. 1, pp. 37–53, Jan. 2010, ISSN: 1432-0533. DOI: 10.1007/s00401-009-0601-5.

[166] E. Alberdi, M. V. Sánchez-Gómez, A. Marino, and C. Matute, "Ca2+ influx through AMPA or kainate receptors alone is sufficient to initiate excitotoxicity in cultured oligodendrocytes," *Neurobiology of Disease*, vol. 9, no. 2, pp. 234–243, Mar. 1, 2002, ISSN: 0969-9961. DOI: 10.1006/nbdi.2001.0457. [Online]. Available: http://www.sciencedirect.com/science/article/pii/S0969996101904577.

[167] C. Matute, I. Torre, F. Pérez-Cerdá, A. Pérez-Samartín, E. Alberdi, E. Etxebarria, A. M. Arranz, R. Ravid, A. Rodríguez-Antigüedad, M. Sánchez-Gómez, and M. Domercq, "P2x(7) receptor blockade prevents ATP excitotoxicity in oligodendrocytes and ameliorates experimental autoimmune encephalomyelitis," *The Journal of Neuroscience: The Official Journal of the Society for Neuroscience*, vol. 27, no. 35, pp. 9525–9533, Aug. 29, 2007, ISSN: 1529-2401. DOI: 10.1523/JNEUROSCI.0579-07.2007.

[168] S. Doyle, D. B. Hansen, J. Vella, P. Bond, G. Harper, C. Zammit, M. Valentino, and R. Fern, "Vesicular glutamate release from central axons contributes to myelin damage," *Nature Communications*, vol. 9, no. 1, pp. 1–15, ISSN: 2041-1723.

[169] S. Baltan, "Age-specific localization of NMDA receptors on oligodendrocytes dictates axon function recovery after ischemia," *Neuropharmacology*, Oligodendrocytes in Health and Disease, vol. 110, pp. 626–632, Nov. 1, 2016, ISSN: 0028-3908. DOI: 10.1016/j.neuropharm.2015.09.015. [Online]. Available: http://www.sciencedirect.com/science/article/pii/S0028390815301076.

[170] M. Buntinx, M. Moreels, F. Vandenabeele, I. Lambrichts, J. Raus, P. Steels, P. Stinissen, and M. Ameloot, "Cytokine-induced cell death in human oligodendroglial cell lines: I. synergistic effects of IFN-gamma and TNF-alpha on apoptosis," *Journal of Neuroscience Research*, vol. 76, no. 6, pp. 834–845, Jun. 15, 2004, ISSN: 0360-4012. DOI: 10.1002/jnr.20118.

[171] J. Li, O. Baud, T. Vartanian, J. J. Volpe, and P. A. Rosenberg, "Peroxynitrite generated by inducible nitric oxide synthase and NADPH oxidase mediates microglial toxicity to oligodendrocytes," *Proceedings of the National Academy of Sciences of the United States of America*, vol. 102, no. 28, pp. 9936–9941, Jul. 12, 2005, ISSN: 0027-8424. DOI: 10.1073/pnas.0502552102.

[172] G. Mifsud, C. Zammit, R. Muscat, G. Di Giovanni, and M. Valentino, "Oligodendrocyte pathophysiology and treatment strategies in cerebral ischemia," *CNS Neuroscience & Therapeutics*, vol. 20, no. 7, pp. 603–612, Jul. 1, 2014, ISSN: 1755-5930. DOI: 10.1111/cns.12263. [Online]. Available: https://onlinelibrary.wiley.com/doi/full/10.1111/cns.12263.

[173] R. Gregersen, T. Christensen, E. Lehrmann, N. Diemer, and B. Finsen, "Focal cerebral ischemia induces increased myelin basic protein and growth-associated protein-43 gene transcription in peri-infarct areas in the rat brain," *Experimental Brain Research*, vol. 138, no. 3, pp. 384–392, Jun. 1, 2001, ISSN: 1432-1106. DOI: 10.1007/s002210100715. [Online]. Available: https://doi.org/10.1007/s002210100715.

[174] K Mandai, M Matsumoto, K Kitagawa, K Matsushita, T Ohtsuki, T Mabuchi, D. R Colman, T. Kamada, and T Yanagihara, "Ischemic damage and subsequent proliferation of oligodendrocytes in focal cerebral ischemia," *Neuroscience*, vol. 77, no. 3, pp. 849–861, Feb. 3, 1997, ISSN: 0306-4522. DOI: 10.1016/S0306-4522(96)00517-9. [Online]. Available: http://www.sciencedirect.com/science/article/pii/S0306452296005179.

[175] T. Mabuchi, K. Kitagawa, T. Ohtsuki, K. Kuwabara, Y. Yagita, T. Yanagihara, M. Hori, and M. Matsumoto, "Contribution of microglia/macrophages to expansion of infarction and response of oligodendrocytes after focal cerebral ischemia in rats.," *Stroke*, vol. 31, no. 7, pp. 1735–1743, 2000. DOI: 10.1161/01.STR.31.7.1735.

[176] X. Shi, Y. Kang, Q. Hu, C. Chen, L. Yang, K. Wang, L. Chen, H. Huang, and C. Zhou, "A long-term observation of olfactory ensheathing cells transplantation to repair white matter and functional recovery in a focal ischemia model in rat," *Brain Research*, vol. 1317, pp. 257–267, Mar. 4, 2010, ISSN: 0006-8993. DOI: 10.1016/j.brainres.2009.12.061. [Online]. Available: http://www.sciencedirect.com/science/article/pii/S0006899309027590.

[177] L. Jiang, F. Shen, V. Degos, M. Schonemann, S. J. Pleasure, S. H. Mellon, W. L. Young, and H. Su, "Oligogenesis and oligodendrocyte progenitor maturation vary in different brain regions and partially correlate with local angiogenesis after ischemic stroke," *Translational stroke research*, vol. 2, no. 3, pp. 366–375, Sep. 2011,

ISSN: 1868-4483. DOI: 10.1007/s12975-011-0078-0. [Online]. Available: https://www.ncbi.nlm.nih.gov/pmc/articles/PMC3196661/.

[178] K. Tanaka, S. Nogawa, S. Suzuki, T. Dembo, and A. Kosakai, "Upregulation of oligodendrocyte progenitor cells associated with restoration of mature oligodendrocytes and myelination in peri-infarct area in the rat brain," *Brain Research*, vol. 989, no. 2, pp. 172–179, Nov. 7, 2003, ISSN: 0006-8993. DOI: 10.1016/S0006-8993(03)03317-1. [Online]. Available: http://www.sciencedirect.com/science/article/pii/S0006899303033171.

[179] E. Irving, D. Bentley, and A. Parsons, "Assessment of white matter injury following prolonged focal cerebral ischaemia in the rat," *Acta Neuropathologica*, vol. 102, no. 6, pp. 627–635, Dec. 1, 2001, ISSN: 1432-0533. DOI: 10.1007/s004010100416. [Online]. Available: https://doi.org/10.1007/s004010100416.

[180] E. A. Irving, K. Yatsushiro, J. McCulloch, and D. Dewar, "Rapid alteration of tau in oligodendrocytes after focal ischemic injury in the rat: Involvement of free radicals," *Journal of Cerebral Blood Flow & Metabolism*, vol. 17, no. 6, pp. 612–622, Jun. 1, 1997, ISSN: 0271-678X.

[181] Pantoni Leonardo, Garcia Julio H., and Gutierrez Jorge A., "Cerebral white matter is highly vulnerable to ischemia," *Stroke*, vol. 27, no. 9, pp. 1641–1647, Sep. 1, 1996. DOI: 10.1161/01.STR.27.9.1641. [Online]. Available: https://www.ahajournals.org/doi/full/10.1161/01.str.27.9.1641.

[182] Y. Chida, Y. Kokubo, S. Sato, A. Kuge, S. Takemura, R. Kondo, and T. Kayama, "The alterations of oligodendrocyte, myelin in corpus callosum, and cognitive dysfunction following chronic cerebral ischemia in rats," *Brain Research*, vol. 1414, pp. 22–31, Sep. 26, 2011.

[183] J. Zhou, J. Zhuang, J. Li, E. Ooi, J. Bloom, C. Poon, D. Lax, D. M. Rosenbaum, and F. C. Barone, "Long-term post-stroke changes include myelin loss, specific deficits in sensory and motor behaviors and complex cognitive impairment detected using active place avoidance," *PloS One*, vol. 8, no. 3, e57503, 2013, ISSN: 1932-6203. DOI: 10.1371/journal.pone.0057503.

[184] A. Kisel, M. Khodanovich, D. Atochin, L. Mustafina, and V. Yarnykh, "Dynamics of myelin content decrease in the rat stroke model," *Journal of Physics: Conference Series*, vol. 886, p. 012008, Aug. 2017, ISSN: 1742-6596. DOI: 10.1088/1742-6596/886/1/012008. [Online]. Available: https://doi.org/10.1088%2F1742-6596%2F886%2F1%2F012008.

[185] S. R. McIver, M. Muccigrosso, E. R. Gonzales, J. M. Lee, M. S. Roberts, M. S. Sands, and M. P. Goldberg, "Oligodendrocyte degeneration and recovery after focal cerebral ischemia," *Neuroscience*, vol. 169, no. 3, pp. 1364–1375, Sep. 1, 2010, ISSN: 1873-7544. DOI: 10.1016/j.neuroscience.2010.04.070.

[186] E. G. Sozmen, A. Kolekar, L. A. Havton, and S. T. Carmichael, "A white matter stroke model in the mouse: Axonal damage, progenitor responses and MRI correlates," *Journal of neuroscience methods*, vol. 180, no. 2, pp. 261–272, Jun. 15, 2009, ISSN: 0165-0270.

[187] Tanaka Yukitaka, Imai Hideaki, Konno Kenjiro, Miyagishima Takaaki, Kubota Chisato, Puentes Sandra, Aoki Takeo, Hata Hidekazu, Takata Kuniaki, Yoshimoto Yuhei, and Saito Nobuhito, "Experimental model of lacunar infarction in the gyrencephalic brain of the miniature pig," *Stroke*, vol. 39, no. 1, pp. 205–212, Jan. 1, 2008.

[188] R. D. Souza-Rodrigues, A. M. R. Costa, R. R. Lima, C. D. Dos Santos, C. W. Picanço-Diniz, and W. Gomes-Leal, "Inflammatory response and white matter damage after microinjections of endothelin-1 into the rat striatum," *Brain Research*, vol. 1200, pp. 78–88, ISSN: 0006-8993.

[189] C.-W. Han, K.-H. Lee, M. G. Noh, J.-M. Kim, H.-S. Kim, H.-S. Kim, R. G. Kim, J. Cho, H.-I. Kim, and M.-C. Lee, "An experimental infarct targeting the internal capsule: Histopathological and ultrastructural changes," *Journal of Pathology and Translational Medicine*, vol. 51, no. 3, pp. 292–305, May 2017, ISSN: 2383-7837.

[190] P. Cougo-Pinto, L. Cloonan, A. Kanakis, K. Fitzpatrick, K. Furie, J. Rosand, and N. Rost, "White matter hyperintensity volume predicts long-term full recovery in patients with mild acute ischemic stroke," Feb. 12, 2015.

[191] H.-J. Kang, R. Stewart, M.-S. Park, K.-Y. Bae, S.-W. Kim, J.-M. Kim, I.-S. Shin, K.-H. Cho, and J.-S. Yoon, "White matter hyperintensities and functional outcomes at 2 weeks and 1 year after stroke," *Cerebrovascular Diseases (Basel, Switzerland)*, vol. 35, no. 2, pp. 138–145, 2013, ISSN: 1421-9786. DOI: 10.1159/000346604.

[192] T. W. Kim, Y.-H. Kim, K. H. Kim, and W. H. Chang, "White matter hyperintensities and cognitive dysfunction in patients with infratentorial stroke," *Annals of Rehabilitation Medicine*, vol. 38, no. 5, pp. 620–627, Oct. 2014, ISSN: 2234-0645. DOI: 10.5535/arm.2014.38.5.620.

[193] H. Ihle-Hansen, B. Thommessen, M. W. Fagerland, T. B. Wyller, K. Engedal, A. R. Øksengård, V. Stenset, K. Løken, and B. Fure, "Impact of white matter lesions on cognition in stroke patients free from pre-stroke cognitive impairment: A one-year follow-up study," *Dementia and Geriatric Cognitive Disorders EXTRA*, vol. 2, no. 1, pp. 38–47, Mar. 28, 2012, ISSN: 1664-5464. DOI: 10.1159/000336817. [Online]. Available: https://www.ncbi.nlm.nih.gov/pmc/articles/PMC3350344/.

[194] M. R. Borich, K. E. Brown, and L. A. Boyd, "Motor skill learning is associated with diffusion characteristics of white matter in individuals with chronic stroke," *Journal of neurologic physical therapy: JNPT*, vol. 38, no. 3, pp. 151–160, Jul. 2014, ISSN: 1557-0584. DOI: 10.1097/NPT.0b013e3182a3d353.

[195] B. Lakhani, K. S. Hayward, and L. A. Boyd, "Hemispheric asymmetry in myelin after stroke is related to motor impairment and function," *NeuroImage: Clinical*, vol. 14, pp. 344–353, Jan. 1, 2017, ISSN: 2213-1582. DOI: 10.1016/j.nicl.2017.01.009. [Online]. Available: http://www.sciencedirect.com/science/article/pii/S2213158217300098.

[196] M. Wang, X. Hua, H. Niu, Z. Sun, L. Zhang, Y. Li, L. Zhang, and L. Li, "Cornel iridoid glycoside protects against white matter lesions induced by cerebral ischemia in rats via activation of the brain-derived neurotrophic factor/neuregulin-1 pathway," *Neuropsychiatric Disease and Treatment*, vol. 15, pp. 3327–3340, Dec. 2, 2019, ISSN: 1176-6328. DOI: 10.2147/NDT.S228417. [Online]. Available: https://www.ncbi.nlm.nih.gov/pmc/articles/PMC6898993/.

[197] M. A. Ying, N. Maruschak, R. Mansur, A. F. Carvalho, D. S. Cha, and R. S. McIntyre, "Metformin: Repurposing opportunities for cognitive and mood dysfunction," *CNS & neurological disorders drug targets*, vol. 13, no. 10, pp. 1836–1845, 2014, ISSN: 1996-3181.

[198] B. Qi, L. Hu, L. Zhu, L. Shang, L. Sheng, X. Wang, N. Liu, N. Wen, X. Yu, Q. Wang, and Y. Yang, "Metformin attenuates cognitive impairments in hypoxia–ischemia neonatal rats via improving remyelination," *Cellular and Molecular Neurobiology*, vol. 37, no. 7, pp. 1269–1278, Oct. 1, 2017, ISSN: 1573-6830. DOI: 10.1007/s10571-016-0459-8. [Online]. Available: https://doi.org/10.1007/s10571-016-0459-8.

[199] L. Otero-Ortega, M. Gutiérrez-Fernández, J. Ramos-Cejudo, B. Rodríguez-Frutos, B. Fuentes, T. Sobrino, T. N. Hernanz, F. Campos, J. A. López, S. Cerdán, J. Vázquez, and E. Díez-Tejedor, "White matter injury restoration after stem cell administration in subcortical ischemic stroke," *Stem Cell Research & Therapy*, vol. 6, no. 1, Jun. 19, 2015, ISSN: 1757-6512.

[200] Ramos-Cejudo Jaime, Gutiérrez-Fernández María, Otero-Ortega Laura, Rodríguez-Frutos Berta, Fuentes Blanca, Vallejo-Cremades Maria Teresa, Hernanz Teresa Navarro, Cerdán Sebastián, and Díez-Tejedor Exuperio, "Brain-derived neurotrophic factor administration mediated oligodendrocyte differentiation and myelin formation in subcortical ischemic stroke," *Stroke*, vol. 46, no. 1, pp. 221–228, Jan. 1, 2015. DOI: 10.1161/STROKEAHA.114.006692. [Online]. Available: https://www-ahajournals-org.login.ezproxy.library.ualberta.ca/doi/full/10.1161/STROKEAHA.114.006692.

[201] R. M. Kessler, M. S. Ansari, P. Riccardi, R. Li, K. Jayathilake, B. Dawant, and H. Y. Meltzer, "Occupancy of striatal and extrastriatal dopamine d2 receptors by clozapine and quetiapine," *Neuropsychopharmacology: Official Publication of the American College of Neuropsychopharmacology*, vol. 31, no. 9, pp. 1991–2001, Sep. 2006, ISSN: 0893-133X. DOI: 10.1038/sj.npp.1301108.

[202] A. J. Cross, D Widzowski, C Maciag, A Zacco, T Hudzik, J Liu, S Nyberg, and M. W. Wood, "Quetiapine and its metabolite norquetiapine: Translation from in vitro pharmacology to in vivo efficacy in rodent models," *British Journal of Pharmacology*, vol. 173, no. 1, pp. 155–166, ISSN: 0007-1188.

[203] S. Nyberg, A. Jucaite, A. Takano, M. Kågedal, Z. Cselényi, C. Halldin, and L. Farde, "Norepinephrine transporter occupancy in the human brain after oral administration of quetiapine XR," *The International Journal of Neuropsychopharmacology*, vol. 16, no. 10, pp. 2235–2244, Nov. 2013, ISSN: 1469-5111. DOI: 10.1017/S1461145713000680.

[204] N. H. Jensen, R. M. Rodriguiz, M. G. Caron, W. C. Wetsel, R. B. Rothman, and B. L. Roth, "N-desalkylquetiapine, a potent norepinephrine reuptake inhibitor and partial 5-HT1a agonist, as a putative mediator of quetiapine's antidepressant activity," *Neuropsychopharmacology: Official Publication of the American College of Neuropsychopharmacology*, vol. 33, no. 10, pp. 2303–2312, Sep. 2008, ISSN: 1740-634X. DOI: 10.1038/sj.npp.1301646.

[205] Y. Zhang, H. Xu, W. Jiang, L. Xiao, B. Yan, J. He, Y. Wang, X. Bi, X. Li, J. Kong, and X.-M. Li, "Quetiapine alleviates the cuprizone-induced white matter pathology in the brain of c57bl/6 mouse," *Schizophrenia Research*, vol. 106, no. 2, pp. 182–191, Dec. 2008, ISSN: 0920-9964. DOI: 10.1016/j.schres.2008.09.013.

[206] H.-n. Wang, G.-h. Liu, R.-g. Zhang, F. Xue, D. Wu, Y.-c. Chen, Y. Peng, Z.-w. Peng, and Q.-r. Tan, "Quetiapine ameliorates schizophrenia-like behaviors and protects myelin integrity in cuprizone intoxicated mice: The involvement of notch signaling pathway," *International Journal of Neuropsychopharmacology*, vol. 19, no. 2, Feb. 1, 2016, ISSN: 1461-1457. DOI: 10.1093/ijnp/pyv088. [Online]. Available: https://academic-oup-com.login.ezproxy.library.ualberta.ca/ijnp/article/19/2/pyv088/2910077.

[207] L. Xiao, H. Xu, Y. Zhang, Z. Wei, J. He, W. Jiang, X. Li, L. E. Dyck, R. M. Devon, Y. Deng, and X. M. Li, "Quetiapine facilitates oligodendrocyte development and prevents mice from myelin breakdown and behavioral changes," *Molecular Psychiatry*, vol. 13, no. 7, pp. 697–708, Jul. 2008, ISSN: 1476-5578. DOI: 10.1038/sj.mp.4002064. [Online]. Available: http://www.nature.com/articles/4002064.

[208] Y. Zhang, H. Zhang, L. Wang, W. Jiang, H. Xu, L. Xiao, X. Bi, J. Wang, S. Zhu, R. Zhang, J. He, Q. Tan, D. Zhang, J. Kong, and X.-M. Li, "Quetiapine enhances oligodendrocyte regeneration and myelin repair after cuprizone-induced demyelination," *Schizophrenia Research*, vol. 138, no. 1, pp. 8–17, Jun. 2012, ISSN: 1573-2509. DOI: 10.1016/j.schres.2012.04.006.

[209] F. Mei, S. P. J. Fancy, Y.-A. A. Shen, J. Niu, C. Zhao, B. Presley, E. Miao, S. Lee, S. R. Mayoral, S. A. Redmond, A. Etxeberria, L. Xiao, R. J. M. Franklin, A. Green, S. L. Hauser, and J. R. Chan, "Micropillar arrays as a high-throughput screening platform for therapeutics in multiple sclerosis," *Nature Medicine*, vol. 20, no. 8, pp. 954–960, Aug. 2014, ISSN: 1546-170X. DOI: 10.1038/nm.3618.

[210] J. Gonzalez Cardona, M. D. Smith, J. Wang, L. Kirby, J. T. Schott, T. Davidson, J. L. Karnell, K. A. Whartenby, and P. A. Calabresi, "Quetiapine has an additive effect to triiodothyronine in inducing differentiation of oligodendrocyte precursor cells through induction of cholesterol biosynthesis," *PloS One*, vol. 14, no. 9, e0221747, 2019, ISSN: 1932-6203. DOI: 10.1371/journal.pone.0221747.

[211] Q. Bian, T. Kato, A. Monji, S. Hashioka, Y. Mizoguchi, H. Horikawa, and S. Kanba, "The effect of atypical antipsychotics, perospirone, ziprasidone and quetiapine on microglial activation induced by interferon-gamma," *Progress in Neuro-Psychopharmacology & Biological Psychiatry*, vol. 32, no. 1, pp. 42–48, Jan. 1, 2008, ISSN: 0278-5846. DOI: 10.1016/j.pnpbp.2007.06.031.

[212] H. Wang, S. Liu, Y. Tian, X. Wu, Y. He, C. Li, M. Namaka, J. Kong, H. Li, and L. Xiao, "Quetiapine inhibits microglial activation by neutralizing abnormal STIM1-mediated intercellular calcium homeostasis and promotes myelin repair in a cuprizone-induced mouse model of demyelination," *Frontiers in Cellular Neuroscience*, vol. 9, Dec. 21, 2015, ISSN: 1662-5102. DOI: 10.3389/fncel.2015.00492. [Online]. Available: https://www.ncbi.nlm.nih.gov/pmc/articles/PMC4685920/.

[213] Z. Zhao, G. Luo, M. Liu, H. Guo, M. Xue, X. Wang, X.-M. Li, and J. He, "Quetiapine reduces microglial number in the hippocampus of a transgenic mouse model of alzheimer's disease," *Neuroreport*, vol. 25, no. 11, pp. 870–874, Aug. 6, 2014, ISSN: 1473-558X. DOI: 10.1097/WNR.0000000000000209.

[214] F. Mei, S. Guo, Y. He, L. Wang, H. Wang, J. Niu, J. Kong, X. Li, Y. Wu, and L. Xiao, "Quetiapine, an atypical antipsychotic, is protective against autoimmune-mediated demyelination by inhibiting effector t cell proliferation," *PloS One*, vol. 7, no. 8, e42746, 2012, ISSN: 1932-6203. DOI: 10.1371/journal.pone.0042746.

[215] H. Xu, H. Wang, L. Zhuang, B. Yan, Y. Yu, Z. Wei, Y. Zhang, L. E. Dyck, S. J. Richardson, J. He, X. Li, J. Kong, and X.-M. Li, "Demonstration of an anti-oxidative stress mechanism of quetiapine: Implications for the treatment of alzheimer's disease," *The FEBS journal*, vol. 275, no. 14, pp. 3718–3728, Jul. 2008, ISSN: 1742-464X. DOI: 10.1111/j.1742-4658.2008.06519.x.

[216] O. Bai, Z. Wei, W. Lu, R. Bowen, D. Keegan, and X.-M. Li, "Protective effects of atypical antipsychotic drugs on PC12 cells after serum withdrawal," *Journal of Neuroscience Research*, vol. 69, no. 2, Jul. 15, 2002, ISSN: 0360-4012. DOI: 10.1002/jnr.10290.

[217] M. Padurariu, A. Ciobica, I. Dobrin, and C. Stefanescu, "Evaluation of antioxidant enzymes activities and lipid peroxidation in schizophrenic patients treated with typical and atypical antipsychotics," *Neuroscience Letters*, vol. 479, no. 3, pp. 317–320, Aug. 2, 2010, ISSN: 1872-7972. DOI: 10.1016/j.neulet.2010.05.088.

[218] S.-W. Park, S.-K. Lee, J.-M. Kim, J.-S. Yoon, and Y.-H. Kim, "Effects of quetiapine on the brain-derived neurotrophic factor expression in the hippocampus and neocortex of rats," *Neuroscience Letters*, vol. 402, no. 1, pp. 25–29, Jul. 10, 2006, ISSN: 0304-3940. DOI: 10.1016/j.neulet.2006.03.028.

[219] F. Fumagalli, R. Molteni, F. Bedogni, M. Gennarelli, J. Perez, G. Racagni, and M. A. Riva, "Quetiapine regulates FGF-2 and BDNF expression in the hippocampus of animals treated with MK-801," *Neuroreport*, vol. 15, no. 13, pp. 2109–2112, Sep. 15, 2004, ISSN: 0959-4965. DOI: 10.1097/00001756-200409150-00022.

[220] S. W. Park, C. H. Lee, H. Y. Cho, M. K. Seo, J. G. Lee, B. J. Lee, W. Seol, B. S. Kee, and Y. H. Kim, "Effects of antipsychotic drugs on the expression of synaptic proteins and dendritic outgrowth in hippocampal neuronal cultures," *Synapse (New York, N.Y.)*, vol. 67, no. 5, pp. 224–234, May 2013, ISSN: 1098-2396. DOI: 10.1002/syn.21634.

[221] Z. Kokaia, G. Andsberg, A. Martinez-Serrano, and O. Lindvall, "Focal cerebral ischemia in rats induces expression of p75 neurotrophin receptor in resistant striatal cholinergic neurons," *Neuroscience*, vol. 84, no. 4, pp. 1113–1125, Jun. 1998, ISSN: 0306-4522. DOI: 10.1016/s0306-4522(97)00579-4.

[222] K. Irmady, K. A. Jackman, V. A. Padow, N. Shahani, L. A. Martin, L. Cerchietti, K. Unsicker, C. Iadecola, and B. L. Hempstead, "Mir-592 regulates the induction and cell death-promoting activity of p75ntr in neuronal ischemic injury," *The Journal of Neuroscience: The Official Journal of the Society for Neuroscience*, vol. 34, no. 9, pp. 3419–3428, Feb. 26, 2014, ISSN: 1529-2401. DOI: 10.1523/JNEUROSCI.1982-13.2014.

[223] G. Dechant and Y.-A. Barde, "The neurotrophin receptor p75(NTR): Novel functions and implications for diseases of the nervous system," *Nature Neuroscience*, vol. 5, no. 11, pp. 1131–1136, Nov. 2002, ISSN: 1097-6256. DOI: 10.1038/nn1102-1131.

[224] X. Bi, Y. Zhang, B. Yan, S. Fang, J. He, D. Zhang, Z. Zhang, J. Kong, Q. Tan, and X.-M. Li, "Quetiapine prevents oligodendrocyte and myelin loss and promotes maturation of oligodendrocyte progenitors in the hippocampus of global cerebral ischemia mice," *Journal of Neurochemistry*, vol. 123, no. 1, pp. 14–20, 2012, ISSN: 1471-4159. DOI: 10.1111/j.1471-4159.2012.07883.x. [Online]. Available: http://www.onlinelibrary.wiley.com/doi/abs/10.1111/j.1471-4159.2012.07883.x.

[225] B. Yan, X. Bi, J. He, Y. Zhang, S. Thakur, H. Xu, A. Gendron, J. Kong, and X.-M. Li, "Quetiapine attenuates spatial memory impairment and hippocampal neurodegeneration induced by bilateral common carotid artery occlusion in mice," *Life Sciences*, vol. 81, no. 5, pp. 353–361, Jul. 12, 2007, ISSN: 0024-3205. DOI: 10.1016/j.lfs.2007.05.020.

[226] B. Yan, J. He, H. Xu, Y. Zhang, X. Bi, S. Thakur, A. Gendron, J. Kong, and X.-M. Li, "Quetiapine attenuates the depressive and anxiolytic-like behavioural changes induced by global cerebral ischemia in mice," *Behavioural Brain Research*, vol. 182, no. 1, pp. 36–41, Aug. 22, 2007, ISSN: 0166-4328. DOI: 10.1016/j.bbr.2007.05.002.

[227] M. B. Yılmaz, M. Tönge, H. Emmez, F. Kaymaz, and M. Kaymaz, "Neuroprotective effects of quetiapine on neuronal apoptosis following experimental transient focal cerebral ischemia in rats," *Journal of Korean Neurosurgical Society*, vol. 54, no. 1, pp. 1–7, Jul. 2013, ISSN: 2005-3711. DOI: 10.3340/jkns.2013.54.1.1. [Online]. Available: https://www.ncbi.nlm.nih.gov/pmc/articles/PMC3772279/.

[228] X. Bi, B. Yan, S. Fang, Y. Yang, J. He, X.-M. Li, and J. Kong, "Quetiapine regulates neurogenesis in ischemic mice by inhibiting NF-kappaB p65/p50 expression," *Neurological Research*, vol. 31, no. 2, pp. 159–166, Mar. 2009, ISSN: 0161-6412. DOI: 10.1179/174313209X393573.

[229] A. J. Schain, R. A. Hill, and J. Grutzendler, "Label-free in vivo imaging of myelinated axons in health and disease with spectral confocal reflectance microscopy," *Nature medicine*, vol. 20, no. 4, pp. 443–449, Apr. 2014, ISSN: 1078-8956. DOI: 10.1038/nm.3495. [Online]. Available: https://www.ncbi.nlm.nih.gov/pmc/articles/PMC3981936/.

[230] R. Mostany and C. A Portera-Cailliau, "A craniotomy surgery procedure for chronic brain imaging," *J. Vis. Exp.*, vol. 12, no. e680, 2008. DOI: 10.3791/680.

[231] N. P. Mc Loughlin and G. G. Blasdel, "Wavelength-dependent differences between optically determined functional maps from macaque striate cortex," *NeuroImage*, vol. 7, no. 4, pp. 326–336, 1998. DOI: doi:10.1006/nimg.1998.0329.

[232] T. Bonhoeffer and A. Grinvald, "Optical imaging based on intrinsic signals. the methodology.," in *Brain mapping: the methods*, A. Toga and J. Mazziota, Eds., London: Academic Press, 1996, pp. 55–97.

[233] N. Ogawa, Y. Hirose, S. Ohara, T. Ono, and Y. Watanabe, "A simple quantitative bradykinesia test in MPTP-treated mice," *Research Communications in Chemical Pathology and Pharmacology*, vol. 50, no. 3, pp. 435–441, Dec. 1985, ISSN: 0034-5164.

[234] M. Balkaya, J. M. Kröber, A. Rex, and M. Endres, "Assessing post-stroke behavior in mouse models of focal ischemia," *Journal of Cerebral Blood Flow & Metabolism*, vol. 33, no. 3, pp. 330–338, Mar. 2013, ISSN: 0271-678X. DOI: 10.1038/jcbfm.2012.185. [Online]. Available: https://www.ncbi.nlm.nih.gov/pmc/articles/PMC3587814/.

[235] K. L. Schaar, M. M. Brenneman, and S. I. Savitz, "Functional assessments in the rodent stroke model," *Experimental & Translational Stroke Medicine*, vol. 2, p. 13, Jul. 19, 2010, ISSN: 2040-7378. DOI: 10.1186/2040-7378-2-13. [Online]. Available: https://www.ncbi.nlm.nih.gov/pmc/articles/PMC2915950/.

[236] X. Li, K. K. Blizzard, Z. Zeng, A. C. DeVries, P. D. Hurn, and L. D. McCullough, "Chronic behavioral testing after focal ischemia in the mouse: Functional recovery and the effects of gender," *Experimental Neurology*, vol. 187, no. 1, pp. 94–104, May 2004, ISSN: 0014-4886. DOI: 10.1016/j.expneurol.2004.01.004.

[237] E. Boldog, T. E. Bakken, R. D. Hodge, M. Novotny, B. D. Aevermann, J. Baka, S. Bordé, J. L. Close, F. Diez-Fuertes, S.-L. Ding, N. Faragó, K. Kocsis, B. Kovács, Z. Maltzer, J. M. McCorrison, J. A. Miller, G. Molnár, G. Oláh, A. Ozsvár, M. Rózsa, S. I. Shehata, K. A. Smith, S. M. Sunkin, D. N. Tran, P. Venepally, A. Wall, L. G. Puskás, P. Barzó, F. J. Steemers, N. J. Schork, R. H. Scheuermann, R. S. Lasken, E. S. Lein, and G. Tamás, "Transcriptomic and morphophysiological evidence for a specialized human cortical GABAergic cell type," *Nature Neuroscience*, vol. 21, no. 9, pp. 1185–1195, Sep. 2018, ISSN: 1546-1726. DOI: 10.1038/s41593-018-0205-2. [Online]. Available: https://www.nature.com/articles/s41593-018-0205-2.

[238] S. Shipp, "Structure and function of the cerebral cortex," *Current Biology*, vol. 17, no. 12, R443–R449, Jun. 19, 2007, ISSN: 0960-9822. DOI: 10.1016/j.cub.2007.03.044. [Online]. Available: https://www.cell.com/current-biology/abstract/S0960-9822(07)01148-7.

[239] P. Rubio-Garrido, F. Pérez-de Manzo, C. Porrero, M. J. Galazo, and F. Clascá, "Thalamic input to distal apical dendrites in neocortical layer 1 is massive and highly convergent," *Cerebral Cortex (New York, N.Y.: 1991)*, vol. 19, no. 10, pp. 2380–2395, Oct. 2009, ISSN: 1460-2199. DOI: 10.1093/cercor/bhn259.

[240] L. Muckli, F. De Martino, L. Vizioli, L. Petro, F. Smith, K. Ugurbil, R. Goebel, and E. Yacoub, "Contextual feedback to superficial layers of v1," *Current Biology*, vol. 25, no. 20, pp. 2690–2695, Oct. 19, 2015, ISSN: 0960-9822. DOI: 10.1016/j.cub.2015.08.057. [Online]. Available: https://www.ncbi.nlm.nih.gov/pmc/articles/PMC4612466/.

[241] M. Larkum, "A cellular mechanism for cortical associations: An organizing principle for the cerebral cortex," *Trends in Neurosciences*, vol. 36, no. 3, pp. 141–151, Mar. 2013, ISSN: 1878-108X. DOI: 10.1016/j.tins.2012.11.006.

[242] M. M. Gresle, B. Jarrott, N. M. Jones, and J. K. Callaway, "Injury to axons and oligodendrocytes following endothelin-1-induced middle cerebral artery occlusion in conscious rats," *Brain Research*, vol. 1110, no. 1, pp. 13–22, Sep. 19, 2006, ISSN: 0006-8993. DOI: 10.1016/j.brainres.2006.06.111.

[243] V. Valeriani, D. Dewar, and J. McCulloch, "Quantitative assessment of ischemic pathology in axons, oligodendrocytes, and neurons: Attenuation of damage after transient ischemia," *Journal of Cerebral Blood Flow and Metabolism: Official Journal of the International Society of Cerebral Blood Flow and Metabolism*, vol. 20, no. 5, pp. 765–771, May 2000, ISSN: 0271-678X. DOI: 10.1097/00004647-200005000-00002.

[244] P. S. Yam, D. Dewar, and J. McCULLOCH, "Axonal injury caused by focal cerebral ischemia in the rat," *Journal of Neurotrauma*, vol. 15, no. 6, pp. 441–450, Jun. 1, 1998, ISSN: 0897-7151. DOI: 10.1089/neu.1998.15.441. [Online]. Available: https://www.liebertpub.com/doi/abs/10.1089/neu.1998.15.441.

[245] I. Whishaw and B. Kolb, *The Behavior of the Laboratory Rat: A Handbook with Tests*. Oxford University Press, Sep. 30, 2004, ISBN: 978-0-19-986389-1. [Online]. Available: https://www.oxfordscholarship.com/view/10.1093/acprof:oso/9780195162851.001.0001/acprof-9780195162851.

[246] T. Tanaka, Y. Fujita, M. Ueno, L. D. Shultz, and T. Yamashita, "Suppression of SHP-1 promotes corticospinal tract sprouting and functional recovery after brain injury," *Cell Death & Disease*, vol. 4, no. 4, e567–e567, Apr. 2013, ISSN: 2041-4889. DOI: 10.1038/cddis.2013.102. [Online]. Available: https://www.nature.com/articles/cddis2013102.

[247] S. Ji, G. Kronenberg, M. Balkaya, K. Färber, K. Gertz, H. Kettenmann, and M. Endres, "Acute neuroprotection by pioglitazone after mild brain ischemia without effect on long-term outcome," *Experimental Neurology*, vol. 216, no. 2, pp. 321–328, Apr. 2009, ISSN: 1090-2430. DOI: 10.1016/j.expneurol.2008.12.007.

[248] G. Royl, M. Balkaya, S. Lehmann, S. Lehnardt, K. Stohlmann, U. Lindauer, M. Endres, U. Dirnagl, and A. Meisel, "Effects of the PDE5-inhibitor vardenafil in a mouse stroke model," *Brain Research*, vol. 1265, pp. 148–157, Apr. 10, 2009, ISSN: 1872-6240. DOI: 10.1016/j.brainres.2009.01.061.

[249] T. Freret, V. Bouet, C. Leconte, S. Roussel, L. Chazalviel, D. Divoux, P. Schumann-Bard, and M. Boulouard, "Behavioral deficits after distal focal cerebral ischemia in mice: Usefulness of adhesive removal test," *Behavioral Neuroscience*, vol. 123, no. 1, pp. 224–230, Feb. 2009, ISSN: 0735-7044. DOI: 10.1037/a0014157.

[250] Q. Guo, G. Wang, X. Liu, and S. Namura, "Effects of gemfibrozil on outcome after permanent middle cerebral artery occlusion in mice," *Brain Research*, vol. 1279, pp. 121–130, Jul. 7, 2009, ISSN: 1872-6240. DOI: 10.1016/j.brainres.2009.04.055.

[251] J. V. Cramer, B. Gesierich, S. Roth, M. Dichgans, M. Düring, and A. Liesz, "In vivo widefield calcium imaging of the mouse cortex for analysis of network connectivity in health and brain disease," *NeuroImage*, vol. 199, pp. 570–584, Oct. 1, 2019, ISSN: 1053-8119. DOI: 10.1016/j.neuroimage.2019.06.014. [Online]. Available: http://www.sciencedirect.com/science/article/pii/S1053811919304999.